BLAST PERFORMANCE QUANTIFICATION STRATEGIES FOR REINFORCED MASONRY SHEAR WALLS WITH BOUNDARY ELEMENTS

BLAST PERFORMANCE QUANTIFICATION STRATEGIES FOR REINFORCED MASONRY SHEAR WALLS WITH BOUNDARY ELEMENTS

By

Tarek Hany Mohamed El-Hashimy

B.Sc., M.Sc.

A Thesis Submitted to the School of Graduate Studies in Partial Fulfillment of the Requirements for the Degree Doctor of Philosophy

McMaster University

April 2019

Doctor of Philosophy (2019) McMaster University

(Civil Engineering) Hamilton, Ontario

TITLE: BLAST PERFORMANCE QUANTIFICATION STRATEGIES FOR REINFORCED MASONRY SHEAR WALLS WITH BOUNDARY ELEMENTS

AUTHOR: Tarek El-Hashimy

B.Sc., M.Sc. (Ain Shams University)

SUPERVISORS: Prof. Wael El-Dakhakhni

Prof. Michael Tait

NUMBER OF PAGES: xiv, 179

Abstract

Structural systems have been evolving in terms of material properties and construction techniques, and their levels of protection against hazardous events have been the focus of different studies. For instance, the performance of the lateral force resisting systems has been investigated extensively to ensure that such systems would provide an adequate level of strength ductility capacity when subjected to seismic loading. However, with the increased occurrence of accidental and deliberate explosion incidents globally by more than three fold from 2004 to 2012 (Lange 2013), more studies have been focusing on the performance of such systems to blast loads and the different methods to quantify the inflicted damage.

Although both blast and seismic design requires structures to sustain a level of ductility to withstand the displacement demands, the distributions of such demands from seismic ground excitation and blast loading throughout the structural system are completely different. Therefore, a ductile seismic force resisting system may not necessarily be sufficient to resist a blast wave. To address this concern, North American standards (ASCE 59-11 (ASCE 2011), CSA S850-12 (CSA 2012a) provide response limits that define the different damage states that components may exhibit prior to collapse.

Over the past ten years, a new configuration of reinforced masonry (RM) shear walls utilizing boundary elements (BEs) at the vertical edges of the wall has been investigated as an innovative configuration that enhances the wall's in-plane performance. As such, they are included in the North American Masonry design standards, CSA S304-14 (CSA 2014a) and TMS 402-16 (TMS 2016) as an alternative means to enhance the ductility of seismic force resisting systems. However, investigations regarding the out-of-plane performance of such walls are generally scarce in literature which hindered the blast design standards from providing unique response limits that can quantify the different damage states for RM walls with BEs.

This dissertation has highlighted that some relevant knowledge gaps may lead to unconservative designs. Such gaps include (a) the RM wall with BEs out-of-plane behavior and damage sequence; and more specifically, (b) the BEs influence on the wall load-displacement response; as well as, (c) the applicability of using of the current response limits originally assigned for conventional RM walls to assess RM walls with BEs. Addressing these knowledge gaps is the main motivation behind this dissertation.

In this respect, this dissertation reports an experimental program, that focuses on bridging the knowledge gap pertaining to the out-of-plane performance

of seismically-detailed RM shear walls with BEs, which were not designed to withstand blast loads.

Meanwhile, from the analytical perspective, plastic analyses were carried out taking into account the different mechanisms that the wall may undergo until peak resistance is achieved. This approach was adopted in order to quantify the resistance function of such walls and determine the contribution of the BEs and web to the overall wall resistance. In addition, the experimental results of the tested walls were used to validate a numerical finite element model developed to compare the resistance function of RM walls with and without BEs. Afterwards, the model was further refined to capture the walls' performance under blast loads. The pressure impulse diagrams were generated to assess the capability of the current response limits in quantifying the different damage states for walls with different design parameters.

Furthermore, new response limits were proposed to account for the out-of-plane ductility capacities of different wall components. Finally, a comparison between conventional rectangular walls and their counterparts with BEs using the proposed limits was conducted in the form of pressure-impulse diagram to highlight the major differences between both wall configurations.

Dedications

To

My Father & Mother,

Nehal,

Noureen & Nadine

Acknowledgments

All praise and gratitude be to Allah the Most Gracious, the Most Compassionate and the Most Merciful with the blessings of Whom the good deeds are fulfilled.

First, I would like to express my deep appreciation to my co-supervisors Prof. Wael El-Dakhakhni and Prof. Michael Tait. I was lucky to be mentored by such professors with high ethical values, and who are humble, supportive, energetic, open-minded, and creative. I am grateful for our discussions that significantly impacted the quality of the dissertation. Special thanks are due to my supervisory committee members, Dr. Lydell Wiebe and Dr. Tracy Becker for their valuable guidance and suggestions. Their helpful comments and discussions during our meetings are greatly appreciated.

No words can express my gratitude to my brother and travelling companion Dr. Shady Salem for his continuous support. The experimental work would have never been completed without his help. I would also like to deeply thank Dr. Mohamed Ezzeldin, Mr. Moustafa Morsy, Dr. Ahmad Siam, and their families whom I consider my second family in Canada.

Special thanks are due to the Applied Dynamics laboratory (ADL) team; Mr. Kent Wheeler and Mr. Paul Heerema, for the help, advice and dedication they provided, my experience in the ADL would not be the same without them. I would also like to thank Dr. Manuel Campedelli for the time and help he provided. I also like to thank all of my friends and colleagues Dr. Yasser Al-Anany, Dr. Ahmed Ashour, Feras Alsheet, Heba Bayoumy, Nathan Buccella, Mohamed El-Sefy, Ahmed Ghith, Maysara Ghaith, Ahmed Ismail, Dr. Yasser Khalifa, Kevin McNamara, Vahid Mohsenzadeh, Mehdi Shafikhani, Taylor Steele, Ahmed Yassin and Ahmed Yosri for their help and useful discussions during all stages of my experimental and analytical studies.

I am thankful for the research funding support provided through the Natural Sciences and Engineering Research Council of Canada, and the Canada Masonry Design Centre. Many thanks to Mr. David Stubbs and Dr. Bennett Banting for providing valuable comments on the reinforced masonry practice in Canada, and the provisions by their expert masons. The supply of the scaled blocks by the Canadian Concrete Masonry Producers Association is gratefully acknowledged. Support was also provided by the McMaster University Centre for Effective Design of Structures, funded through the Ontario Research and Development Challenge Fund of the Ministry of Research and Innovation. Additional advancements have

also been provided by the McMaster Institute for Multi-Hazard Systemic Risk Studies.

At last but by no means the least, I would like to say that no words can express my sincere gratitude to my parents, Hany El-Hashimy and Fatma Shaker, for the motivation and guidance they provided, and to my wife, Nehal, for her patience, understanding, and endless encouragement and support throughout both the tough and the good times at McMaster. She has happily supported me far beyond her fair share. I would also like to acknowledge my daughters, Noureen and Nadine, for their positive energy that eased the long nights of work.

Co-Authorship

This thesis has been prepared in accordance with the regulations for a sandwich thesis format or as a compilation of research papers stipulated by the Faculty of Graduate Studies at McMaster University. This research presents experimental and analytical work carried out solely by Tarek El-Hashimy. Advice and guidance were provided for the whole thesis by the academic supervisors Dr. Wael El-Dakhakhni and Dr. Michael Tait. Information presented from outside sources, which has been used towards analysis or discussion, has been cited where appropriate; all other materials are the sole work of the author. This thesis consists of the following manuscripts in the following chapters:

Chapter 2

El-Hashimy, T., Ezzeldin, M., Tait, M. and El-Dakhakhni, W. (2019). "Out-of-Plane Performance of Reinforced Masonry Shear Walls Constructed with Boundary Elements." *J. Struct. Eng.*, Submitted on December 28, 2017 and approved on November 16, 2018. 10.1061/(ASCE)ST.1943-541X.0002337.

Chapter 3

El-Hashimy, T., Ezzeldin, M., El-Dakhakhni, W., and Tait M. (2019). "Out-of-Plane performance of Seismically-Detailed Reinforced Concrete Block Shear Walls with Boundary Elements." *J. Struct. Eng.* Submitted on November 25, 2018 and approved on May 11, 2019.

Chapter 4

El-Hashimy, T., Ezzeldin, M., El-Dakhakhni, W., and Tait M. (2019). "Reinforced Masonry Shear Wall Blast Response Limits for ASCE 59 and CSA S850" *J. Struct. Eng.*. submitted in March 4th, 2019.

Table of Content

List of Figures

List of Tables

CHAPTER 1

INTRODUCTION

1.1 BACKGROUND AND MOTIVATION

Structural systems have been evolving in terms of material properties and construction techniques, and their levels of protection against hazardous events have been the focus of different studies. These hazardous events are usually associated with dynamic loads that may negatively affect the structural system and may thus require special design considerations. For instance, the performance of lateral force resisting systems have been investigated extensively to ensure that such systems would provide an adequate level of strength ductility capacity when subjected to seismic loading. More recently, with the increased occurrence of accidental and deliberate explosion incidents globally by more than three folds from 2004 to 2012 (Lange 2013), more studies have been focusing on the performance of such key systems to blast loads and the different methods to quantify the inflected damage.

Although both blast and seismic design requires structures to sustain a certain level of ductility in order to withstand the displacement demands, the distributions of such demands from seismic ground excitation and blast wave throughout the structural system are different (Dusenberry 2010). A seismic ground excitation induces forces that are distributed on the structural *system* based on the mass and stiffness associated with each component, whereas blast loads effects are concentrated on specific components according to their location and stand-off

distance from the shock wave source (FEMA 2010). Therefore, a ductile seismic force resisting system may not necessarily be appropriate or sufficient to resist a blast wave. To address this concern, North American standards (ASCE 59-11 (ASCE 2011), CSA S850-12 (CSA 2012a) and CSA S851-12 (CSA 2012b) were developed to address the design requirements of structural components that might be subjected to blast loads. In addition, these standards provided response limits that defined the different damage states that components may exhibit prior to collapse.

Over the past ten years, a new type of reinforced masonry (RM) shear wall that utilize boundary elements (BEs) at the vertical edges of the wall has been investigated. This innovative BEs configuration enhances the wall's in-plane performance. The research studies of Shedid et al. (2010) and Banting and El-Dakhakhni (2014) have demonstrated that the in-plane ductility enhancement that BEs provided was due to the presence of dual layer of reinforcement and confinement reinforcement ties within the BEs. Recently, Ezzeldin et al. (2017) showed that a high level of ductility and small strength degradation were achieved at the structural system level when conventional walls were replaced with equivalent (i.e. same in-plane flexural capacity) walls with BEs. In light of these findings, and the perceived performance enhancement, RM walls with BEs were included in the North American Masonry design standards, CSA S304-14 (CSA 2014a) and TMS 402-16 (TMS 2016) as an alternative means to enhance the ductility of seismic force resisting systems.

Since RM shear walls are typically designed to sustain seismic demands (forces and displacements) within their in-plane direction, their out-of-plane performance investigation is generally scarce in literature (Abboud et al. 1996; Azimikor et al. 2017; ElSayed et al. 2016; Zhang et al. 2001). Nonetheless, ASCE 59 recommends that load bearing walls be constructed with a column at each end (i.e. with BEs) to provide an alternative load path for the axial load in the event of wall collapse. Simonds (2014) conducted the first and only known experimental study to date to evaluate the performance of such walls when subjected to live explosive-generated blast loading and showed that BEs provided significant support to the wall web (i.e. the part of the wall between the BEs). In particular, the cracking pattern suggested the formation of a two-way bending mechanism within the wall web. However, no further quantification or illustration of the BEs influence on the wall resistance capacity, displacement response and failure mode were conducted. In addition, the lack of experimental data hindered blast design standards from providing unique response limits that are able to quantify the different damage states for RM walls with BEs.

In this dissertation, some relevant knowledge gaps are highlighted that may lead to unconservative designs. Such gaps include (a) the RM wall with BEs out-of-plane behavior and damage sequence; and more specifically, (b) the BEs influence on the wall load-displacement response; as well as, (c) the applicability of using of the current response limits originally assigned for conventional RM walls to assess RM walls with BEs. Addressing these knowledge gaps is the main motivation behind this dissertation.

In this respect, this dissertation reports an experimental program, that consists of two phases, focusing on bridging the knowledge gap pertaining to the out-of-plane performance of seismically-detailed RM shear walls with BEs which were not designed to withstand blast loads. In *Phase I*, three scaled shear walls with different reinforcement ratios were tested in their out-of-plane direction using a load-controlled airbag until the peak resistance was reached. *Phase I* focused on evaluating the behavior of the walls including their damage pattern, load-displacement response (i.e. resistance function), stiffness degradation and ductility capacity under monotonically increasing load. In *Phase II*, the testing focused on investigating additional parameters that may influence the performance of the walls; such as the reinforcement ratio distribution through the web and the BEs; the wall aspect ratio; the axial load and the BEs alignment with respect to the wall web. Accordingly, seven additional scaled walls were tested under quasi-static displacement-controlled cyclic loading to capture the wall post peak behavior along with different damage sequence that may occur in the BEs (e.g. BE-web interface failure or BEs damage due torsional behavior) as will be discussed in Chapter 4.

From the analytical perspective, plastic analyses were carried out to quantify the resistance function of such walls and determine the contribution of the BEs and web to the overall wall resistance. In addition, the experimental results of the tested walls were used to validate a numerical finite element model developed to compare the resistance function of RM walls with and without BEs. Subsequently the model was further developed to capture the walls' performance under blast loads. Pressure impulse diagrams were generated to assess the capability of the current response

limits in quantifying the different damage states for walls with different design parameters. In addition, new response limits were proposed to account for the out-of-plane ductility capacities of different wall components. Finally, a comparison between conventional rectangular walls and their counterparts with BEs using the proposed limits was conducted in the form of pressure-impulse diagrams to highlight the major differences between the two wall configurations.

1.2 RESEARCH OBJECTIVES

The main goal of this dissertation is to evaluate the out-of-plane performance of seismically-detailed RM shear walls with BEs when subjected to blast loads, and to assess their subsequent damage states. As such, the following objectives were identified:

1.a. Quantify the influence of BEs on the wall displacement, ultimate resistance and ductility capacities. A preliminary experimental investigation was conducted on three RM walls with BEs (*Phase I*).

1.b. Gain a better understanding of the out-of-plane performance of shear walls with BEs, through comparing them to conventional RM walls. Therefore, a layered-shell element numerical model was developed and validated to simulate the out-of-plane performance of RM walls without and with BEs.

2. Assess the influence of different design parameters on the out-of-plane resistance function and damage sequence of RM walls with BEs by experimentally testing seven RM walls with BEs (*Phase II*). The parameters

investigated include the web and BEs vertical reinforcement ratio and distribution, BEs alignment with the respect to the wall web, as well as the axial load level and the wall aspect ratio. In addition, use plastic analysis approaches to replicate the test walls response in order to facilitate wall resistance function generation for RM wall blast design.

3.a. Assess the current ASCE 59-11 and CSA S850-12 response limits and propose new blast response limits that are capable of accounting for the wall's ductility performance. This was done through developing P-I diagrams for RM walls with and without BEs

3.b. Evaluate the out-of-plane dynamic behavior of RM walls with BEs when subjected to far-field blast loading demands relative to conventional RM using the previously proposed limits.

1.3 ORGANIZATION OF THE DISSERTATION

This section summarizes the content of each of the five chapters in the dissertation as follows:

- Chapter 1 introduces the background and motivation of the research as well as the dissertation objectives and an overview of its arrangement.
- Chapter 2 focuses on investigating the out-of-plane behavior of seismically-detailed RM shear walls under monotonically increasing quasi-static load to identify the influence of BEs on the wall performance. In this respect, an

experimental investigation (*Phase I*) was carried out on three scaled RM shear walls with BEs to evaluate their displacement responses, ductility capacities and damage states until ultimate resistance was reached. In order to generate additional results of RM shear walls without BEs to allow for a direct comparison with those experimentally tested, a simplified numerical model was developed and validated to simulate the out-of-plane performance of RM walls without and with BEs.

- Chapter 3 outlines *Phase II* of the experimental program, which included additional scaled RM walls selected to investigate the influence of different design parameters on the wall performance and more specifically the BEs damage. These aspects included the web and BEs vertical reinforcement ratio and distribution, BEs alignment, the axial load level and the wall aspect ratio. The BEs interaction with the web was evaluated based on the BEs and web deformations coupled with the observed damage. Finally, the test walls were analyzed using different plastic analysis approaches to predict their experimental behaviors and quantify the contribution of the BEs in the wall resistance.
- Chapter 4 evaluates the performance of different RM walls with BEs at different damage states using ASCE 59-11 and CSA S850-12 and the proposed response limits. In this respect, the numerical model (Constructed in Chapter 2) was used to simulate and validate the effects of blast load on the wall performance. The model was subsequently used to generate pressure-impulse diagrams that were used to assess the capability of the current response limits of conventional RM

walls in quantifying the different damage states. Subsequently a new response limit which is able to more accurately quantify the different damage states was proposed. Finally, a comparison between RM walls with and without BEs were conducted to highlight the enhancements in pressure and impulse demand for different damage states using BEs.

- Chapter 5 presents the dissertation summary, major conclusions and recommendations for future research work.

It should be noted that, although each chapter presents a standalone journal manuscript, Chapters 2, 3, 4 collectively form a cohesive research program as described in the introduction and conclusion chapters of the dissertation. However, for completeness of the individual standalone chapters/manuscripts, some overlap might exist.

1.4 REFERENCES

Abboud, B. E., Hamid, A. A., and Harris, H. G. (1996). "Flexural behavior of reinforced concrete masonry walls under out-of-plane monotonic loads." *ACI Structural Journal*, 93(3), 327–335.

ASCE (2011). "Blast Protection of Buildings." *ASCE 59-11*, Reston, Va.

Azimikor, N., Brzev, S., Elwood, K. J., Anderson, D. L., and Mcewen, W. (2017). "Out-of-plane instability of reinforced masonry uniaxial specimens under reversed cyclic axial loading." *Canadian J. Civ. Eng.*, 376(March), 367–376.

Banting, B. R., and El-Dakhakhni, W. W. (2014). "Seismic Design Parameters for Special Masonry Structural Walls Detailed with Confined Boundary Elements." *Journal of Structural Engineering*, 140(10), 04014067.

CSA (Canadian Standards Association). (2012). "Design and assessment of buildings subjected to blast loads." *CSA S850-12*, Mississauga, ON, Canada.

Dusenberry, D. O. (2010). *Handbook for blast-resistant design of buildings*. *Assessment*.

ElSayed, M., El-Dakhakhni, W., and Tait, M. (2016). "Resilience Evaluation of Seismically Detailed Reinforced Concrete-Block Shear Walls for Blast-Risk Assessment." *Journal of Performance of Constructed Facilities*, 30(4), 04015087.

Ezzeldin, M., El-Dakhakhni, W., and Wiebe, L. (2017). "Experimental assessment of the system-level seismic performance of an asymmetrical reinforced concrete block wall building with boundary elements." *Journal of Structural Engineering*, 143(8)

FEMA. (2010). *Blast-Resistant Benefits of Seismic Design. Phase 2 Study: Performance of Structural Steel Strengthening Systems (FEMA P-439B).*

Lange, D. (2013). "A review of blast loading and explosions in the context of multifunctional buildings." *SP Arbetsrapporter NV - 2013:11*.

Shedid, M. T., El-Dakhakhni, W. W., and Drysdale, R. G. (2010). "Alternative strategies to enhance the seismic performance of reinforced concrete-block

shear wall systems." *J. Struct. Eng.*, 10.1061/(ASCE)ST.1943-541X.0000164, 676–689.

Simonds, K. (2014). "Performance of reinforced concrete block structural walls with boundary elements under multiple design basis blast threat levels". M.Eng. thesis, McMaster University, Hamilton, ON, Canada.

The Masonry Society (TMS). (2016). "Building code requirements and specifications for masonry structures." *TMS 402-16*Detroit.

Zhang, X. (David), Singh, S., Bull, D. K., and Cooke, N. (2001). "Out-of-Plane Performance of Reinforced Masonry Walls with Openings." *Journal of Structural Engineering*, 127(1), 51–57.

CHAPTER 2

OUT-OF-PLANE PERFORMANCE OF REINFORCED MASONRY SHEAR WALLS CONSTRUCTED WITH BOUNDARY ELEMENTS

2.1. ABSTRACT

Reinforced Masonry shear walls with boundary elements have been introduced recently as a seismic force resisting system as alternative to conventional reinforced masonry shear walls with rectangular cross sections. The introduction of the boundary elements enhances the wall's in-plane performance because of the confinement action of the horizontal steel ties within the boundary elements, that increase the latter's compressive strain capacity, and thus improve the overall wall displacement ductility. However, the performance of such reinforced masonry shear wall system has not yet been well experimentally or analytically investigated under out-of-plane loading (e.g. blast and wind loads). As such, the study, in this chapter, evaluates the contribution of boundary elements to the wall out-of-plane performance in terms of enhanced ultimate resistance load and displacement capacities. In this respect, three reinforced masonry shear walls with boundary elements, with different reinforcement ratios and distributions, were tested under quasi-static loading to evaluate the wall displacement response, mode of failure, damage state, ductility capacity and energy absorption. Furthermore, a numerical (*OpenSees*) model was developed and utilized to generate additional results of walls with similar in-plane or out-of-plane load resistance to those tested experimentally, but with rectangular cross sections, to allow for a performance comparison. The

results showed that reinforced masonry shear walls with boundary elements achieved higher ductility capacity and energy absorption levels compared to their counterparts with rectangular cross sections. This chapter presents some of the key experimental and numerical data that will facilitate quantifying several aspects pertaining to the out-of-plane performance of reinforced masonry shear walls with BEs within the next editions of relevant North American codes and standards.

2.2. INTRODUCTION

In the last decade, reinforced masonry (RM) shear walls with boundary elements (BEs) have been investigated as an innovative solution to enhance the wall's in-plane performance compared to conventional RM shear walls with rectangular cross sections (Shedid et al. 2010a). The same authors demonstrated that the enhancement was mainly attributed to the presence of confinement reinforcement ties comprising the BEs that in turn increased the ultimate compressive strain of the section, and subsequently its corresponding curvature capacity. Banting and El-Dakhakhni (2014) also reported that BEs delayed the buckling of the compression reinforcement until significant drift ratios were reached. Recently, Ezzeldin et al. (2017) showed that a high level of ductility and small strength degradation were achieved at the system level when conventional walls were replaced with identical (i.e. same flexural capacity) walls with BEs. Based on the above conclusions, CSA S304-14 (CSA 2014a) standards, similar to the TMS 402-16 (TMS 2016), included RM walls with BEs as an alternative system to resist seismic loading.

Wall seismic force resisting systems are not typically designed to sustain seismic demands in their out-of-plane (low stiffness) direction. As such, studies focused on assessing the out-of-plane behavior of RM walls are very scarce in literature. A limited number of studies has been carried out to assess the different parameters that influence this behavior. For example, Abboud et al. (1996) reported that high out-of-plane ductility capacity and energy absorption levels were achieved by RM shear walls (tested experimentally), when low vertical reinforcement ratios, ρ_v, (i.e. less than 0.2) were used. Zhang et al. (2001) and ElSayed et al. (2016) respectively also demonstrated the influence of wall openings and reinforcement ratio on the wall resistance and displacement response of RM walls. Several studies also investigated the out-of-plane performance of unreinforced masonry walls including infill walls (Tu et al. 2010; Moghadam and Goudarzi 2010) and confined walls (Varela-Rivera et al. 2011, 2012). Moreno-Herrera et al. (2016) evaluated the main parameters that affect the out-of-plane performance of confined unreinforced masonry walls such as the aspect ratio (h_w/l_w), slenderness ratio (h_w/t_w), axial load and the in-plane stiffness of the surrounding elements. Varela-Rivera et al. (2011) also demonstrated the influence of the wall aspect ratio on the out-of-plane strength and displacement response, whereas Tu et al. (2010) studied the influence of slenderness ratio on infill walls. The results showed that slenderness ratio affects the wall's strength significantly. However, to the best of the authors' knowledge, no similar studies were conducted on RM walls with BEs. In general, the out-of-plane performance of RM shear walls, constructed with or without BEs, has received little attention, compared to those tested under in-plane loading, and

subsequently their corresponding resistance and ductility capacities are not well quantified (Hatzinikolas et al 2015).

Although ASCE 59-11 (ASCE 2011) and CSA-S850-12 (CSA 2012) standards for Blast Protection of Buildings provide response limits to assess the damage of conventional (i.e. with rectangular cross sections) RM shear walls in the out-of-plane direction, no corresponding limits are available for their counterparts with BEs. According to the above two standards, a non-load bearing wall would exhibit a heavy damage state when its chord support rotation exceeds 2 degrees. However, Simonds (2014) tested nine RM walls with BEs to quantify their performance under blast loading in the out-of-plane direction. The same author reported that BEs acted as partial supports that prevented wall edges from rotating freely, thus initiating a two-way bending mechanism of the wall web. Subsequently, some tested walls recorded support rotations of more than 2 degrees, without significant inelastic deformations being observed. This clearly demonstrates the conservative values of the response limits listed in the ASCE 59-11 (ASCE 2011) and CSA-S850-12 (CSA 2012) when BEs are adopted. This conservatism was based on the lack of relative experimental and/or analytical studies at the time when both standards were originally developed. To address this, distinctive values are needed for RM shear walls with BEs to account for their enhanced performance.

This chapter focuses on quantifying the influence of BEs on the wall displacement and ultimate resistance capacities in order to facilitate a better understanding of the out-of-plane performance of RM shear walls. In this respect,

a preliminary experimental investigation (*Phase I*) was carried out on three scaled RM shear walls with BEs under quasi-static loading to evaluate their damage states, displacement responses, ductility capacities and energy absorption. In order to generate additional results of RM shear walls without BEs to allow for a direct comparison with those experimentally tested, a three-dimensional layered-shell element macro numerical model was developed using *OpenSees* (McKenna et al. 2013) to simulate the out-of-plane performance of RM walls without and with BEs. The model was validated using experimental results from different programs to account for walls with different configurations. Subsequently, the study focused on comparing the load displacement response of RM walls without and with BEs with different design criteria.

2.3. EXPERIMENTAL PROGRAM (*PHASE I*)

2.3.1. Test Specimens and Material Properties

The experimental program was designed to assess the out-of-plane performance of three one-third scale RM shear walls with BEs that were originally designed for in-plane seismic load resistance, as shown in Fig. 2.1, through quantifying their out-of-plane performance. The CSA S304-14 (CSA 2014a) specifies a maximum slenderness ratio of 16 for ductile RM walls with thicker edges (i.e. boundary elements). As such, all the tested walls had a height, h_w, and thickness, t_w, of 990 mm and 63 mm respectively, corresponding to 2970 mm and 200 mm in full-scale. Since a two-way mechanism was observed in previous experimental studies (Simonds 2014), the aspect ratio of all walls was selected approaching unity to

maximize this mechanism. Therefore, the length, l_w, of all walls was 945 mm, corresponding to 2,835 mm in full-scale.

All tested walls had reinforcement details in accordance with CSA S304-14 (CSA 2014a) and TMS 402-16 (TMS 2016) to provide enough in-plane inelastic deformation and rotational capacity to withstand seismic loading demands (i.e. ductile/special shear walls). Although TMS (2016) waives the maximum reinforcement ratio requirements when BEs are confined with ties, CSA (2014a) specifies minimum and maximum reinforcement ratios of 0.125 % and 2%, respectively. Therefore, three vertical reinforcement ratios (ρ_v) were used for the tested walls, as presented in Table 2.1, to provide different flexural and curvature capacities. Wall ($W_{BE\text{-}L}$) had a D4 bar every other cell in the web, while its BEs had one bar in every cell. This distribution resulted in a 0.48% reinforcement ratio, classifying the wall as lightly reinforced in this study. To investigate the influence of the reinforcement ratio in the web, D4 bars were placed in every cell in wall ($W_{BE\text{-}M}$). This in turn increased the reinforcement ratio to 0.64%, and thus the wall was classified as moderately reinforced. Finally, wall ($W_{BE\text{-}H}$) was classified as a heavily reinforced because its reinforcement ratio reached a value of 1.20% by using D7 bars in every cell. The shear reinforcement and BEs confinement ties were placed every other course in wall $W_{BE\text{-}L}$ and every course in walls $W_{BE\text{-}M}$ and $W_{BE\text{-}H}$, as presented in Table 2.1.

The use of scaled models of reinforced masonry walls has been performed by several studies (Abboud et al. 1990, Shedid et al. 2010a, ElSayed et al. 2016 and

Smith et al 2016). In addition, use of scaled blocks and reinforcement bars has been well documented in the text by Harris and Sabnis (1999). In this respect, a one-third scale version of the standard 200 mm concrete blocks (190 x 190 x 390 mm) was used in the current study for all walls (Harris and Sabnis 1999). The blocks were 130 mm in length and 63 mm in both width and height, while the face-shell thickness was 10 mm. A number of these blocks were randomly tested to determine their axial compressive strength according to CSA A165-14 (CSA 2014b). The blocks had an average compressive strength of 20.1 MPa (coefficient of variation (c.o.v. = 12.0%)). Meanwhile, the mortar used in construction was classified as Type S according to CSA A179-14 (CSA2014c). The testing method specified within the same standards was used to determine the mortar average axial compressive strength which was found to be 29.6 MPa (c.o.v. = 10.1%). All blocks were laid in a running bond pattern, while the BEs were constructed in a configuration similar to that adopted by Shedid et al. (2010a), where two blocks are laid adjacent to each other, and thus the BEs dimensions were 130 mm in both directions. All walls were fully grouted, where notches were provided in all blocks to ensure the full grout encasement of the horizontal reinforcement along the entire length of the wall to provide an anchorage between the web and its corresponding BEs. The grout used was fine grout that had an average axial compressive strength of 22.4 MPa (c.o.v. = 14.2%) according to CSA A179-14 (CSA2014c).

Samples of standard unconfined grouted prisms were assembled and tested, and their average compressive strength was 19.4 MPa (c.o.v. = 15.9%) according

to CSA S304-14 (CSA 2014a). Tension tests were also conducted, according to CSA G30.18-09 (CSA 2014d), on the D4 and D7 (vertical reinforcement), and W1.7 (horizontal reinforcement) to determine their yield and ultimate strengths. The D4 (25 mm^2) and D7 (45 mm^2) vertical reinforcement had average yield strengths, f_y, of 484 MPa (c.o.v. = 4.2%) and 477 MPa (c.o.v = 4.1%), respectively, while their average ultimate strengths, f_u, were 546 MPa (c.o.v. = 1.8%) and 516 MPa (c.o.v. = 0.5%), respectively. For the W1.7 horizontal reinforcement, the average yield and ultimate strengths were 268 (c.o.v = 2.4%) and 362 MPa (c.o.v. = 2.2%), respectively.

All walls were constructed within a steel frame in order to provide a top and bottom support system that can be connected to the test setup, as shown in Fig. 2.2. The top and bottom edges of the steel frame (i.e. C-sections) were assumed rigid enough to represent diaphragm supports in the wall's out-of-plane directions (for both the web and BEs). This prevented the translation of the wall, but they allowed rotation along the wall entire length. These C-sections were welded to the wall's web and BEs vertical bars to provide them the required anchorage. Afterwards, vertical steel plates were welded to the C-sections to simulate the effect of different floor diaphragms. These *diaphragms* do not move, with respect to each other, in the vertical direction when the walls deform in the out-of-plane direction.

2.3.2. Test Setup and Instrumentation

This test setup comprised of a force-controlled system that loaded all walls until they reached their ultimate capacities, without capturing their post-peak descending

responses. The test setup included a rigid frame connected to a self-reacting frame as shown in Fig. 2.3(a). The C-sections of the walls were placed on two hinged supports. Four load cells were installed between the top and bottom C-sections and the rigid frame to directly measure the applied load on the wall. Out-of-plane load demands on walls are typically uniformly distributed as in the case of far-field blast loads. To simulate this load distribution within the experimental setup, a pneumatic bag was used to produce a uniform pressure load on the wall's surface. The pneumatic bag had a square configuration of 820 mm in each direction, with a capacity of 250 kN and a maximum stroke of 400 mm. The pneumatic bag was placed between the tested wall and a self-reacting frame connected to the test setup, as shown in Fig. 2.3(a). Meanwhile, Fig. 2.3(b) shows the instrumentation used throughout the test to capture the displacement responses of the wall at different locations. Three displacement potentiometers were mounted on the back-side of the walls to monitor their displacements. More specifically, potentiometers (web and BE) were positioned at the center of the web and the BE, respectively, while potentiometer (web') was installed at the mid-distance between the two former potentiometers.

2.3.3. Damage State Criteria

Three damage states were adopted within the current study following the response limits identified by ASCE 59-11 (ASCE 2011) and CSA S850-12 (CSA 2012) for flexural members. When the wall deformation remains less than the yield displacement (i.e. ductility ≤ 1), only a *superficial damage* is considered to be

realized. Beyond this ductility limit, the support chord rotation (θ_s) would be the governing parameter for the wall damage. A wall is considered to exhibit a *moderate damage* state until it reaches a θ_s equal to 2 degrees (i.e. 18 mm at the web center (Δ_{web}) according to the tested wall dimensions), where permanent, but repairable, deformations are expected before this rotation limit. Beyond this limit, a *heavy damage* state is considered to be realized, where significant (i.e. causing unrepairable damage) permanent deformations develop in the wall. Although these limits are intended to be used for dynamic loading that considers the strain rate effect and inertial forces, they are used in this study to facilitate a direct comparison due to the lack of explicit code limits for quasi-static loading.

2.4. EXPERIMENTAL RESULTS

2.4.1. Damage Sequence and Failure Modes

All walls showed a consistent cracking pattern throughout their tests, as shown in Fig. 2.4, where horizontal and vertical cracks were observed at the center of the webs. There was slightly unsymmetrical crack formation, based on this observation, future studies ought not assume symmetrical behavior of the wall and subsequently, more than one potentiometer should be used at the same horizontal level. In the tension side, the vertical and horizontal cracks were initiated at the wall mid-height till they reached 40% and 20% of the wall height and length, respectively. Afterwards, the vertical cracks were extended diagonally, with almost 45 degrees, until they reached the wall corners passing through the BEs. This crack pattern

confirms the influence of BEs to restrain the vertical edges of the wall, resulting in a two-way bending mechanism along its web, as shown in Fig. 2.5.

On the compression side, damage/crushing patterns similar to the crack patterns on the tension side were observed. As shown in Fig. 2.4, these patterns verify the presence of in-elastic rotations along these lines which resulted in concrete crushing and eventually flexural failures for all three walls. However, all walls showed additional corner cracks that were perpendicular to the web diagonals. This indicated a degree of corner restraining, where BEs along with the top and bottom supports restrained the web's vertical edge deformation, introducing diagonal moments on the web and torsional moments on the BEs, similar to that in two-way slabs (Park and Gamble, 2000). In slabs, corner cracks are typically avoided by adding steel reinforcement to resist such diagonal moment, as suggested by ACI 318-14 (2014). However, adding such reinforcement in RM shear walls is not possible due to the limitations associated with concrete masonry unit geometrical configuration and construction techniques. As such, this restriction results in damage to the BEs, as shown in Fig. 2.4. Similar torsional behavior were reported by Moreno-Herrera et al. (2015) that investigated the performance of confined unreinforced masonry walls (i.e. different system than that of the current study) under out-of-plane loading demands. Therefore, BEs need to be designed against such torsional moments to prevent the corresponding damages. This can be implemented through 1) increasing the vertical reinforcement of BEs; 2) increasing

the confinement ties; and 3) increasing the size of the BEs to provide higher torsional resistance.

It is worth noting that, at the ultimate resistance load, only Wall $W_{BE\text{-}L}$ experienced fracture in the horizontal reinforcement due to its lower ratio (ρ_h = 0.14%) relative to Walls $W_{BE\text{-}M}$ and $W_{BE\text{-}H}$ (ρ_h = 0.26%). This confirms that the load was transferred horizontally to the boundary element throughout the test and that the horizontal reinforcement contributed to the wall's out-of-plane performance. Such contribution is not possible in conventional RM shear walls with rectangular cross sections, that would only experience one-way bending.

2.4.2. Load-Displacement Response

Figure 2.6(a) presents the experimental load-displacement relationship of walls ($W_{BE\text{-}L}$, $W_{BE\text{-}M}$ and $W_{BE\text{-}H}$) to evaluate the influence of the steel reinforcement ratio on their out-of-plane performance. As can be seen in Fig. 2.6(a), the initial stiffness values of all walls are almost the same regardless of their reinforcement ratios. This is mainly attributed to the identical gross dimensions of all walls. However, wall $W_{BE\text{-}H}$ achieved higher ultimate resistance load of 86.5 kN compared to those of walls ($W_{BE\text{-}M}$ and $W_{BE\text{-}L}$) reaching 74 kN and 60 kN, respectively. The difference in the ultimate resistance load between the three walls demonstrates the significant influence of the reinforcement ratio on altering the out-of-plane performance of RM shear walls with BEs. More specifically, unlike conventional RM walls, the use of BEs at both wall ends facilitates the use of dual layer of vertical reinforcement that subsequently increases the wall's cross-section flexural capacity.

Figure 2.6(a) shows that the ultimate resistance load values of walls ($W_{BE\text{-}L}$, $W_{BE\text{-}M}$ and $W_{BE\text{-}H}$) were reached at θ_s = 2.4, 3.9 and 3.0 degrees, respectively. These values indicate that all walls were able to reach the ASCE 59-11 and CSA 850-12 standards' heavy damage state rotation limit/indicator ($\theta_s > \theta_{max}$ = 2 degrees), without actually reaching their ultimate resistance load and prior to experiencing significant inelastic deformations. During the test of wall $W_{BE\text{-}L}$, a distortion in the test setup was observed at the bottom support that limited the wall rotation and subsequently resulted in an increased perceived wall stiffness, as shown in Figs. 6(a and b). This distortion was avoided during the test of the subsequent walls by providing enough clearance between the steel frame and the bottom C-sections to allow its rotation.

Figures 2.6 (b, c and d) show the load-displacement responses of walls ($W_{BE\text{-}L}$, $W_{BE\text{-}M}$ and $W_{BE\text{-}H}$), respectively, at different wall locations (i.e. BEs, Web and Web'). These figures also present the walls mid-height displacement profiles at their corresponding yield and ultimate resistance loads. For all walls, at their early loading stages (up to R = 15 kN), displacement responses (Δ_{BEs}, $\Delta_{web'}$, Δ_{web}) were essentially the same at the BEs, Web' and Web, respectively. However, at later stages of loading (from R > 15 kN), these displacement responses were different, as shown in Figs. 2.6 (b, c and d). This is mainly attributed to the BEs that partially restrained the edges of the wall, forcing the web to deform into a two-way bending mechanism. The discrepancy between these displacement responses (i.e. Δ_{BEs} and Δ_{web}) showed an increasing non-linear trend for all walls that was linked to the wall

reinforcement ratio. For example, $W_{BE\text{-}M}$ had ($\Delta_{web}/\Delta_{BEs}$) ratio of 1.9 at yield load that increased to 2.3 at the ultimate resistance load. Similarly, for $W_{BE\text{-}L}$, ($\Delta_{web}/\Delta_{BEs}$) had a wider range of 1.43 and 2.67 at yield and ultimate resistance loads, respectively. This is due to the lower web reinforcement ratio of $W_{BE\text{-}L}$ (ρ_{vw} = 0.32%) relative to that of $W_{BE\text{-}M}$ (ρ_{vw} = 0.64%), as can be seen in Table 2.1, since both walls had the same boundary reinforcement ratio ($\rho_{v\text{-}BEs}$ = 0.64%).

To further quantify the influence of the BEs on the wall bending mechanism, the chord rotation about the BEs axis (θ_{BE}), shown in Fig. 2.5, was evaluated for the test walls. At their ultimate resistance loads, walls ($W_{BE\text{-}L}$, $W_{BE\text{-}M}$, and $W_{BE\text{-}H}$) achieved θ_{BE} value of 1.85, 2.2 and 1.8 degrees, respectively. These values are lower than their corresponding θ_s, which indicates that the latter indicator still controls the damage state, as mentioned earlier in this study, regardless of the presence of the two-way bending mechanism.

Defining the onset of yielding for a composite wall system that is composed of different materials (i.e. concrete blocks, grout, mortan and reinforcement bars) is a controversial research point that has not find a general consensus. Specifically, yielding of a bar does not necessarily represent the onset of yielding of the wall, as discussed by Tomaževič (1998). As such, the idealization of the load-displacement response was used to identify the wall's yielding point using ASCE 41-13(ASCE 2014) instead of relying on strain gages, as shown in Fig. 2.7. This idealization is characterized by the effective yield displacement (Δ_y), reinforcement yield load (R_y), effective elastic lateral stiffness (K_e), ultimate resistance load (R_u) and ultimate

displacement (Δ_u). As can be seen in Fig. 2.7, the load-displacement response is idealized to a bi-linear elastoplastic relationship. According to ASCE 41-13(ASCE 2014), K_e was calculated as the secant stiffness at 60% of R_y, while R_u was set corresponding to the maximum load achieved. Based on the aforementioned criteria, Δ_y and R_y were calculated to maintain an equivalent system of the actual load-displacement response that has the same energy absorption level. (i.e. same area under curve). Table 2.2 presents the idealization results for all walls. $W_{BE\text{-}L}$ (ρ_v = 0.48%) achieved lower R_y of 40.3 kN compared to those of 58.3 kN and 64.5 kN achieved by walls ($W_{BE\text{-}M}$ and $W_{BE\text{-}H}$) with higher vertical reinforcement ratio, ρ_v, of 0.64% and 1.20%, respectively.

2.4.3. Displacement Ductility and Energy Absorption

Displacement ductility (μ) is the ability of the wall to deform beyond its yielding state without losing appreciable strength. Typically, it is defined by the ratio of some target ultimate displacement to the yield displacement (Paulay and Priestley 1992). Since there is no consensus in the literature on how to determine the yield displacement, Δ_y, the idealization approach in ASCE 41-13 (ASCE 2014), mentioned earlier, was used in this study. The target displacement was defined as the web displacement (Δ_{web}) corresponding to the ultimate resistance load. $W_{BE\text{-}L}$ achieved the highest ductility performance with μ of 6.56, corresponding to ρ_v of 0.48%, compared to those of 4.37 and 4.10 achieved by Walls $W_{BE\text{-}M}$ and $W_{BE\text{-}H}$ with higher vertical reinforcement ratio ρ_v of 0.64% and 1.20%, respectively. Related observations were reported for RM shear walls tested by Shedid et al.

(2008), albeit in their in-plane directions, where the increase in the reinforcement ratio led to limited ductility capacities.

Energy absorption, E_A, is an important aspect in blast design (Dusenberry, 2010), where blast demands can be reduced through plastic deformations, which occurs within walls with high ductility capacities (Biggs 1964). Therefore, E_A of each wall was evaluated at two damage states, moderate and heavy, and at the ultimate resistance loads level for comparison purposes. E_A was quantified as the area enclosed by the load-displacement relationship. As can be seen in Fig. 2.8(a), all walls showed low E_A levels at early loading stages before any significant plastic deformations development in the wall. Later on, at higher displacement levels, the E_A values increased significantly relative to early loading stages reflecting the increased wall resistance, damage and ductility levels.

The wall normalized energy absorption, defined as the ratio between the E_A required to reach a specific damage state (i.e. heavy damage state or ultimate resistance loads) to that at the moderate damage state (Shedid et al. 2008), is shown in Fig. 2.8(b). Normalization was utilized in this study to eliminate the influences of different wall responses so as to monitor the trend of increase of energy absorption. As can be seen in Fig. 2.8(b), wall $W_{BE\text{-}L}$ showed the highest normalized energy absorption in both heavy damage state and ultimate resistance load with values of 12.0 and 14.6, respectively, compared to 3.7 and 9.4 for Wall $W_{BE\text{-}M}$ and 5.1 and 8.4 for Wall $W_{BE\text{-}H}$ at the same demand levels. This comparison indicates that although Wall $W_{BE\text{-}L}$ had the lowest ultimate resistance load among the walls,

it possessed the highest energy absorption after yield which is key in blast resistant construction.

2.5. RM WALL OUT-OF-PLANE NUMERICAL MODEL

In order to further investigate the influence of BEs on the RM walls out-of-plane performance and expand the result database beyond that of the three walls reported earlier, a numerical or analytical model is needed. The objective was to utilize such model to generate RM shear walls without and with BEs with identical characteristics to allow for a direct comparison between the walls' out-of-plane performances. Several models were developed to simulate the in-plane behavior of RM shear walls (Karapitta et al. 2011; Ezzeldin et al. 2016). However, the limited amount of published research to date has focused on developing experimentally validated models to simulate the out-of-plane performance of only unreinforced and infill masonry walls (Drysdale and Essawy 1988 and Varela-Rivera et al. 2012). In addition, such studies required well-defined boundary conditions at the wall edges (unlike the case of BEs which provide partial wall web out-of-plane restraints). Several other studies (Cerioni and Donida. 1994, and Hallinan and Guan 2007) have demonstrated that layered finite element model (LFEM) is efficient in simulating the coupled bending/shear behavior of both concrete and masonry walls. Therefore, a macro numerical *OpenSees* model was developed in terms of simple level of detailing requirements and material modeling, as will be discussed in this section.

2.5.1. Material Model

Two main material models were used for simulating the grouted concrete block masonry and the steel reinforcement. For the masonry, a concrete model, developed by Lu et al. (2015) specifically for the LFEM in *OpenSees*, was used. This concrete model follows the smeared crack approach that accounts for the concept of damage mechanics. More specifically, once the wall reaches its cracking limit, the damage model considers its material to have an orthotropic nature. Afterwards, the model implements directional damage factors to the elastic constitutive matrix based on the crack direction. The model adopts the crack band theory (Bažant and Oh 1983), where fracture is modeled as a smeared crack band instead of discrete crack. The tension strain within the developed crack is then distributed along a crack band width, and subsequently, the tension stress-strain relationship is influenced by the cracking stage where tension softening is included (Rots 1997).

In order to account for the enhanced performance of the BEs (i.e. higher ultimate strain capacity), both confined and unconfined concrete materials were modeled within the current study. The unconfined concrete material was assigned an axial compressive strength, f'_m, equal to that of the tested prisms, as mentioned earlier in the paper, whereas the elastic modulus, E_m, and the shear modulus, G, were calculated according to TMS 402-16 (TMS 2016) as 900 f'_m and 0.4 E_m, respectively. Damage due to shear was considered by using a shear retention factor, β, that reduced the elastic shear modulus according to Rots et al. (1985). Finally, the strain at ultimate compressive strength, ε_{cu}, was assumed to be 0.0025 according

to prisms test data reported by Shedid et al.(2010b) and Elezz et al. (2015). As mentioned earlier, unlike the web part of the wall, BEs allow for closed ties that provide confinement to the grouted masonry within the BE cores and subsequently delay the buckling of the enclosed vertical reinforcement. This confinement enhances the strength and ductility capacities of the concrete material within the BEs. Subsequently, the confined concrete material within the BEs, Mander et al. (1988) model was implemented to determine the enhanced compressive strength, f'_m, and strain, ε_{ccu}, due to the confinement.

In the LFEM, both the vertical and horizontal reinforcement details/ratios were modeled as an equivalent thickness of steel layers. In this respect, the PlateRebar material model (available in *OpenSees*) was used. The yield strength, f_y, for each type of reinforcement was defined based on experimental tension tests and the strain hardening ratio (ratio between post-yield and initial elastic tangents (Filippou et al. 1983)) of 1% was assumed and the steel Young's modulus, E_s, was taken as 200 GPa.

2.5.2. Model Description

A three-dimensional model was generated using *OpenSees* (McKenna et al. 2013) version 6.50, Figs. 2.9 (a and b) presents a schematic diagram of the model, showing nodes and elements distribution. The LFEM SHELLMITC4 shell element (available in *OpenSees*) was used to simulate the out-of-plane response of the wall. A comprehensive description of the SHELLMITC4 multi-layer shell element formulation can be found elsewhere (Lu et al. 2015). Figs. 2.9 (c and d) shows a

schematic diagram of the material distribution among the wall cross-section used in the model for walls without and with BEs, respectively. The unconfined and confined masonry areas were divided into several layers each, to properly capture the material non-linearity of the section, as suggested by (Lu et al. 2015).

The crack band approach minimizes the influence of geometrical node spacing (i.e. shell meshing) on the numerical results through strain localization phenomena. This was confirmed by Lu et al. (2015) for concrete walls using the SHELLMITC4 shell elements, where the crack band width is a function of the element size. Although this is valid for elements made of isotropic materials, masonry elements require additional limitations to avoid inaccurate simulation (Lotfi and Shing 1991; Rots 1997; Hoiseth and Kvande 2000). More specifically, Lotfi and Shing (1991) recommended appropriate mesh size to avoid localization of the inelastic deformations within some elements.

Square SHELLMITC4 shell elements were used to avoid introducing analysis bias by adopting an unrealistic crack path in a certain direction, as suggested by Bažant and Oh (1983). Since it is common in RM shear walls to have cracks through their mortar joints, four different square mesh sizes functions of the block height, h_b, were assumed to determine an appropiate meshing size. However, in the current study, the tested walls were subjected to force-controlled loading, which prevented the descending loading branch from being captured. Therefore, a RM rectangular wall (Wall W_1), tested by Abboud et al. (1996), was used to show the sensitivity of the wall out-plane-response to the meshing size within the

developed model. Full details of the wall dimensions and material properties are presented in Table 2.3, while the wall boundary conditions and loading scheme can be found in Abboud et al. (1996). The model results, shown in Fig. 2.10, showed good agreement with the experimental results when the model mesh size was equal to h_b, as the model was able to capture the wall's ultimate resistance load and its corresponding displacement with maximum deviations of 16% and 5%, respectively. As can be see also in Fig. 2.10, a large mesh size (1.50 h_b) results in larger ductility capacity of the wall and no strength degradation, whereas a small mesh size (0.25 h_b or 0.50 h_b) underestimates the ductility capacity of the wall. This is mainly attributed to the unrealistic strain distribution attributed to using either mesh size. Accordingly, a mesh with square element sizes equal to h_b was used in the current study.

All the nodes in the top and bottom rows of the mesh were restrained according to the boundary conditions. The tested RM shear walls with BEs (i.e. $W_{BE\text{-}L}$, $W_{BE\text{-}M}$ and $W_{BE\text{-}H}$), discussed earlier in this study, had C-sections that were assumed to behave as diaphragms, therefore, any translation throughout the test was ignored. This was considered in the numerical model by restraining all the nodes at the C-sections to prevent their translations. However, the presence of a dual layer of reinforcement coupled with the larger wall thickness in the BEs region restrained the C-section rotation relative to the web, thus inducing partial fixation to the BEs. As such, to simulate this behavior, a plastic spring was added to BEs support as shown in Fig. 2.9 (b), using a zero-length element (available in *OpenSees*). The

properties of this spring were based on the moment rotation relation using mechanics base elastic analysis. The validity of this behavior was assessed by modeling Wall $W_{BE\text{-}M}$ using four different approaches to simulate the boundary conditions. The first approach provided a complete fixation for all the supports (i.e. web and BEs). In the second approach, the BEs were assumed to be fully fixed, while the web was considered simply supported. The third approach considered hinged boundary conditions at the web and four plastic springs at the BEs. Finally, a hinged support was assumed in the fourth approach for both web and BEs. For all approaches, the numerical results were compared to the experimental load-displacement relationships, as shown in Fig. 2.11. The results show the sensitivity of the wall's out-of-plane response to its simulated boundary conditions. As can be seen in Fig. 2.11, the first and second approaches overestimated the ultimate resistance load resistance by 70% and 60%, respectively, while the same parameter was underestimated by 20% in the fourth approach. However, the third approach showed a good agreement with the experimental results in terms of the ultimate resistance load and its corresponding displacement predictions (i.e. deviation < 3%). Therefore, the third approach was used throughout the current study to simulate the behavior of RM shear walls with BEs.

2.5.3. Model Validation

The developed model was validated using a fully grouted conventional (i.e. with rectangular cross-section) RM shear wall (Wall W_3) tested by Abboud et al. (1996). The wall material and reinforcement properties are presented in Table 2.3. As can

be seen in Figs. 12 (a and b) for walls W_1 (shown earlier in Fig. 2.10) and W_3, respectively, the model captured the different characteristics of wall in term of initial stiffness value, load resistances, and corresponding displacements until flexural failure was observed at wall mid-height. For example, for Wall W_3, the model was able to capture the ultimate resistance load and its corresponding displacement with maximum deviations of 7% and 13%, respectively. To verify the effectiveness of the developed model for walls with BEs, the numerical results were compared to the experimental results of Wall $W_{BE\text{-}H}$, as shown in Fig. 2.12(c). The numerical model effectively captured the load-displacement response with maximum deviations of 6% and 4% at yield and ultimate resistance loads, respectively. In addition, Fig. 2.12(d) compared the numerical results of Wall $W_{BE\text{-}M}$ to its experimental results, shown earlier in the previous section, for completeness of the model validation.

To further demonstrate the effectiveness of the developed model, the damage (crack) pattern in the tension side of wall $W_{BE\text{-}M}$, (i.e. based on the tension strains in the outermost layers of the shell element) was compared to that of the test, as shown in Fig. 2.13(a). This figure confirms that the model can predict the concentration of the tension strains within the mid-height of the web that extended diagonally to the corners of the wall, as shown in Fig. 2.13(b).

2.6. INFLUENCE OF BES ON THE WALLS' OUT-OF-PLANE RESPONSE

The influence of introducing BEs on the out-of-plane performance of RM shear walls was evident from the experimental results, discussed earlier in this study.

However, quantification of this influence, compared to conventional walls, is key. As such, displacement response numerical results of five walls (i.e. four rectangular and one with BEs) were generated, compared to the three walls previously tested experimental program, and shown in Fig. 2.1. The in-plane and out-of-plane capacities were the aspects of design considered for wall selection as the in-plane capacity is used for walls designed as a part of the seismic force resisting systems, whereas the out-of-plane capacity is considered for blast and wind loads. All walls had the same length, height, block dimensions and material properties as the tested walls. The reinforcement ratios and details for each wall are presented in Fig. 2.14.

The first comparison was for walls having the same in-plane capacity. In this respect, Walls $W_{R\text{-}L}$, $W_{R\text{-}M}$ and $W_{R\text{-}H}$ were designed to match the in-plane capacity of the previously tested Walls $W_{BE\text{-}L}$, $W_{BE\text{-}M}$, and $W_{BE\text{-}H}$, respectively, but with rectangular cross-sections. As can be seen in Fig. 2.15, the initial stiffness and ultimate resistance load values of Walls $W_{BE\text{-}L}$, $W_{BE\text{-}M}$, and $W_{BE\text{-}H}$ were almost double those of Walls $W_{R\text{-}L}$, $W_{R\text{-}M}$ and $W_{R\text{-}H}$. This enhancement is attributed to the geometrical configuration of the BEs and the use of dual layer of reinforcement, which in turn increase the wall's out-of-plane flexural capacity. In addition, Walls $W_{BE\text{-}L}$, $W_{BE\text{-}M}$, and $W_{BE\text{-}H}$ show also improvement in terms of their displacement capacities, where the BEs enhanced the wall ultimate displacement, Δ_u, by 35% on average. It is worth mentioning that ρ_v for each conventional wall was higher than their corresponding wall with BEs by approximately 35%, however, higher load

resistance and ultimate displacement values were achieved by walls with BEs because of the steel distribution as mentioned earlier.

Walls W_R and W_{BE} were generated to have similar out-of-plane ultimate resistance load. To achieve this, a heavily reinforced rectangular Wall W_R with a ρ_v of 2.37% was required versus a ρ_v of 0.20% for Wall W_{BE} with the BEs. The load-displacement relationships for both walls were presented in Fig. 2.16. The initial stiffness of Wall W_{BE} was increased by approximately 200% relative to that of Wall W_R. In addition, the numerical model was utilized to determine the wall yield resistance load and its corresponding displacement. Both walls achieved approximately the same yield resistance load, but at different yield displacement levels due to the variations in their reinforcement ratios. Although the ultimate displacement of Wall W_{BE} was lower than that of W_R, as shown in Fig. 2.16, Wall W_{BE} showed higher ultimate ductility capacity with value of 2 relative to 1.2 of W_R.

2.7. CONCLUSIONS

Previous experimental and numerical/analytical studies showed that RM shear walls with BEs experienced an enhanced in-plane performance compared to conventional RM shear walls (i.e. with rectangular cross sections). However, prior to the current study, very limited published work has been conducted on RM shear walls with BEs under out-of-plane loading scenarios. In this respect, an experimental investigation was carried out by testing three scaled RM shear walls with BEs under quasi-static out-of-plane loading. The experimental results were evaluated in terms of the wall displacement response, ductility capacity, and

damage states. To allow for a direct comparison, similar conventional RM shear walls (i.e. with rectangular cross-sections) were generated using a developed three-dimensional layered-shell numerical model. This model was validated through different experimental programs because they included walls with different configurations (i.e. without and with BEs) with a range of aspect ratios, from 1.0 to 3.0.

The influence of the reinforcement ratio on altering the out-of-plane ultimate resistance load of walls with BEs was evident from the experimental results. This influence was mainly attributed to the geometrical configuration of the BEs that enabled the use dual layer of vertical reinforcement at the wall end regions. In addition, similar to RM shear walls subjected to in-plane loading, the out-of-plane ductility capacity and energy absorption were affected by the wall steel reinforcement ratio. More specifically, the results showed that the ductility capacity increased as the wall reinforcement ratio decreased, but with lower energy absorption levels when compared to walls with higher reinforcement ratio. Moreover, the load displacement relationships for all walls clearly demonstrated the discrepancies between the BEs and web displacements as the wall web edges were partially restrained by their BEs. These displacement discrepancies coupled with the observed crack pattern confirmed the presence of two-way bending mechanism along the wall web. This two-way bending mechanism indicates that distinctive response limits should be provided for RM shear walls with BEs. Finally, the numerical results showed that RM shear walls with BEs had higher

initial stiffness values and energy absorption levels compared to conventional walls, when both systems were originally designed to have either identical in-plane or out-of-plane load resistance.

The work in chapter was limited to RM shear walls with specific BEs configuration due to preliminary address lack of experimental data for other wall systems with different loading conditions (e.g. axial load demands). However, a low aspect ratio (h_w/l_w) wall for example may experience an essentially one-way bending mechanism that in turn minimizes the contribution of the BEs. As such, to build on the current study results, additional experimental studies that investigate the influence of the boundary conditions and aspect ratio on the wall performance will be further studied in the next chapter. In addition, although the numerical modeling approach (i.e. three-dimensional layered-shell elements) adopted in the current study captures the experimental results very well, there are other modeling approaches (e.g. the discrete element) and different analysis methods (i.e. two-way section analysis and yield line method) that might need to be considered in future studies for comparison purposes. Overall, this study opens the gate for additional experimental and numerical studies that are still needed to facilitate the adoption of RM shear walls with BEs within the masonry provision of future editions of the ASCE 59 and CSA S850 blast design standards.

2.8. ACKNOWLEDGMENTS

The financial support for this project was provided by a Collaborative Research and Development Grant (CRDG) funded through the Natural Sciences and Engineering

Research Council (NSERC) of Canada and the Canadian Concrete Masonry Producers Association (CCMPA). Provision of mason time by the Ontario Masonry Contractors Association (OMCA) and technical support by the Canada Masonry Design Centre (CMDC) is appreciated. Support was also provided by the McMaster University Centre for Effective Design of Structures (CEDS), funded through the Ontario Research and Development Challenge Fund (ORDCF) of the Ministry of Research and Innovation (MRI).

2.9. NOTATION

The following symbols are used in this paper:

E_A	=	Energy absorption;
E_m	=	Masonry Young's modulus;
E_s	=	Elastic modulus of streel reinforcement;
f'_m	=	Unconfined masonry compressive strength;
f'_{mc}	=	Confined masonry compressive strength;
f_u	=	Reinforcement ultimate strength;
f_y	=	Reinforcement yield strength;
G	=	Masonry shear modulus;
K_e	=	Cross section effective initial stiffness;
l_w	=	Length of the wall;
h_w	=	Height of the wall;
h_b	=	Height of the concrete block;
R	=	Resistance load on the wall;
R_u	=	Ultimate out-of-plane resistance load;
R_y	=	Yield out-of-plane resistance load;
t_w	=	Web thickness;
β	=	Masonry shear retention factor;
Δ_{BE}	=	Out-of-plane displacement at the mid-hight of the boundary element;
Δ_u	=	Out-of-plane displacement corresponding to ultimate resistance load;

Δ_{web}	=	Out-of-plane displacement at web center;
Δ_y	=	Out-of-plane displacement corresponding to reinforcement of yield;
ε_{cu}	=	Unconfined ultimate compressive strain of concrete;
ε_{ccu}	=	Confined ultimate compressive strain of concrete;
$\mu_{\Delta u}$	=	Displacement ductility at ultimate resistance load (Δ_u/Δ_y);
ρ_h	=	Horizontal steel reinforcement ratio;
ρ_v	=	Vertical steel reinforcement ratio in the wall;
ρ_{vw}	=	Vertical steel reinforcement ratio in the web;
$\rho_{v\text{-}BE}$	=	Vertical steel reinforcement ratio in the boundary element;
θ_{BE}	=	Chord rotation of the web about the boundary element axis;
θ_{max}	=	Maximum support rotation corresponding to damage state response limit;
θ_s	=	Chord rotation of the web about the top/bottom support axis.

2.10. REFERENCES

Abboud, B. E., Hamid, A. A., and Harris, H. G. (1990). "Small-scale Modeling of Concrete Block Masonry Structures." *ACI Structural Journal*, (87), 145–155.

Abboud, B., Hamid, A. A., and Harris, H. G., (1996). "Flexural Behavior of Reinforced Concrete Masonry Walls Under Out-of-Plane Monotonic Loads." *ACI Structural Journal*, *93*(3), 327-335.

ACI Committee 318. (2014). *Building Code Requirements for Structural Concrete (ACI 318M-14).* ACI Report, American concrete institute.

ASCE (2011). "Blast Protection of Buildings." *ASCE 59-11*, Reston, Va.

ASCE (2014). "Seismic evaluation and retrofit of existing buildings." *ASCE 41-13*, Reston, VA.

Banting, B., and El-Dakhakhni, W. (2014). "Seismic performance quantification of reinforced masonry structural walls with boundary elements." *J. Struct. Eng*., 10.1061/(ASCE)ST.1943-541X.0000895, 04014001.

Bažant, Z.P., and B.H. Oh. (1983). "Crack band theory of concrete." *Materials and Structures*, 16, 155–177.

Biggs, J. M. (1964). *Introduction to structural dynamics*. McGraw-Hill Inc.

Cerioni, R., and Donida, G. (1994). "A finite element model for the nonlinear analysis of reinforced and prestressed masonry walls." *Computers & Structures*, 53(6), 1291–1306.

CSA (Canadian Standards Association). (2012). "Design and assessment of buildings subjected to blast loads." *CSA S850-12*, Mississauga, ON, Canada.

CSA (Canadian Standards Association). (2014a). "Design of masonry structures." *CSA S304-14*, Mississauga, ON, Canada.

CSA (Canadian Standards Association). (2014b). "CSA Standards on concrete masonry units." *CSA A165 Series-14*, Mississauga, ON, Canada.

CSA (Canadian Standards Association). (2014c). "Mortar and grout for unit masonry." *CSA A179-14*, Mississauga, ON, Canada.

CSA (Canadian Standards Association). (2014d). "Carbon steel bars for concrete reinforcement." *CSA G30.18-09*, Mississauga, ON, Canada.

Drysdale, R. G., and Essawy, A. S. (1988). "Out-of-plane bending of concrete block walls". *Journal of Structural Engineering*, 114(1), 121-133.

Dusenberry, D. O. (Ed.). (2010). *Handbook for blast resistant design of buildings*. John Wiley & Sons.

Elezz, A. A., Seif Eldin, H. M., and Galal, K. (2015). “Influence of confinement reinforcement on the compression stress-strain of grouted reinforced concrete block masonry boundary elements.” *Structures*, Elsevier B.V., 2, 32–43.

ElSayed, M., El-Dakhakhni, W., and Tait, M. (2016). “Resilience Evaluation of Seismically Detailed Reinforced Concrete-Block Shear Walls for Blast-Risk Assessment.” *Journal of Performance of Constructed Facilities*, 30(4), 04015087.

Ezzeldin, M., Wiebe, L., and El-Dakhakhni, W. (2016). “Seismic Collapse Risk Assessment of Reinforced Masonry Walls with Boundary Elements Using the FEMA P695 Methodology.” *Journal of Structural Engineering*, 142(11), 4016108.

Ezzeldin, M., El-Dakhakhni, W., and Wiebe, L. (2017). “Experimental assessment of the system-level seismic performance of an asymmetrical reinforced concrete block wall building with boundary elements.” *Journal of Structural Engineering*, 143(8).

Filippou, F. C., Popov, and E. P., Bertero, V. V. (1983). "Effects of Bond Deterioration on Hysteretic Behavior of Reinforced Concrete Joints". *Report EERC 83-19*, Earthquake Engineering Research Center, University of California, Berkeley.

Hallinan, P., and Guan, H. (2007). “Layered Finite Element Analysis of One-Way and Two-Way Concrete Walls with Openings.” *Advances in Structural Engineering*, 10(1), 55–72.

Harris, H. G., and Sabnis, G. M. (1999). *Structural modeling and experimental techniques*, 2nd Ed., CRC Press, Boca Raton, FL

Hatzinikolas, M., Korany, Y. and Brzev, S. (2015). *Masonry Design for engineers and architects*, Canadian Masonry Publication, Edmonton, Alberta, Canada.

Hoiseth, K. V., and Kvande, T. (2000). "Constitutive Properties of Lightweight Concrete Masonry." *12th International Brick/Block Masonry Conference*, Madrid.

Karapitta, L., Mouzakis, H., and Carydis, P. (2011). "Explicit finite-element analysis for the in-plane cyclic behavior of unreinforced masonry structures." *Earthquake Eng. Struct. Dyn.*, 40(2), 175–193.

Lotfi, H. R., and Shing, P. B. (1991). "An appraisal of smeared crack models for masonry shear wall analysis." *Computers and Structures*, 41(3), 413–425.

Lu, X., Xie, L., Guan, H., Huang, Y., and Lu, X. (2015). "A shear wall element for nonlinear seismic analysis of super-tall buildings using OpenSees." *Finite Elements in Analysis and Design*, Elsevier, 98, 14–25.

Mander, J. B., Priestley, M. J. N., and Park, R. (1988). "Theoretical Stress-Strain Model for Confined Concrete." *Journal of Structural Engineering*, 114(8), 1804–1826.

McKenna, F., Fenves, G. L., and Scott, M. H. (2013). "Open system for earthquake engineering simulation", Version 6.50, Univ. of California, Berkeley, CA.

Moghaddam, H., and Goudarzi, N. (2010). "Transverse resistance of masonry infills." *ACI Structural Journal*, 107(4), 461–467.

Moreno-Herrera, J., Varela-Rivera, J., and Fernandez-Baqueiro, L. (2016). "Out-of-Plane Design Procedure for Confined Masonry Walls." *Journal of Structural Engineering*, 142(2), 04015126.

Park, R., and Gamble, W. L. (2000). *Reinforced concrete slabs (2nd edition)*, John Wiley & Sons.

Paulay, T., and Priestley, M. (1992). *Seismic design of reinforced concrete and masonry buildings*, Wiley, New York.

Rots, J. G., Nauta, P., Kusters, G. M. A., and Blaauwendraad, J. (1985). "Smeared Crack Approach and Fracture Localization in Concrete." *Heron*, 30(1).

Rots. J. G.(1997). *Structural Masonry: An Experimental/ Numerical Basis for Practical Design Rules (CUR Report 171)*.

Shedid, M., Drysdale, R., and El-Dakhakhni, W. (2008). "Behavior of fully grouted reinforced concrete masonry shear walls failing in flexure: Experimental results." *J. Struct. Eng.*, 10.1061/(ASCE)0733-9445(2008) 134:11(1754), 1754–1767.

Shedid, M. T., El-Dakhakhni, W. W., and Drysdale, R. G. (2010a). "Alternative strategies to enhance the seismic performance of reinforced concrete-block shear wall systems." *J. Struct. Eng.*, 10.1061/(ASCE)ST.1943-541X.0000164, 676–689.

Shedid, M. T., El-Dakhakhni, W. W., and Drysdale, R. G. (2010b). "Characteristics of confined and unconfined masonry prisms for seismic performance enhancement of structural walls." *Masonry International*, *23*(2), 69-78.

Simonds, K. (2014). "Performance of reinforced concrete block structural walls

with boundary elements under multiple design basis blast threat levels". M.Eng. project, McMaster University, Hamilton, ON, Canada.

Smith, N. L., Tait, M. J., Asce, M., El-Dakhakhni, W. W., Asce, F., and Mekky, W. F. (2016). "Response Analysis of Reinforced Concrete Block Infill Panels under Blast." *Journal of Performance of Constructed Facilities*, 30(6), 1–12.

The Masonry Society (TMS). (2016). "Building code requirements and specifications for masonry structures." *TMS 402-16/ACI 530-16/ASCE 5-16*, Detroit.

Tomaževič, M. (1998). *Earthquake-resistant design of masonry buildings*, Imperial College Press, London.

Tu, Y.-H., Chuang, T.-H., Liu, P.-M., and Yang, Y.-S. (2010). "Out-of-plane shaking table tests on unreinforced masonry panels in RC frames." *Engineering Structures*, Elsevier, 32(12), 3925–3935.

Varela-Rivera, J. L., Navarrete-Macias, D., Fernandez-Baqueiro, L. E., and Moreno, E. I. (2011). "Out-of-plane behaviour of confined masonry walls". *Engineering Structures*, *33*(5), 1734-1741.

Varela-Rivera, J., Moreno-Herrera, J., Lopez-Gutierrez, I., and Fernandez-Baqueiro, L. (2012). "Out-of-plane strength of confined masonry walls". *Journal of Structural Engineering*, *138*(11), 1331-1341.

Zhang, X. (David), Singh, S., Bull, D. K., and Cooke, N. (2001). "Out-of-Plane Performance of Reinforced Masonry Walls with Openings." *Journal of Structural Engineering*, 127(1), 51–57.

Table 2.1: Test matrix

Specimen	Wall Dimensions (Length x Height)	Vertical Reinforcement					Horizontal Reinforcement	
		Web		BEs		Wall		
		Number and Size of bars	$\rho_{v.w}$(%)	Number and Size of bars	$\rho_{v.BE}$(%)	ρ_v (%)	Number of W1.7 at spacing (mm)	ρ_h (%)
W_{BE-L}	945 mm x 1000 mm	6 D4	0.32	4 D4	0.64	0.48	1 @ 130	0.14
W_{BE-M}		11 D4	0.64	4 D4	0.64	0.64	1 @ 65	0.26
W_{BE-H}		11 D7	1.20	4 D7	1.20	1.20	1 @ 65	0.26

Table 2.2: Summary of measured displacements, idealized yield values and maximum displacements and corresponding load values

Wall	Yield		Ultimate	
	R_y	Δ_y	R_u	Δ_u
	(kN)	(mm)	(kN)	(mm)
W_{BE-L}	40.3	3.2	64.7	21.0
W_{BE-M}	58.3	7.5	76.2	34.0
W_{BE-H}	64.5	6.2	86.5	26.1

Table 2.3: Characteristics of the RM walls used for the model validation.

Wall ID Number	Height (m)	Length (m)	Vertical Reinforcement ρ_v (%)	Horizontal Reinforcement ρ_h (%)	f'_m (MPa)	f_y (MPa)
W_1*	2.60	1.20	0.23	0.1	16	544
W_3*	2.60	1.20	0.44	0.1	13	462

* Based on data from Abboud et al. (1996)

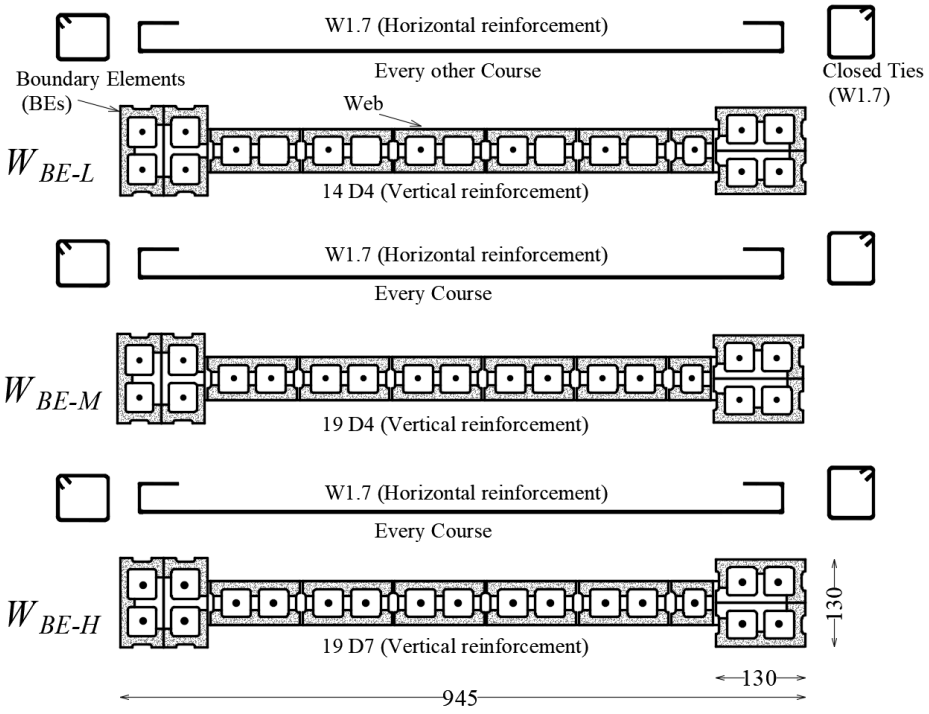

Fig 2.1. Cross-section of the tested walls (all dimensions are in mm)

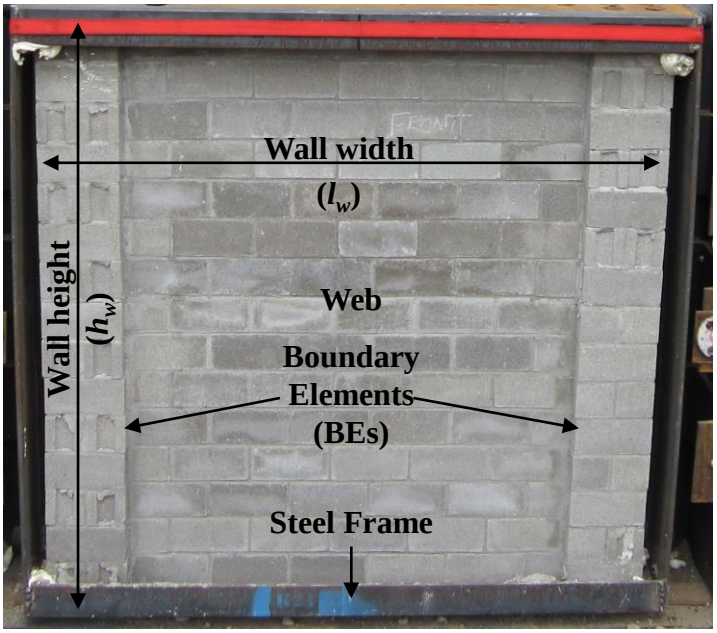

Fig 2.2. One-third scale wall specimen confined by steel frame forming the boundary condition

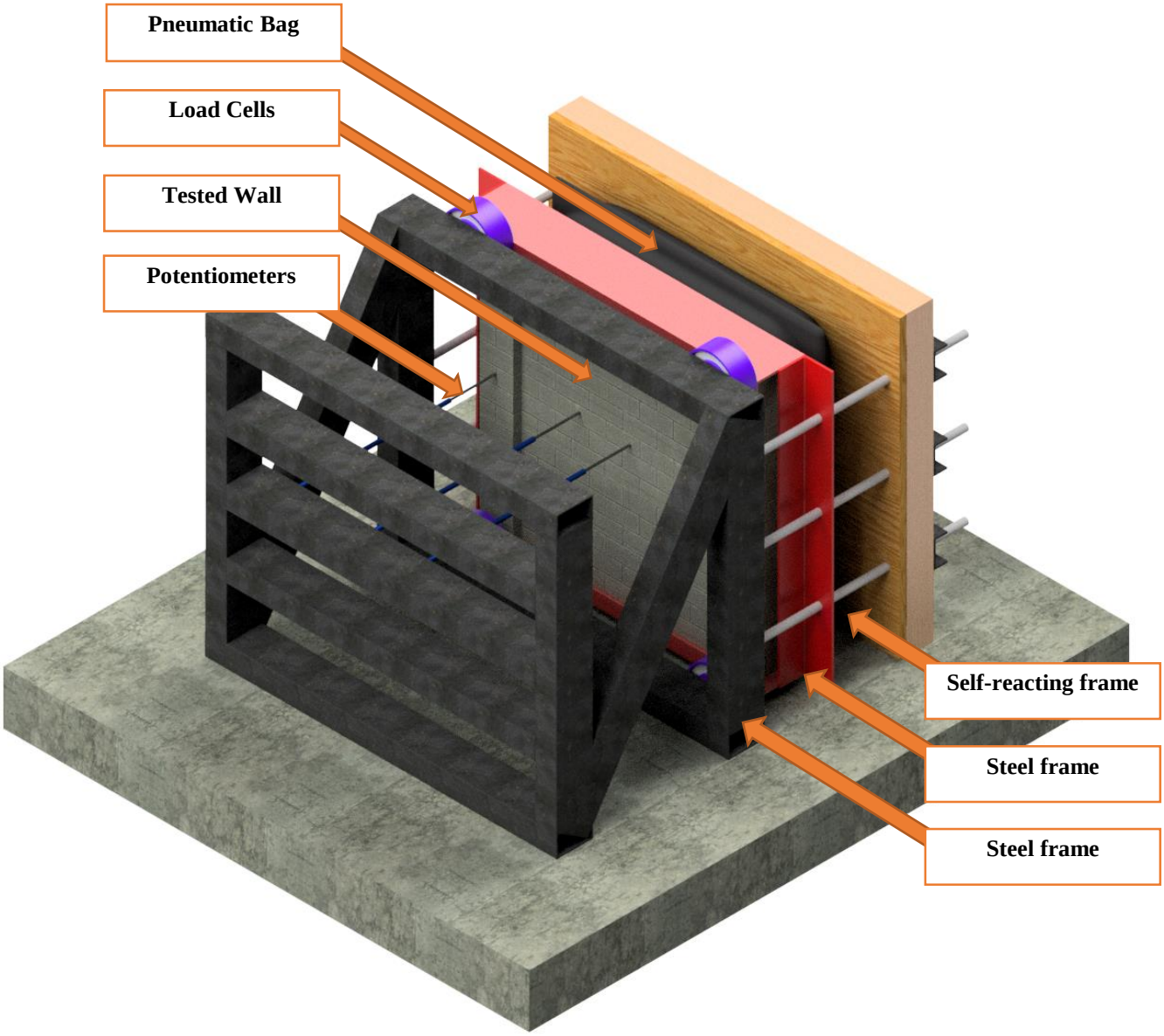

(a)

Fig 2.3. Test setup and instrumentation: (a) 3D view for the test Setup

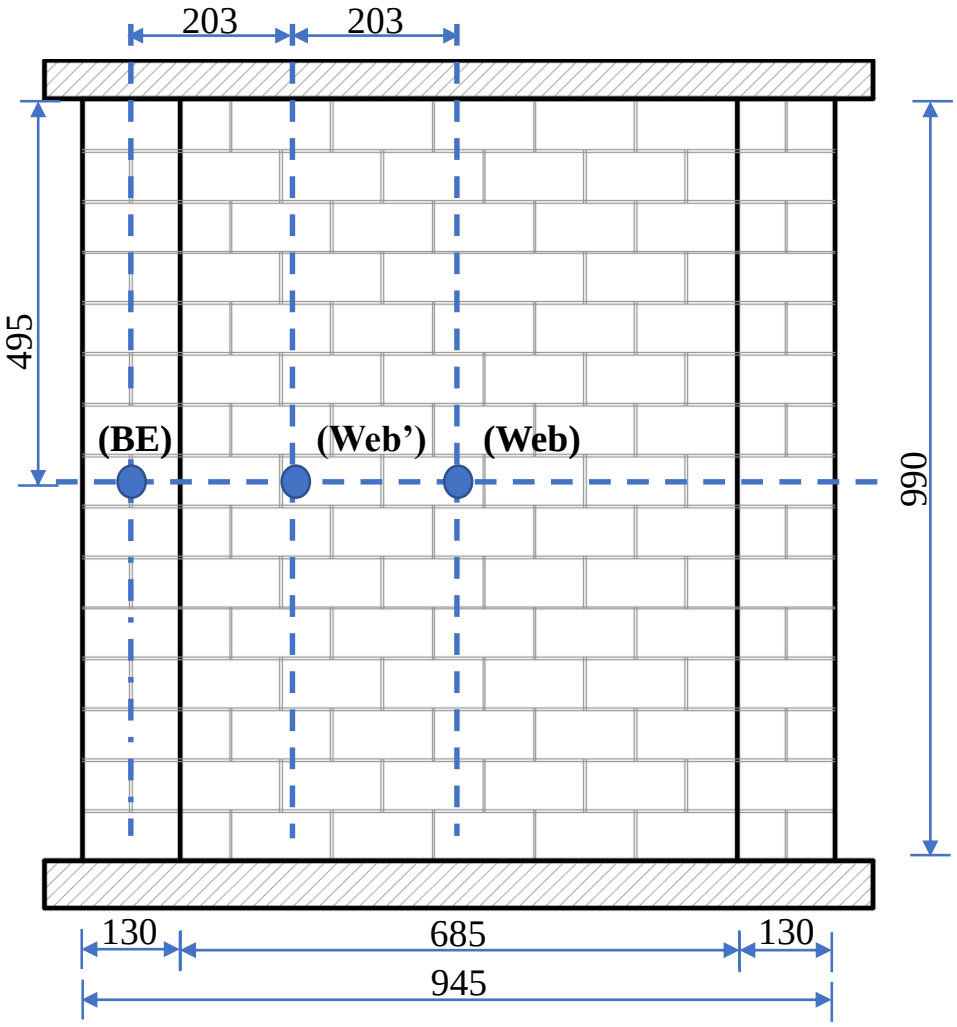

(b)

Fig 2.3(Cont). Test setup and instrumentation: (b)Wall dimension and instrumentation (Potentiometers) locations on the back face

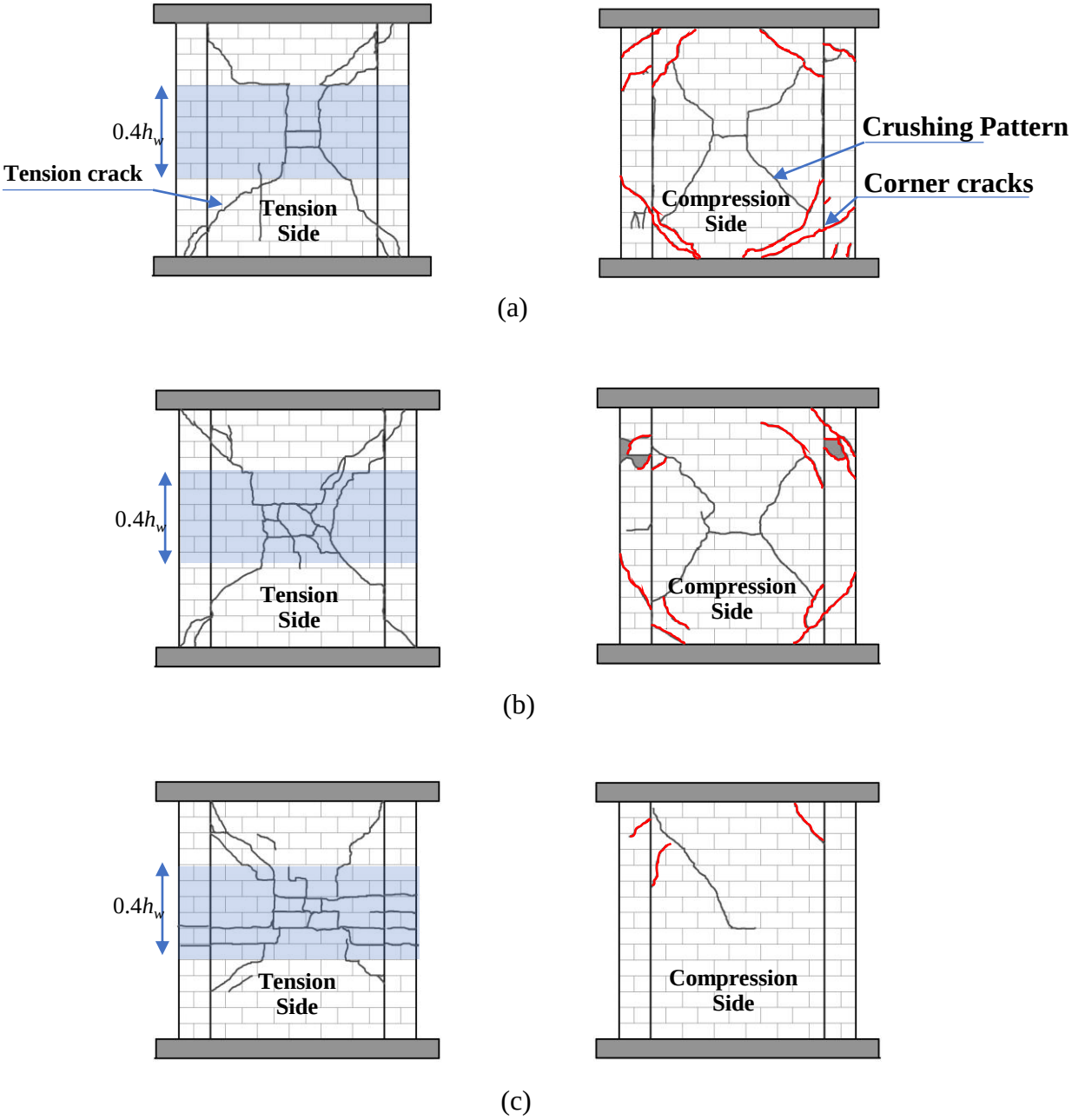

Fig 2.4. Crack pattern at ultimate resistance load:
(a) Wall $W_{BE\text{-}L}$; (b) Wall $W_{BE\text{-}M}$; (c) Wall $W_{BE\text{-}H}$

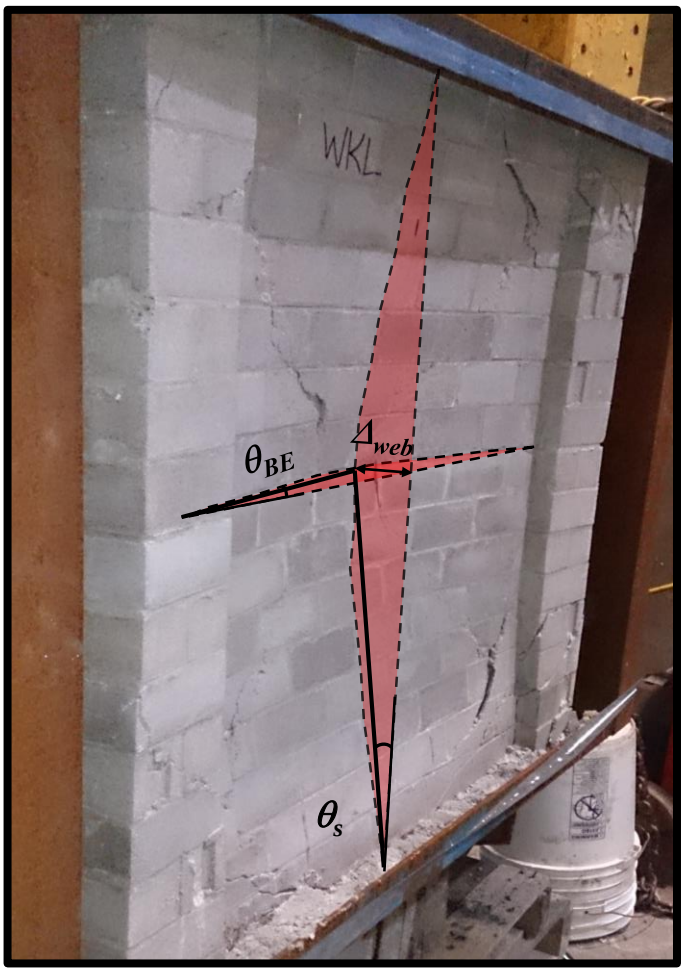

Fig 2.5. BEs wall two-way bending deformed shape

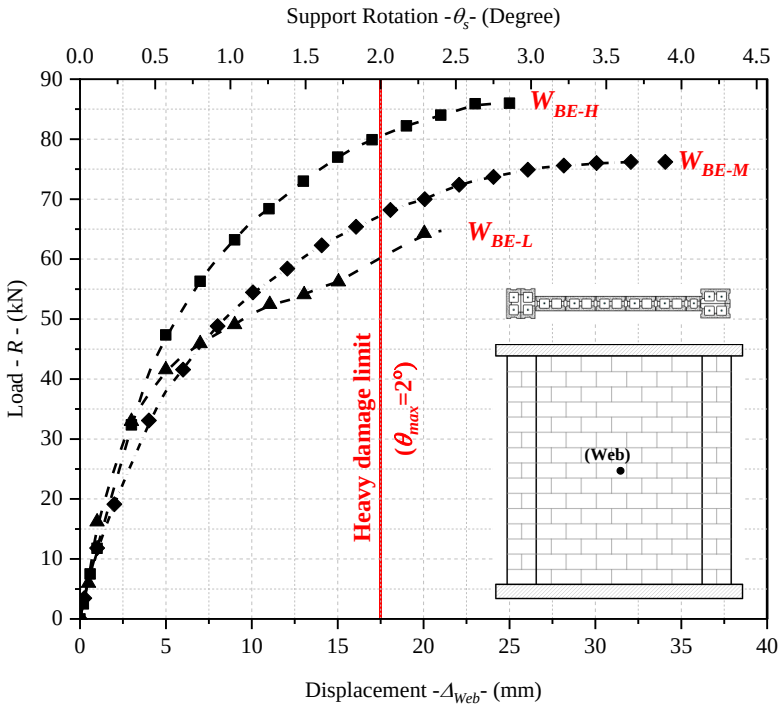

(a)

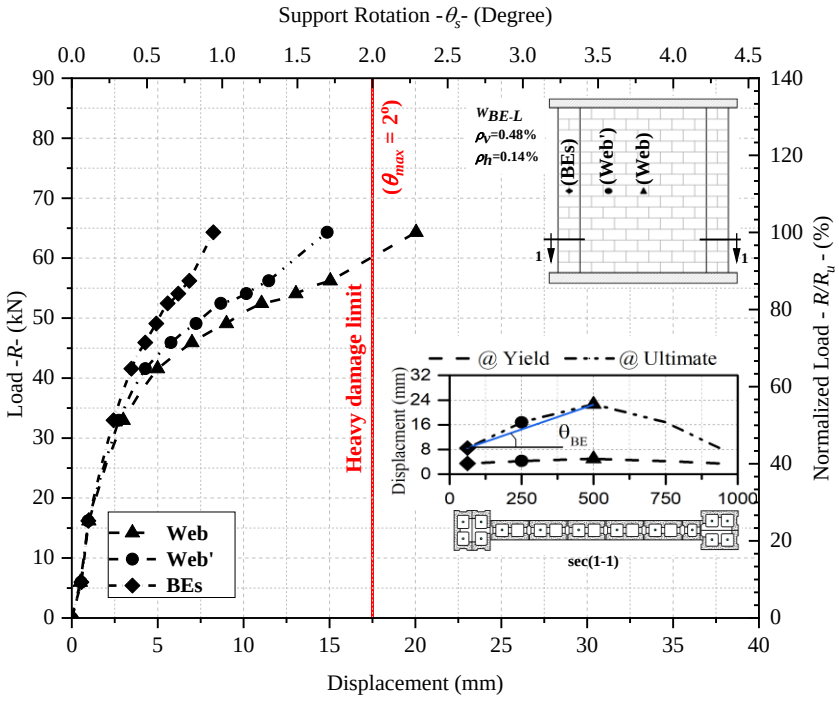

(b)

Fig 2.6. Load-displacement relationship; (a) All walls at Web; (b) Wall W_{BE-L}

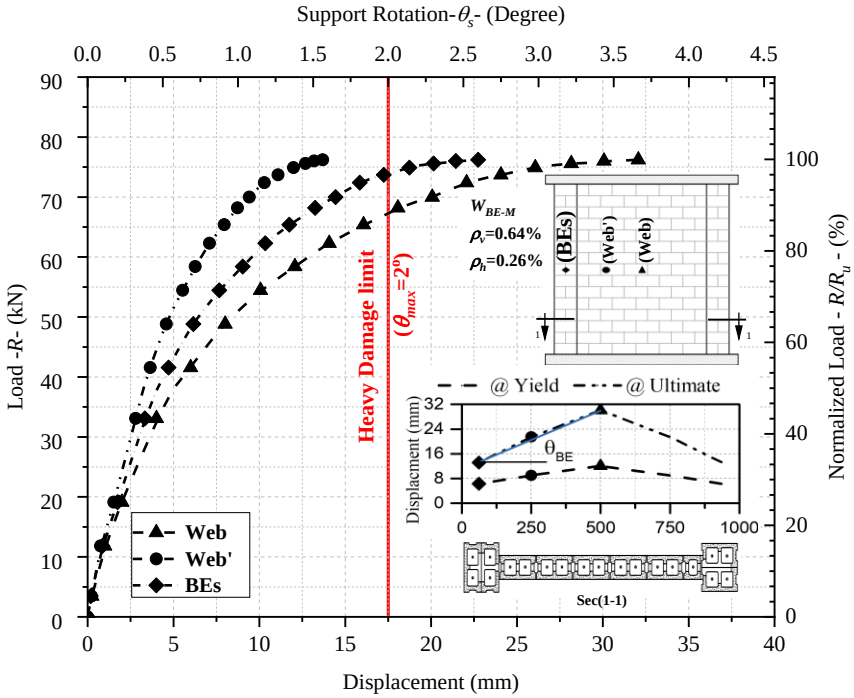

(c)

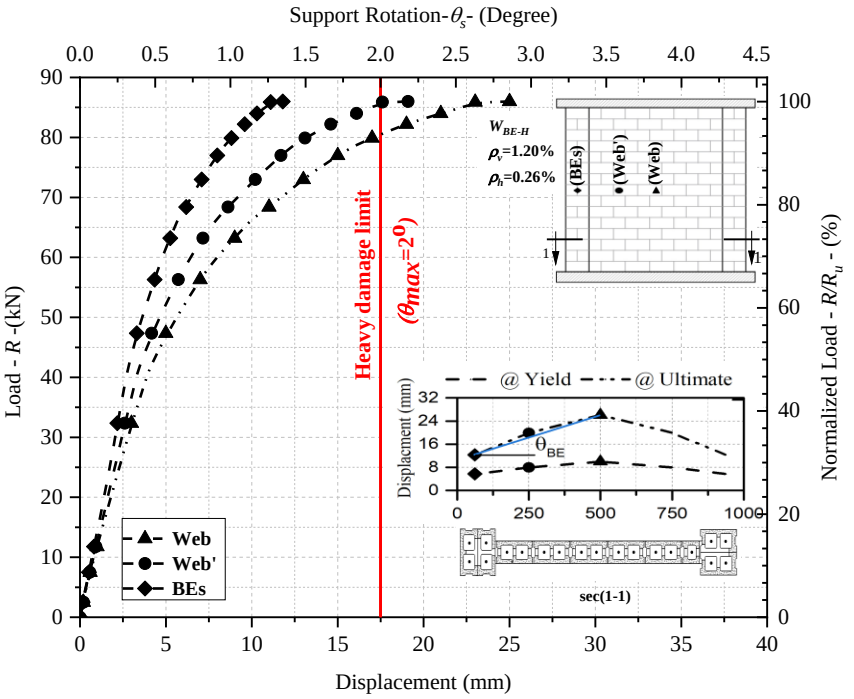

(d)

Fig 2.6 (Cont). Load-displacement relationship: (c) Wall W_{BE-M}; (d) Wall W_{BE-H}

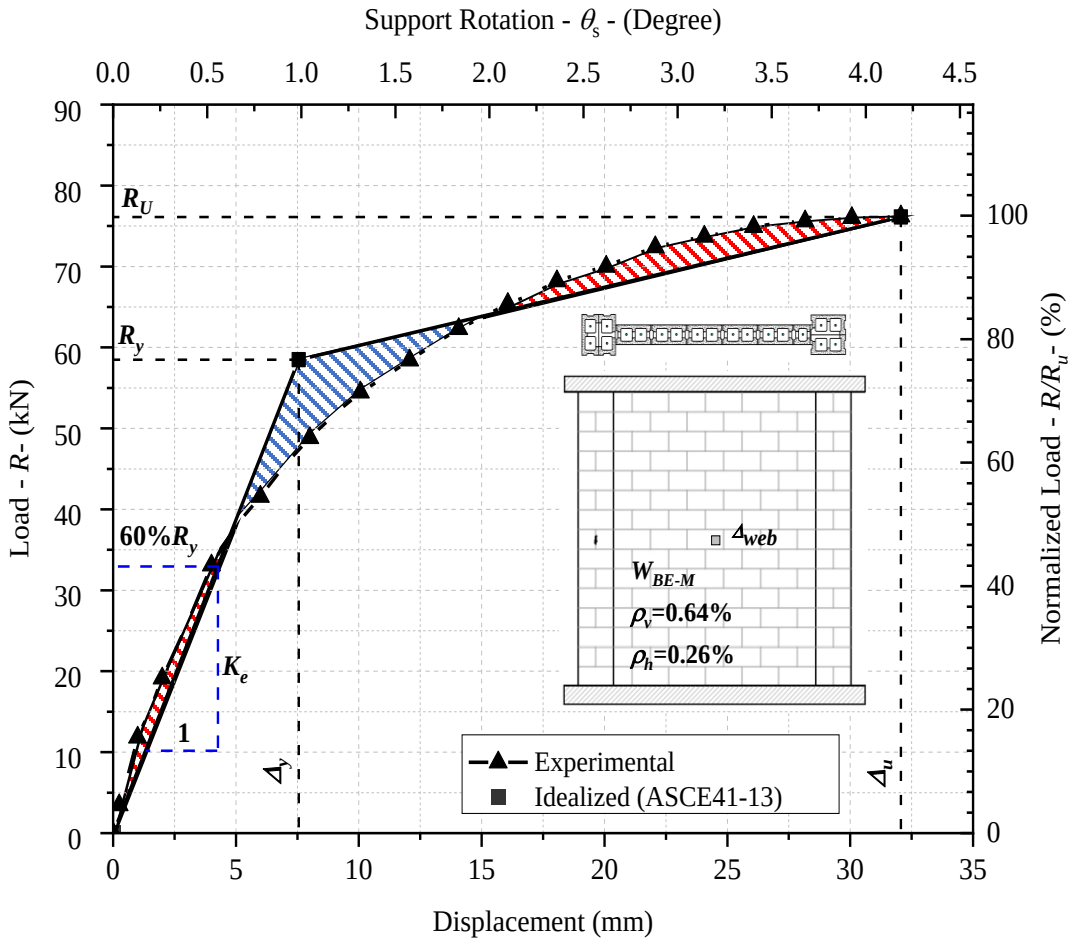

Fig 2.7. Experimental and idealized load-displacement responses according to ASCE 41-13 methodology (ASCE 2014).

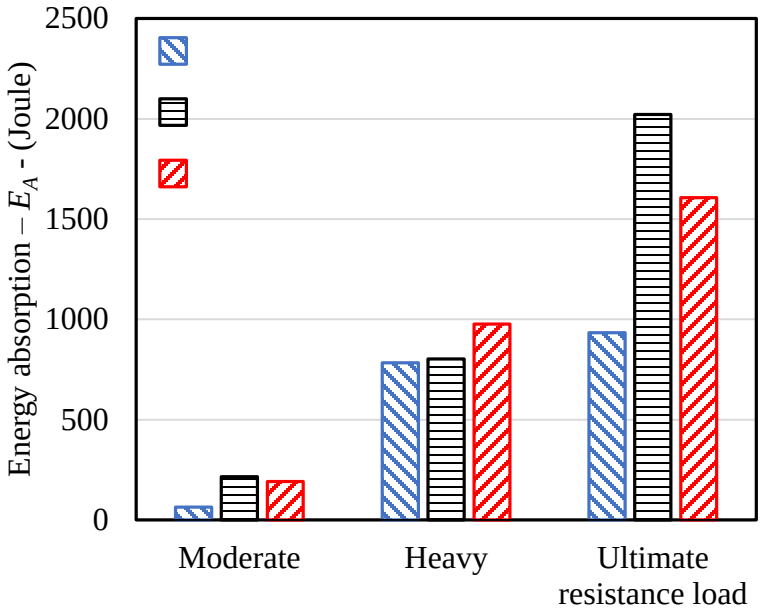

(a)

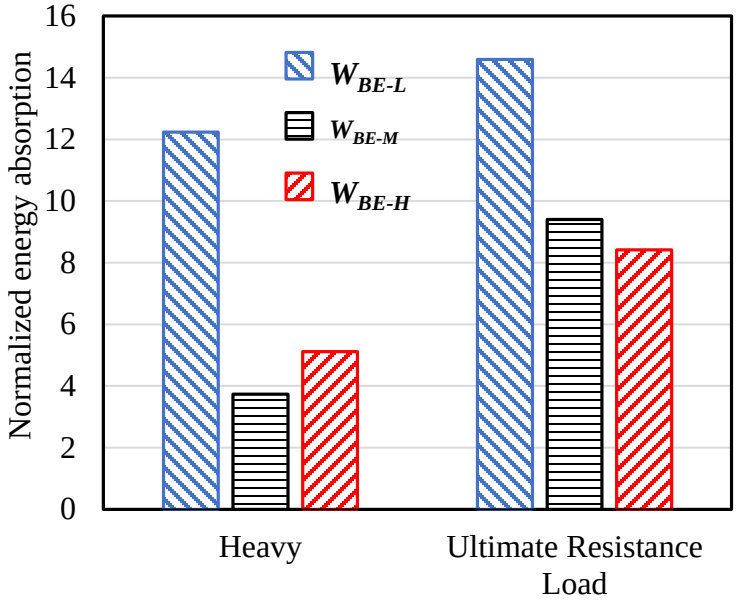

(b)

Fig 2.8. Energy absorption of walls with boundary elements at different demand levels

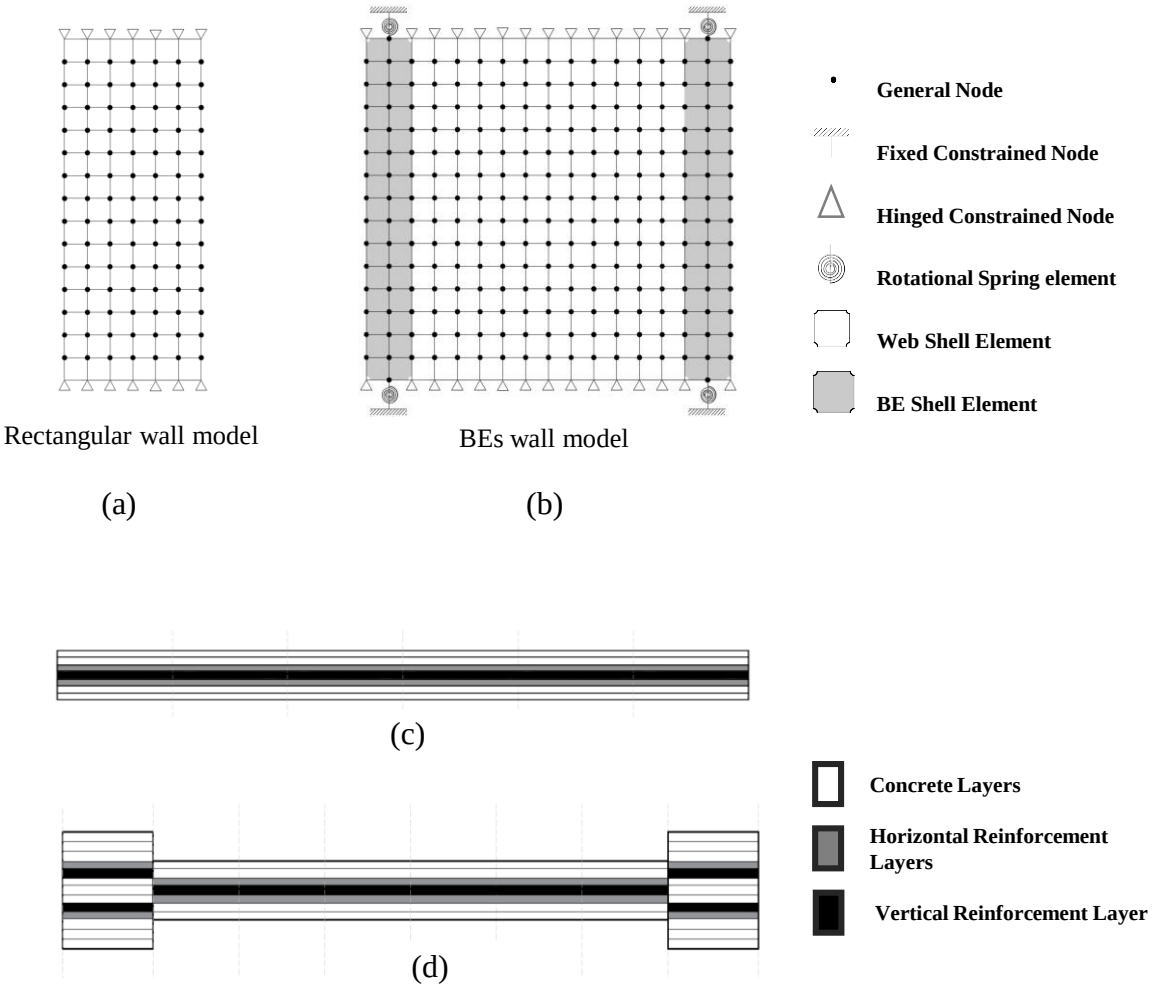

Fig 2.9. Schematic diagram for the developed model:
(a) Rectangular wall; (b) Wall with BEs;
(c) Material layers cross-section of rectangular wall and;
(d) Material layers cross-section of wall with BEs

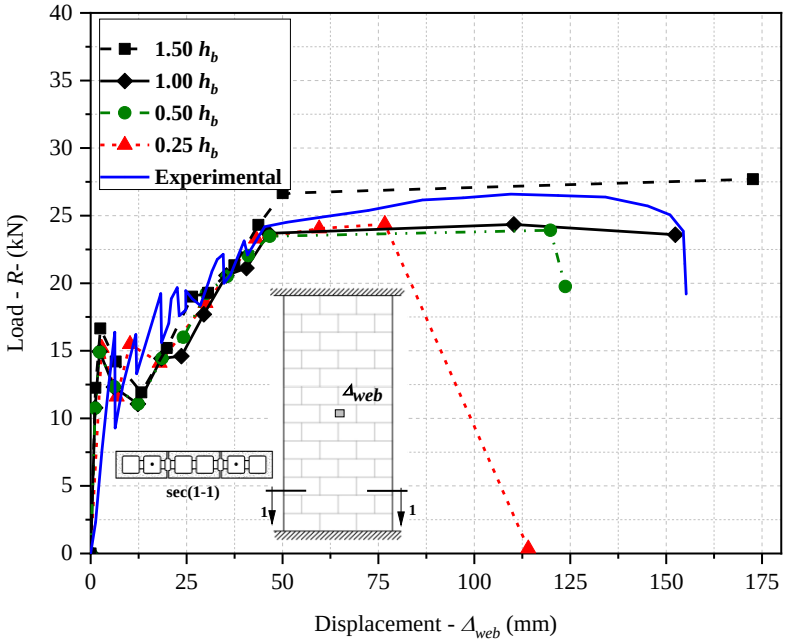

Fig 2.10. Sensitivity of the numerical model to different mesh sizes.

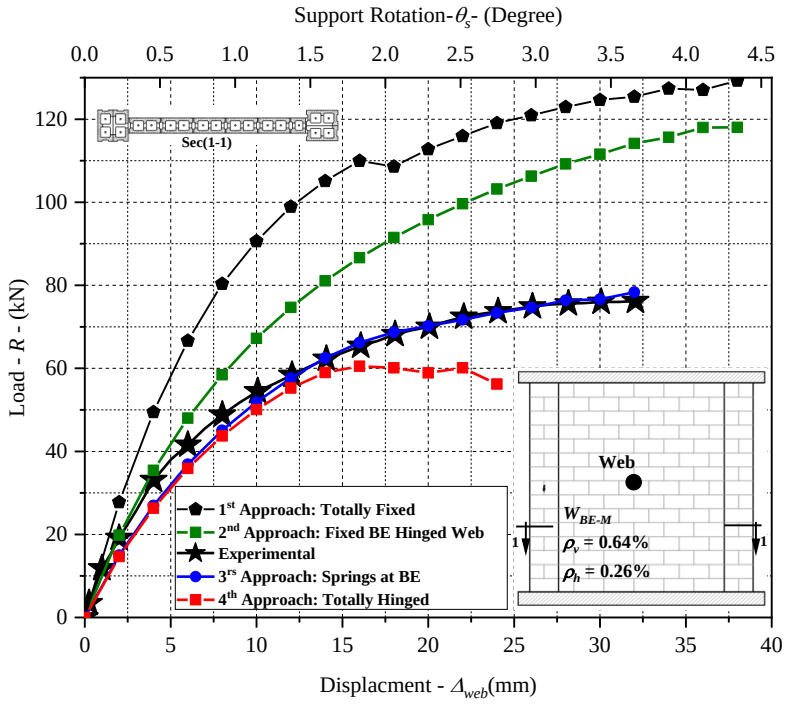

Fig 2.11. Sensitivity of the wall out-of-plane performance to different modeling approaches.

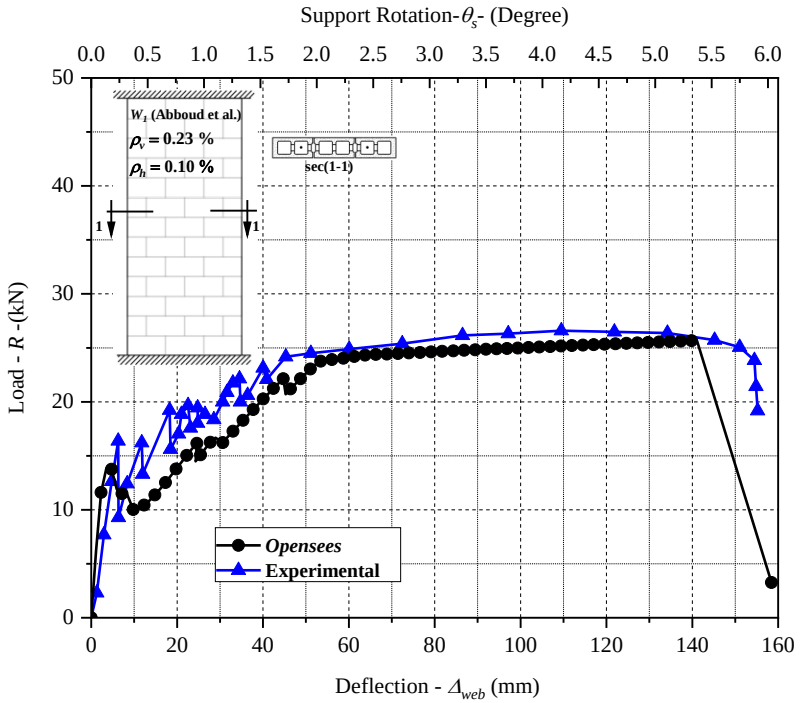

(a)

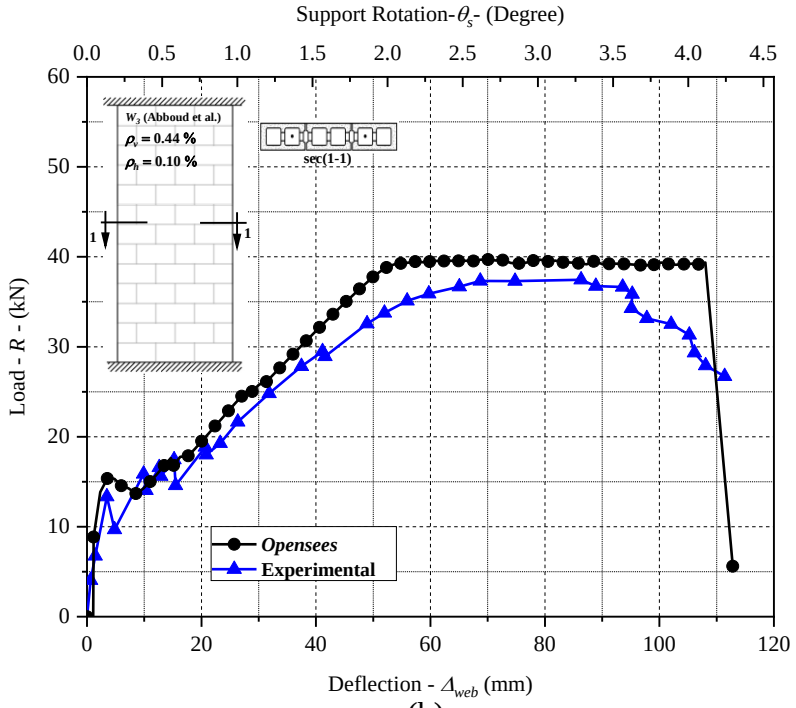

(b)

Fig 2.12. Experimental and numerical load-displacement relationship: (a) wall W_1 ; (b) wall W_3 (data from Abboud et al.1996)

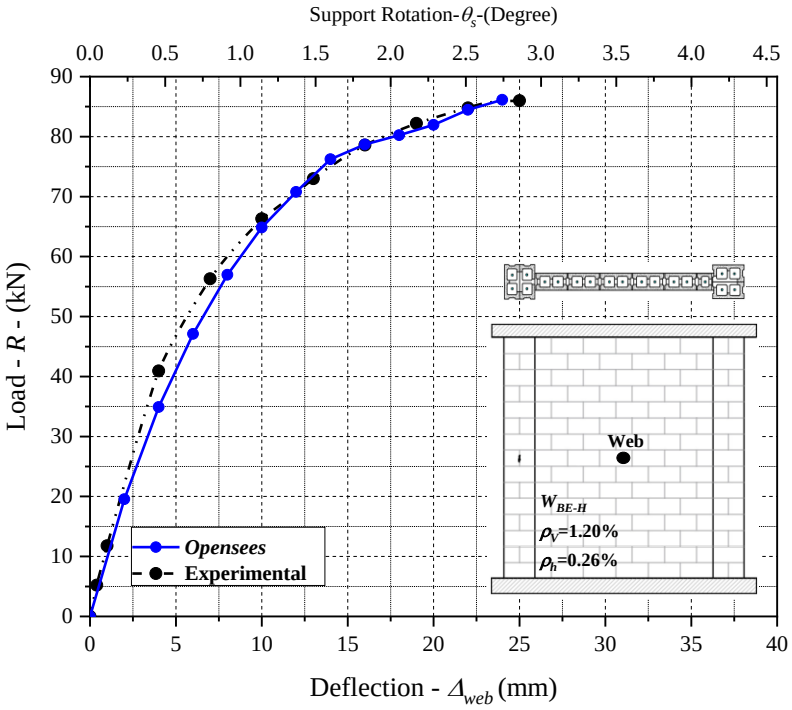

(c)

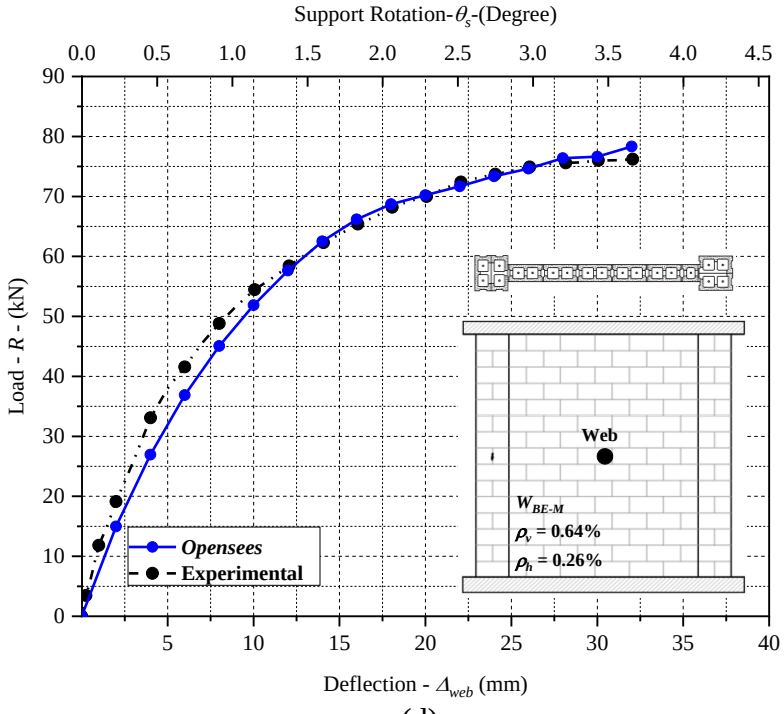

(d)

Fig 2.12 (Cont). Experimental and numerical load-displacement relationship: (c) wall W_{BE-H}; (d) wall W_{BE-M}

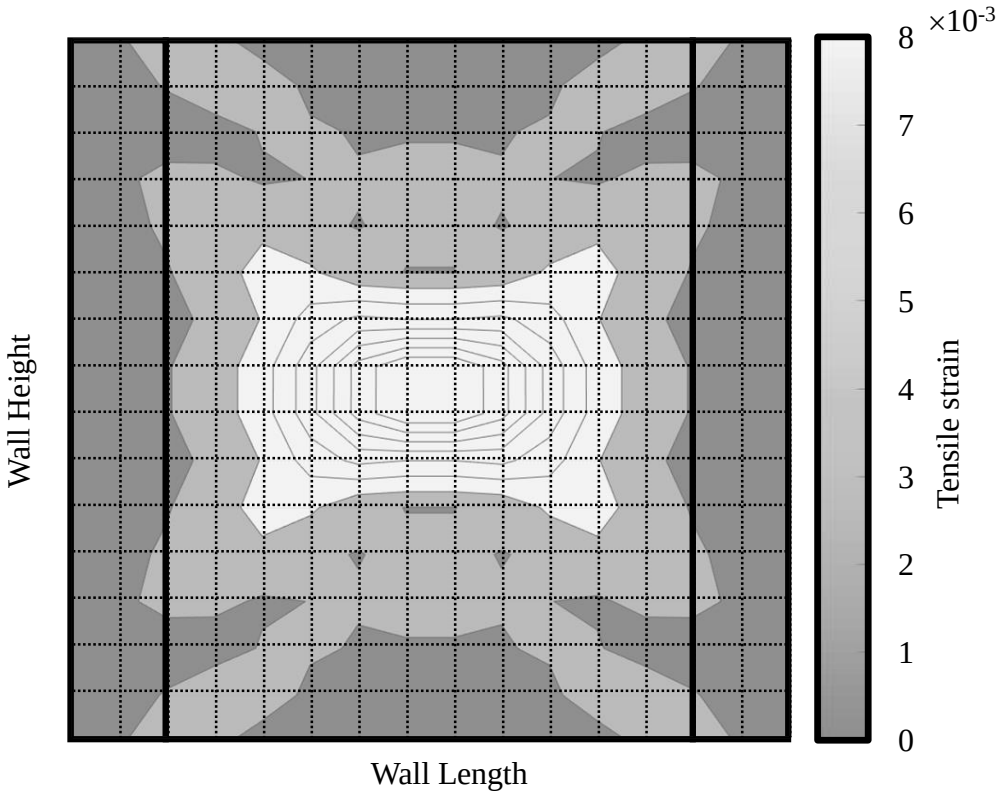

(a)

(b)

Fig 2.13. (a) Predicted tension strain distribution of Wall $W_{BE\text{-}M}$; (b) Actual damage (crack) pattern of Wall $W_{BE\text{-}M}$

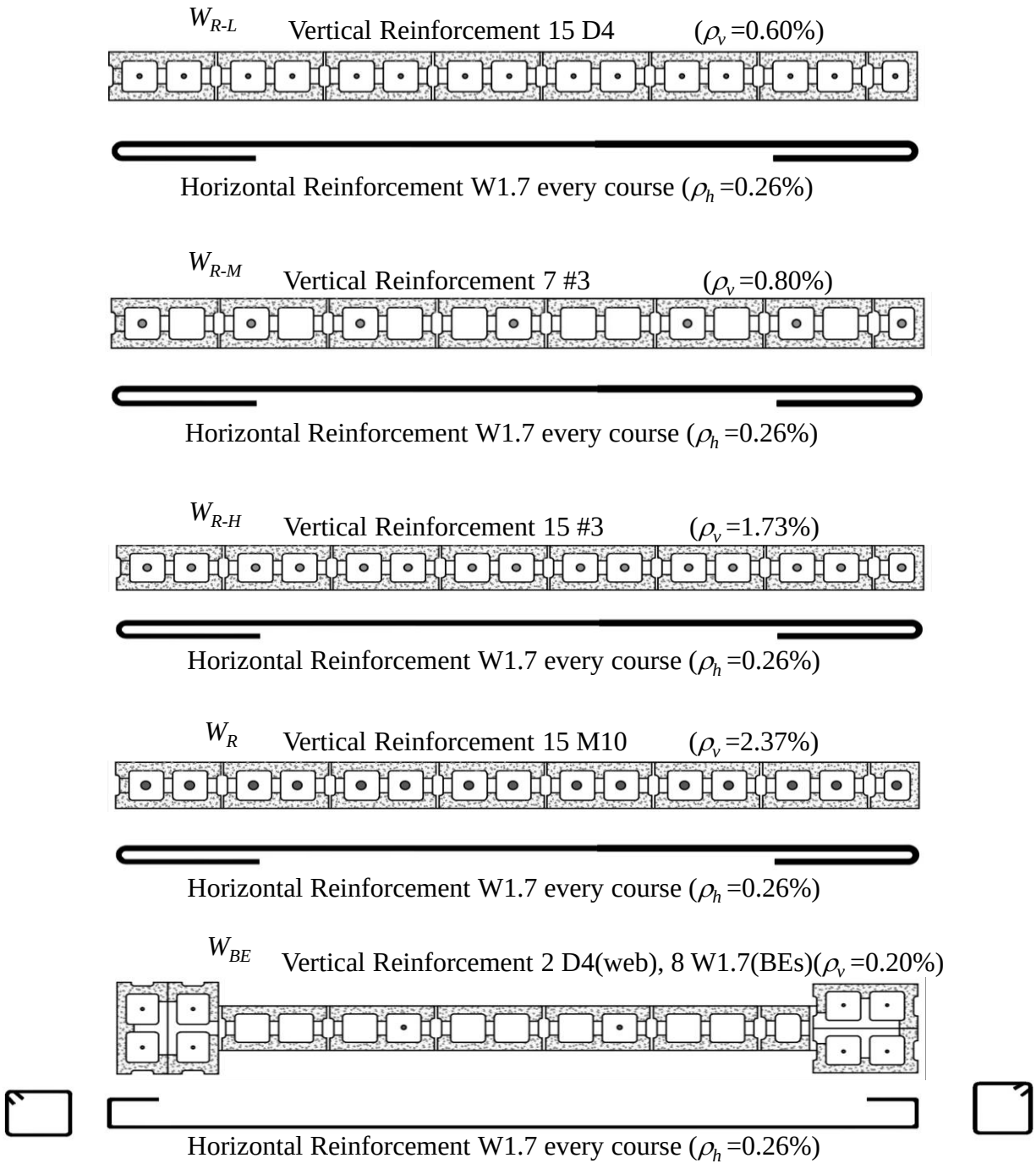

Fig 2.14. Reinforcement details of numerically generated RM shear walls

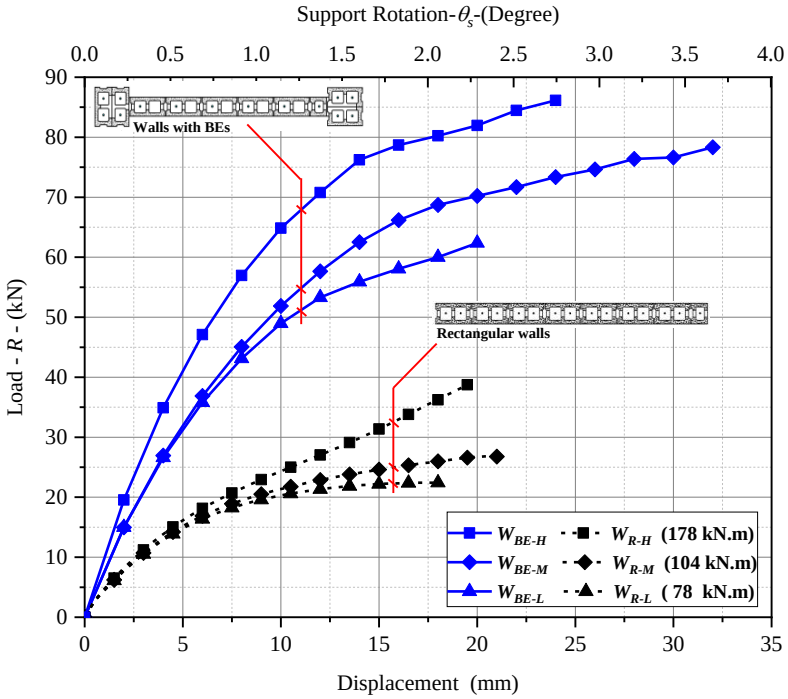

Fig 2.15. Load-displacement relationship of walls with similar in-plane capacities

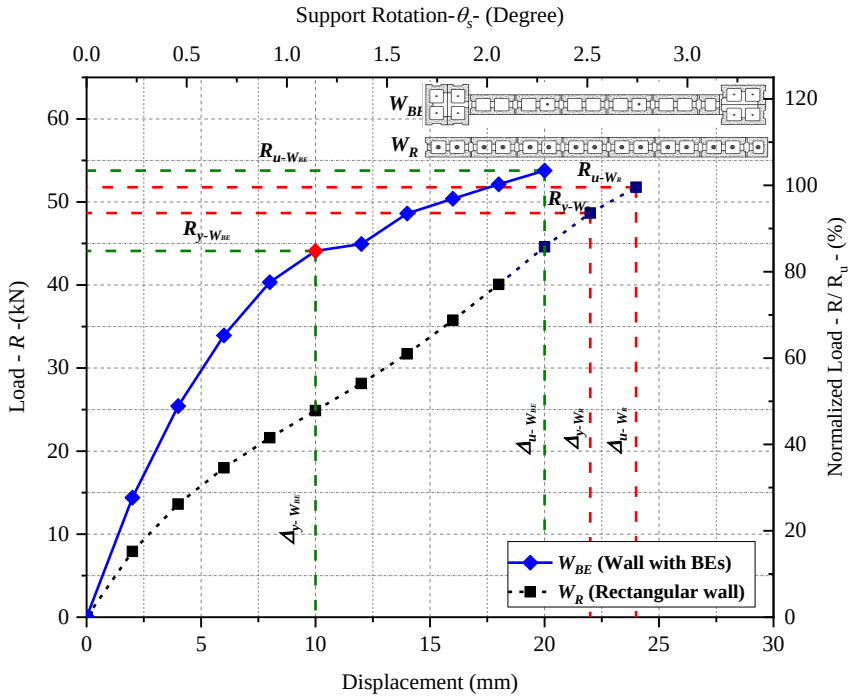

Fig 2.16. Load-displacement relationship of walls with similar out-of-plane capacity

CHAPTER 3

OUT-OF-PLANE PERFORMANCE OF SEISMICALLY-DETAILED REINFORCED CONCRETE BLOCK SHEAR WALLS WITH BOUNDARY ELEMENTS

3.1. ABSTRACT

Although boundary elements have been known to enhance the in-plane performance of reinforced masonry shear walls under seismic loading, their influence on the walls' out-of-plane performance (e.g. due to blast loading) has not been well investigated. Unlike conventional walls with rectangular cross sections, boundary elements allow the use of closed ties and multiple layers of vertical reinforcement, thus enhancing the wall's out-of-plane resistance and stiffness. Nevertheless, the corresponding wall performance and damage sequence beyond the wall peak resistance have neither been experimentally nor analytically quantified to date. As such, current blast standards (e.g. ASCE 59-11 and CSA S850-12) do not assign unique design requirements or response limits for reinforced masonry walls with boundary elements due to the limited number of relevant studies published when these standards were originally developed. To address this knowledge gap, Experimental program (*Phase II*) was carried out to investigate the out-of-plane performance of seven scaled seismically-detailed reinforced masonry walls with boundary elements under quasi-static displacement-controlled cyclic loading. In this respect, several design parameters were considered in the test matrix, which included the wall vertical reinforcement ratio and distribution, the

boundary elements alignment relative to the wall web, as well as the wall aspect ratio and axial load level. The resistance function of the walls and the corresponding damage sequence, as well as the ductility capacity were used to assess the wall out-of-plane performances. Finally, experimentally validated models, based on plastic analysis, were developed to generate the resistance functions of all walls. The experimental and analytical results in the current study demonstrated the importance of considering the two-way bending mechanism associated with reinforced masonry walls with boundary elements, when their performance is evaluated under out-of-plane loading demands.

3.2. INTRODUCTION

Although reinforced masonry (RM) shear walls are typically designed to withstand in-plane loading, they may be also subjected to out-of-plane loading that can cause substantial damage. This is because RM walls, detailed to experience a ductile in-plane behavior, do not necessarily exhibit similar behavior when subjected to out-of-plane loading (Elsayed et al. 2015a). This out-of-plane loading can result from either a hazard scenario (e.g. blast) or an out-of-plane instability due to in-plane loading (e.g. Azimikor et al. 2017; Robazza et al. 2018). As such, the out-of-plane performance of RM walls has recently attracted the interest of several researchers (e.g. Da Porto et al. 2010; Noor-E-Khuda et al. 2016; Al-Jaberi et al. 2018). For example, Noor-E-Khuda and Dhanasekar (2017 and 2018) investigated the influence of the bi-axial loading on an *unreinforced* masonry wall in-plane resistance using different boundary conditions. The results demonstrated that when

the out-of-plane pressure increases beyond a critical threshold, the in-plane resistance rapidly decreases, thus disregarding such interaction between loads may lead to unsafe design.

One alternative to enhance the out-of-plane performance of RM shear walls is to use vertical boundary elements (BEs) at the wall edges. The use of BEs has been introduced in North American design standards (i.e. TMS 2016; CSA 2014a) to enhance the in-plane seismic performance of RM shear walls. This enhancement is mainly attributed to the use of dual layer of vertical reinforcement and closed ties within the BEs that enhance both strength and displacement capacities of the wall.

When experimentally investigated in their in-plane direction by Shedid et al. (2010), RM shear walls with BEs achieved higher ductility capacities compared to conventional RM shear walls with rectangular cross sections. In addition, Banting and El-Dakhakhni (2014) showed that BEs delayed the buckling of the vertical wall reinforcement and subsequently prevented the abrupt drop in the resistance after face shell spalling. At the system-level, Ezzeldin et al. (2017) compared the performance of two buildings constructed without (Ashour et al. 2016) and with (Ezzeldin et al. 2017) BEs. Although both buildings were originally designed to have similar ultimate resistance to allow for a direct comparison, the building constructed with BEs showed higher ductility capacities and less resistance degradation at high drift levels.

In general, the out-of-plane performance investigation of RM walls with BEs in literature is scarce. Simonds (2014) conducted the first reported

experimental study to evaluate the performance of such walls when subjected to blast loading and showed that BEs provided significant support to the wall web. This was evident through load transfer by the horizontal reinforcement, which subsequently created a two-way bending mechanism in the wall web. El-Hashimy et al. (2018) reported a preliminary investigation (Experimental program (*Phase I*) in Chapter 2) of non-load bearing RM walls with BEs tested to their ultimate resistance only but not beyond that point because of the air bag loading mechanism adopted. Thier preliminary results demonstrated that higher out-of-plane stiffness and ultimate resistance were achieved by these walls compared to conventional RM walls due to the BEs configuration and special reinforcement details. However, the influence of BEs on the wall damage mechanism and displacement response beyond the ultimate resistance has not been adequately investigated to date. As such, as a new system, RM walls with BEs are currently assigned no distinct response limits in blast design standards [e.g. ASCE 59-11(ASCE 2011); CSA S850-12(CSA 2012a)].

In blast design, one alternative to enhance the performance of structural components at high displacement demands is to introduce shear reinforcement (e.g. laced reinforcement or ties) in the direction of loading (Woodson 1992). As such, according to UFC 3-340-02 (USDOD 2008), components with shear reinforcement can attain a support rotation up to 6˚ prior to reaching a hazardous damage state, whereas the absence of such reinforcement reduces this rotation limit to only 2˚. Shear reinforcement (e.g. ties) however, requires a dual layer of vertical

reinforcement (to form a cage) that is not practical in conventional RM walls because of limitations associated with concrete block standard sizes/configurations used in North America. As such, the ASCE 59-11 (ASCE 2011) and CSA S850-12 (CSA 2012a) state that RM walls are likely to suffer a complete disengagement of concrete block faceshells with significant spalling and/or scabbing (i.e. hazardous damage state) when the support rotation exceeds 2˚. Although this might be applicable to conventional RM walls, the confinement ties within RM walls with BEs can be considered as shear reinforcement as suggested by Woodson (1992).

The objective of the current study is to evaluate the out-of-plane performance of seismically-detailed RM shear walls with BEs and determine the influence of BEs on the wall's behavior and resistant function, in order to subsequently inform their blast design. Therefore, experimental program (*Phase II*) was carried out on seven scaled RM walls with a range of different design parameters to investigate their influence on the out-of-plane wall performance. These parameters included the web and BEs vertical reinforcement ratio and distribution, BEs alignment relative to the wall web, as well as the axial load level and the wall aspect ratio. In this respect, a description of the experimental program is first presented that includes the material used in construction, test setup and instrumentations used to monitor the wall response. Subsequently, the influence of each design parameter is assessed through the wall load-displacement relationship, damage sequence, and ductility. The BEs interaction with the web is also evaluated based on the BEs and web deformations coupled with the observed damage. Finally,

the test wall responses were replicated using two plastic analysis modeling approaches to facilitate wall resistance function generation for RM wall blast design.

3.3. EXPERIMENTAL PROGRAM (*PHASE II*)

The experimental program was designed to evaluate the out-of-plane performance of seven scaled RM walls with BEs. All walls were subjected to a displacement-controlled quasi-static out-of-plane cyclic loading until they reached a 20% resistance degradation (80% of the maximum resistance on the descending branch of the load-displacement relationship) to capture the wall post-peak resistance behavior. The following subsections provide details on the wall test matrix, material properties and construction, as well as the test setup and instrumentation used to monitor the wall performances.

3.3.1. Test Matrix

Since RM walls with BEs are typically investigated in the context of seismic force resisting systems, the seven fully grouted walls in the current study were originally detailed in accordance with the *special* RM shear walls seismic detailing requirements in their in-plane direction following the TMS 402-16 (TMS 2016). This was mainly to provide enough in-plane inelastic deformation and rotational capacities to withstand seismic loading demands. In addition, the ASCE 59-11 (ASCE 2011) recommends that RM walls should not experience a brittle flexural behavior when subjected to blast loading. This was verified in the current study by performing a preliminary out-of-plane sectional analysis, which indicated that the

steel reinforcement would yield before the masonry reach their crushing strain (e.g. in *Wall 1*, BEs reinforcement bars would yield at a flexural moment of 23 kN.m, whereas the ultimate compression strain develops at approximately 30 kN.m).

The seven half-scaled walls were constructed and tested as listed in Table 3.1 and Fig. 3.1. The control wall (*Wall 1*) had a vertical and horizontal reinforcement ratio (ρ_v and ρ_h) of 0.47% and 0.16%, respectively. The influence of increasing the vertical reinforcement in the BEs and the wall web was considered in *Walls 2* and *3*, respectively. More specifically, in *Wall 2*, the vertical reinforcement ratio of the BEs ($\rho_{v\text{-}BE}$) was 1.10% (i.e. 0.79% in *Wall 1*), whereas the vertical reinforcement ratio of the wall web ($\rho_{v\text{-}w}$) in *Wall 3* (i.e. 0.46%) was double that of *Wall 1* (0.23%). This resulted in two wall cross-sections (i.e. *Walls 2* and *3*) with ρ_v values higher (by 30%) than that of *Wall 1*, as can be seen in Table 3.1.

Several previous studies (e.g. Shedid et al. 2008; Banting and El-Dakhakhni 2012; and Seif ElDin and Galal 2017) showed the negative influence of the wall axial load on the in-plane wall ductility capacity. However, to the best of the authors' knowledge, all the out-of-plane experimental investigations on RM walls with and without BEs (e.g. Abboud et al. 1996; Elsayed et al. 2015b; Browning et al. 2014; Simonds 2014; El-Hashimy et al. 2018) considered only non-load bearing walls that were not subjected to superimposed axial loads. To address this gap, all walls, except *Wall 4*, were subjected to an axial equivalent stress ratio (σ_v) of 10% of their corresponding axial compressive strengths (i.e. a superimposed axial load

of 198 kN). The influnce of the axial load on the wall out-of-plane performance was then investigated through *Wall 4* that was similar to *Wall 1* but with zero axial equivalent stress ratio, as can be seen in Table 3.1.

BEs were symmetrically aligned with their wall web axis in all previous in-plane (e.g. Shedid et al. 2010; Banting and El-Dakhakhni 2014; Ezzeldin et al. 2016) and out-of-plane (e.g. Simonds 2014 and El-Hashimy et al. 2018) studies. However, in consultation with masonry designers and contractors, BEs forming one flush surface with the wall web were thought to facilitate adoption of this system in construction practice as it is architecturally more appealing. As such, all walls in the current study followed this BEs configuration, as shown in Fig. 3.1. Subsequently, all walls were loaded on their flush surface, while *Wall 5* only, shown in Fig. 3.1(d), was loaded from the non-flush surface to facilitate a direct comparison with *Wall 3*. Finally, since the wall web has been shown to result in a two-way bending mechanism (Simonds, 2014 and El-Hashimy et al. 2018), the aspect ratio (i.e. wall height to length ratio) was expected to be key parameter in terms of the out-of-plane load distribution. To evaluate this attribute, all walls had an aspect ratio (A_R) of 1.0 except for *Walls 6* and *7* that had A_R of 1.20 and 0.73, respectively.

3.3.2. Material Properties

The standard hollow concrete blocks (190 mm thickness × 190 mm height × 390 mm length) commonly used in North America were scaled down by half (95 mm thickness × 95 mm height × 185 mm length) and used for the wall construction as

well as 5 mm (half-scaled) mortar joints. The use of scaled models of reinforced masonry walls was reported in several studies (Abboud et al. 1990, Tomaževič and Velechovsky, 1992), Shedid et al. 2010, Elsayed et al. 2015a and Smith et al. 2016). In addition, the use of scaled blocks and reinforcement bars has been well documented in the text by Harris and Sabnis (1999). The blocks were subjected to compression tests according to CSA A165-14 (CSA 2014b) to determine their strengths. The blocks had an average compressive strength of 18.6 MPa (coefficient of variation (C.O.V.) = 14.0%) based on the net area of the block. The grout used in the walls had an average compressive strength of 21.3 MPa (C.O.V. = 15.0%), according to CSA A179-14 (CSA 2014c). A total of 69 masonry prisms were assembled and grouted during the wall construction to evaluate their average compressive strength (f'_{av}) according to CSA (2014a). These prisms were one block in cross-section and four blocks high (90 mm thickness × 375 mm height × 185 mm length). The prisms had a f'_{av} of 11.2 MPa (C.O.V = 13.4%).

The reinforcement bars used in the walls were tested through direct tension tests to determine their yield (f_y) and ultimate (f_{ult}) strengths, according to CSA G30-14 (CSA 2014d). The average f_y was 459 MPa (C.O.V = 4.6%) and 436 MPa (C.O.V. = 1.3%) for bars #3 (area = 73.3 mm^2) and M10 (area = 100 mm^2), respectively. Similarly, the average f_{ult} recorded was 664 MPa (C.O.V. = 3.4%) and 605 MPa (C.O.V. = 1.0%) for the same bars. The D4 bars (area = 25.4 mm^2) were used as horizontal reinforcement in the wall web and as square ties in the BEs.

These bars had average f_y and f_{ult} of 517 MPa (C.O.V. = 6.9%) and 573 MPa (C.O.V. = 5.7%), respectively.

3.3.3. Wall Construction

All walls were constructed on concrete foundations, as shown in Fig. 3.2(a) and vertical bars were extended in each foundation to ensure adequate development length. The ties in the BEs were installed every 65 mm spacing to provide the required confinement according to the CSA S304-14 (CSA 2014a) specifications, as shown in Figs. 2(a and b). An experienced mason laid the courses with face-shell mortar bed joint of approximately 5 mm thickness. The web was built in a running bond pattern using scaled stretcher and half block units following common North American practice, while BEs were built in a stack pattern to facilitate the construction procedure using scaled C-blocks, as shown in Fig. 3.2(b). These blocks were notched to accommodate the wall's horizontal reinforcement in the BEs that was placed either every course or every other course based on the design of the corresponding wall, as presented in Fig. 3.1. The detailing of the horizontal reinforcement followed the requirements of CSA S304 (CSA 2014a) for walls with boundary elements, where a single bar was hooked around the outermost vertical bar, as shown in Fig. 3.1. One of the bar ends had a 90° hook with more than six-bar diameter extension (i.e. taken as 220 mm), while the other end had a 180° hook with extension more than 100 mm (i.e. taken as 200 mm). The continuity of the wall's vertical reinforcement was facilitated by laying six additional courses above

the top wall support (slab/diaphragm) level to ensure an adequate development length, as shown in Fig. 3.2(c).

At the top wall support, two channels were installed from each side using steel bolts. Although this connection restrained the wall lateral displacement at its top support, it was also detailed to not prevent the wall vertical displacements and its out-of-plane rotations. This was to simulate actual construction conditions, where the slab may provide only out-of-plane horizontal displacement restraint at their level, but does not prevent wall rotation due to typical masonry wall reinforcement detailing (Tanner and Klingner, 2017) and its non-monolithic connection with concrete floor slabs. Conversely, as mentioned earlier, the wall's vertical reinforced bars were extended into the foundation, which was rigid enough to prevent displacements at the bottom support and limit the rotation (i.e. fixed support), as will be discussed later.

3.3.4. Test Setup

The test setup used can be divided into three main systems, as shown in Fig. 3.3(a). The first system was a self-reacting frame that supported the horizontal and vertical loading systems and the test wall. The horizontal actuators, which provided the out-of-plane loading, comprised the second system. The third system included a vertical actuator loading system to apply the required axial load on the wall. The wall foundation was anchored and prestressed to the self-reacting frame, and the top support channels were attached to two stiff horizontal beams that restrained the wall displacements in the out-of-plane direction but allowed for vertical displacements

as shown in Fig. 3.3(b). These beams were subjected to downward force from each side by two vertical actuators with a capacity of 110 kN each, which exerted the axial load on the wall. This latter force-controlled vertical loading system maintained the same axial load from each side throughout the test to prevent in-plane bending.

Although out-of-plane loads are usually applied experimentally using airbags (Ghobarah and El Mandooh Galal 2004; Smith et al. 2016; Winkel and Smith 2010), the proposed test setup was designed to overcome the drawbacks including those pertaining to airbag sudden energy release, air pressure relaxations, and the alignment of the airbag systems, typically used for testing such components (Dizhur et al. 2010; Hamoush et al. 2001). Therefore, for the horizontal loading system, the out-of-plane loads were applied through a displacement-controlled hydraulic actuator (with a capacity of 800 kN and a maximum cyclic stroke of 500 mm) that was positioned at the center of the wall, as shown in Fig. 3.3(b). The actuator load was distributed on the wall through nine identical secondary hydraulic actuators that experienced the same hydraulic pressure and were mounted on a rigid frame connected to the main actuator, as can be seen in Fig. 3.3(b). This approach was to maintain the same load on all secondary actuators throughout the test while allowing their displacements to follow the wall's deformed shape. This was an essential criterion during the design stage of the test setup because, unlike their conventional (i.e. with rectangular cross-sections) walls counterparts, RM walls with BEs were expected to experience a two-way bending mechanism in their webs

resulting in different horizontal displacements at the same height. The secondary actuators applied the loads on the wall through nine thick rubber pads (300m×300mm×60mm), as shown in Fig. 3.4(a), to avoid any stress concentration or wall punching shear failure while also not restraining the wall deformations.

In order to monitor the load distribution through the nine secondary actuators during the test, three load cells (LC1 to LC3) were centered on three rubber pads, as shown in Fig. 3.4(a). The maximum deviation between the three load cells was monitored for each wall at different displacement demands. The maximum deviation between the load cells is 5% which demonstrates the ability of the secondary actuators system to distribute the applied load on the wall surface.

3.3.5. Instrumentation and Test Procedure

The out-of-plane wall displacements at the web and BEs were monitored by nine displacement potentiometers (D1 to D9), as shown in Fig. 3.4(b). In addition, nine strain gauges (S1 to S9) were mounted on the bars prior to wall construction. The locations of these strain gauges, as shown in Fig. 3.4(c), were selected to monitor the initial yielding of the reinforcement as well as the extent of this yielding throughout the web and BEs reinforcement.

The test walls were subjected to varying out-of-plane displacement-controlled cyclic loading, while the axial load was maintained constant throughout the test. The cyclic loading was carried out to evaluate the wall rebound (unloading) response at different chord rotation demands that can be subsequently used to validate nonlinear numerical blast models in future studies. It is acknowledged that

strength degradation may have affected the load displacement relation, however the results are still considered conservative compared to single pulse loading. In each cycle, the target displacement at the wall center was increased in increments corresponding to the wall support rotation (i.e. defined as the angle enclosed between the vertical centerline of the wall and the chord from the support to the center of web). Support rotation was used in the current study, in alignment with the current blast design standards (ASCE (2011) and CSA (2012a)) approaches, to quantify the damage state of RM walls. To select the displacement increment values, the theoretical yield displacement of the walls was preliminary estimated (i.e. based on UFC 3-340-02) to be 4.5 mm corresponding to a chord support rotation of 3/8°. Thus, the rotation increment was selected to be 1/8° degree equivalent to a displacement at the wall center of 1.65 mm. Thus, the cycles displacement amplitudes ranged from 1.65 mm to 108.9 mm. This loading procedure continued until the test walls resistance degraded to 80% of peak resistance, which was considered a failure criterion in the current experimental program.

3.4. TEST RESULTS

The test walls experienced several response stages until failure. First, the elastic resistance (R_e) point was considered in the current study to represent the onset of reinforcement bar yielding based on the strain gauge measurements, which indicated the formation of the first yield line. Afterwards, the distribution of moments changed throughout the wall, which resulted in the formation of additional

yield lines. Subsequently, the wall behaved in an essentially plastic manner until reaching its ultimate resistance (R_{ult}) (USDOD, 2008). Beyond R_{ult}, the wall attained a slightly higher peak resistance (R_{Peak}), that was approximately 5% more than R_{ult} due to the strain hardening of the steel reinforcement bars that was observed when similar bars were individually tested. Finally, the wall resistance started to degrade until the test was terminated at 80% of the R_{Peak} ($R_{80\%}$). The following sections discuss the damage sequence, resistance, displacement responses and ductility capacities of the test walls at different stages, whereas a summary of the wall resistances and their corresponding web displacements (Δ) and support chord rotations (θ_s) is presented in Table 3.2.

3.4.1. Damage Sequence

The cracking patterns of the walls were monitored at different loading stages (i.e. elastic, peak and 20% resistance degradation), as shown in Fig. 3.5. For all test walls, at early loading stages, horizontal flexural cracks in the bed joints were observed at the mid-height of the wall unloaded side and at the bottom course of its loaded side. This was followed by vertical head joint cracks at the center of the wall, which progressed diagonally through the blocks towards the web corners. Based on the strain gauge measurements, the walls reached R_e when yielding occurred in the vertical BEs bars at the mid-height for all walls except for *Wall 5*, where the web reinforcement bars yielded first. The measurements of different strain gauges in the wall bars at the elastic resistances are presented in Fig. 3.6. As can be inferred from the figure, the strains at the top supports were very minor compared to those at the

bottom support and wall the mid height. This observation indicated that the top support, unlike the bottom support, did not provide significant rotational restraint. Subsequently, more diagonal cracks developed and propagated throughout the wall web, combined with additional diagonal spiral cracks appearing in the BEs, as shown in Fig. 3.5. These cracks were also accompanied by yielding in the horizontal reinforcement bars, which confirmed their contributions to the wall resistance and the formation of a two-way bending mechanism that continued until R_{peak} was reached and early signs of flexural crushing were observed at wall mid-height. In addition, Fig. 3.6 also shows that yielding in all walls except Wall 5 occurred at wall mid-height before bottom support. This is attributed to the unsymmetrical wall cross-section which affects the wall yielding flexural capacity (M_y). For instance, cross-section analysis indicates that M_y of Wall 3 were 18 kN.m and 34 kN.m at the mid-height and bottom support respectively, therefore the mid-height cross-section yields first. Whereas, in *Wall* 5, as the wall loaded from the opposite directions the cross-sections interchange and consequently the bottom cross-section yields first.

Beyond the peak resistance, wide horizontal and vertical cracks were observed in the web while more spiral diagonal torsional cracks developed at the bottom of the BEs accompanied by face shell spalling, as shown in Fig. 3.5 at 20% resistance degradation. In addition, *Wall 7* in particular experienced a local shear damage at the web near the top support, as shown in Fig. 3.7. This shear damage caused a sudden 16% drop in the wall resistance.

3.4.2. BEs Torsional Behavior

Although flexural crushing damage was the dominant mode of failure in all walls, except *W7* as mentioned earlier, the wall BEs experienced torsional moments to maintain compatible deformations with the wall web edges. This *compatibility torsion* (ACI 2014) eventually led to a significant damage of the BEs, as shown in Fig. 3.8. According to Collins and Lampert (1973), the compatibility torsion is influenced by the torsional stiffness of the supporting component (i.e. BEs) and the flexural behavior of the supported component (i.e. web). Thus, when the BEs were cracked under torsion, their torsional stiffness decreased and subsequently, the loads were redistributed to the wall web in the vertical direction, limiting further twisting of the BEs. This can be observed in the test walls as the diagonal torsional cracks were limited, as shown in Figs. 3.8 (a and b). Similar observations were reported by El-Hashimy et al. (2018) when the boundary elements were even symmetrically aligned with their wall web. Once flexural failure occurred in the wall web due to load transfer in the vertical direction, the loads were redistributed again horizontally, which subsequently increased the torsional moment and twist demand on the wall BEs, as shown in Figs. 3.8 (c and d).

The reinforcement of the wall web and the geometrical configuration of the wall influenced the extent of the BEs damage despite the fact that all walls had BEs with an identical confinement ties arrangement (i.e. same spacing and diameter). For example, at $R_{80\%}$, the BEs of *Wall 3* were heavily damaged as face shell spalling was observed in the bottom five courses, on the other hand, for *Wall 1*, the face

shell spalling did not exceed the second course. This was mainly attributed to the higher horizontal reinforcement ratio in the web of *Wall 3* (i.e. compared to that of *Wall 1*) that facilitated transferring more loads to the BEs and subsequently increasing their corresponding torsional moment demands, as mentioned earlier. Similarly, the BEs height influenced this damage as shown in Fig. 3.5 for *Walls 6* and *7*. The former wall experienced spalling of the BEs' face shells in the bottom four courses, unlike the latter wall that only had inclined spiral cracks with no spalling observed at the BEs. As the wall height increased (i.e. *Wall 6*), the ratio of horizontal load increased and subsequently the torsional moment demand at the bottom of the BEs increased.

To further assess this torsional behavior numerically, the torsional (cracking and ultimate) moment capacities of the selected BEs were evaluated in accordance with ACI 318-14 (ACI 2014) as the current CSA S304-14 (CSA 2014a) does not include any design provisions for torsion. Since all walls had BEs with the same dimensions and reinforcement ties configuration, the cracking torsional moment was found to be 2.4 kN.m, while the ultimate torsional moment which considered the ties and longitudinal reinforcement of the BEs was 4.0 kN.m. The torsional moment demand was calculated at R_{peak} assuming the load to be carried entirely by the web in the horizontal direction. The analysis showed that the torsional moment demand ranged between 7.6 to 9.4 kN.m, which is almost double the ultimate torsional moment capacity of the BEs. This observation highlights the importance of considering torsion in the design of BEs to limit the possible post peak damage

that may affect the overall wall out-of-plane behavior. In this respect, the current study proposes that BEs should be designed for torsional moment demands in future editions of relevant design standards (CSA 2014a and TMS 2016), as suggested by the ACI318 -14 (ACI 2014) to reduce excessive cracking and minimize BEs face shell spalling, thus ensuring prolonged two-way bending action.

3.4.3. BEs-Web Connection Damage

In addition to the previously discussed damanges, *Wall 5* also showed BEs-web connection failure, as shown in Fig. 3.9. Unlike the BEs-web connection of all other walls shown in Fig. 3.10(a), the horizontal reinforcement of *Wall 5*, shown in Fig. 3.10(b), was placed in a manner that did not prevent further crack propagation, which subsequently led to excessive splitting cracks and BEs-web connection failure. Similar behavior was described by Park and Paulay (1975) as a failure mode for reinforced concrete components, which is fundamentally affected by the loading direction. In order to mitigate this BEs-web connection failure, it is proposed to introduce horizontal shear dowels at the expected wall tension side, that extends beyond BEs-web connection development length, to ensure such dowels would arrest the crack propagation, as shown in Fig. 3.10(c). This complies with the ACI 318-14 (ACI 2014) detailing requirements for reinforced concrete slabs with spandrel beams. Further experimental tests are still required to physically evaluate the performance of such proposed detail for BEs of RM walls.

3.4.4. Walls Resistance

The influence of vertical reinforcement can be evaluated through considering the response of *Walls 1*, *2* and *3*. For example, Table 3.2 shows that the R_e values were 16% and 4% higher for *Walls 2* and *3*, respectively, than that of *Wall 1*. This indicates that the high BEs reinforcement ratio in *Wall 2* had a notable influence on the wall's R_e compared to *Wall 3* with high web reinforcement ratio. As can be seen also from Table 3.2, *Walls 2* and *3* (i.e. ρ_v =0.61%) exhibited an increase in their R_{peak} values by 10% and 13%, respectively, relative to *Wall 1* (i.e. ρ_v =0.47%). It is also worth mentioning that *Walls 2* and *3* reached similar R_{peak} values (i.e. less than 3% difference), indicating that the vertical reinforcement distribution had low influence on the R_{peak} values for both walls.

W*alls 3* and *5* had similar design parameters but they were loaded from opposite sides. The wall resistances were almost identical, where the R_e and R_{peak} values of *Wall 5* were only 8% and 5%, respectively, higher than those of *Wall 3*. This slight difference indicates that the alignment of BEs, with the currently used dimensions (i.e. 2 x 2 cells), had an insignificant impact on the overall wall resistances. This is because the loads on *Wall 5*, mainly responsible for that BEs-web connection failure, were redistributed in the horizontal direction after the wall R_{peak} was reached, as mentioned earlier. Therefore, the splitting cracks and the subsequent BEs-web connection failure mainly influenced the post-peak response of *Wall 5* relative to that of *Wall 3* that had different BEs-web connection, as shown in Figs. 10 (b and a), respectively.

Although *Walls 1* and *4* had similar vertical and horizontal reinforcement details, the axial load affected their R_e values. As presented in Table 3.2, *Wall 1* had higher R_e than *Wall 4* by 46%, which was mainly attributed to the high compressive stresses on the cross-section of *Wall 1* that counteracted the tension stresses that resulted from the out-of-plane flexural stresses and subsequently delayed reinforcement yielding. However, the peak resistance, R_{peak}, of *Wall 1* was only 10% higher than that of *Wall 4.* This is because the axial load increased the compression forces and the compression block depth; which subsequently reduces the wall's cross-section flexural lever arm. To further validate this observation numerically, sectional analysis using strain compatibility was carried out for *Walls 1* and *4*. The results the peak flexural capacities were 37.0 and 30.2 kN.m for *Walls 1* and *4*, respectively, with only 22% difference, whereas their corresponding elastic flexural capacities were 29 kN.m and 19 kN.m with 52% difference.

3.4.5. Walls Displacement Responses

Figure 3.11 shows the hysteretic cyclic load-displacement/rotation relationships of the walls based on the horizontal displacements at the wall center and the corresponding chord support rotations. For each wall, the envelope of the load-displacement relationship represents the resistance function (USDOD 2008). The resistance functions of all walls are compared in Fig. 3.12 which shows the influence of the different design parameters. For instance, the absence of axial load in *Wall 4* clearly enhanced the wall displacement at peak resistance, Δ_{peak}, compared to its axially loaded counterpart (*Wall 1)*, which experienced approximately half the

displacement at approximately the same load. On the other hand, for *Wall 2* and *3*, the reinforcement ratio value and distribution did not affect the displacement responses, as shown in Fig. 3.12.

According to the current blast design standards (i.e. ASCE 2011; USDOD 2008), a wall reaches a hazardous damage state (i.e. likely to fail) when its support rotation exceeds 2˚. However, as can be seen in Fig. 3.12, all the walls achieved high support rotation values (i.e. in excess of 4˚) before their resistances degraded to 80% of their peak resistance. For example, *Wall* 7 had vertical support rotation of 4.1˚ at 20% resistance degradation, as shown in Fig. 3.12. At a similar support rotation, (i.e. 4˚), all of the walls had some permanent deformations and excessive cracking, but no collapse. This behavior discrepancy shows the large level of conservatism in the current blast design limits that were originally developed based on a limited number of experimental and analytical studies, mainly of stiff non-civilian buildings/structures (e.g. bunkers).

The BEs of all walls attained similar displacement values that were almost 60% of those at the wall web, as shown in Fig. 3.13. This figure confirms that all walls experienced a two-way bending mechanism throughout the test. However, *Wall 4* showed a higher ratio between the BEs and web displacements (i.e. compared to all other walls). This can be attributed to the absence of the axial load that reduced the stiffness of the BEs (Paulay and Priestley 1992; Bonet et al. 2011) and subsequently limited the stiffness of the web in the horizontal direction. It is also worth mentioning that the behavior of *Wall 5* was initially similar to all other

walls until a failure in the BEs-web connection occurred, as shown in Fig. 3.13 and discussed earlier.

3.4.6. Ductility Capacities

In blast design, flexurally-governed structural components are expected to sustain large displacement demands without experiencing brittle failures (ASCE 2011). Therefore, the ductility of RM walls is an important aspect in controlling the performance of such walls under blast load scenarios (CSA 2012b), especially considering the fact that RM shear walls would most likely be also the main structural components responsible for sustaining the overall building gravity loads. As such, the wall ductility capacities (μ_{peak} and $\mu_{80\%}$) was defined in the current study as the ratio between the center of web displacement at peak, Δ_{peak}, or at degradation to 80% of peak resistance, $\Delta_{80\%}$, and the yield displacement (i.e. elastic displacement, Δ_e, corresponding to R_e), respectively (Shedid et al. 2008). The ductility capacity of each wall is shown in Fig. 3.11 at different loading stages (μ_{peak} and $\mu_{80\%}$), while Fig. 3.14 compares these values based on different design parameters.

Figure 3.14(a) shows that the ductility capacities of *Walls 1, 2* and *3*, were essentially the same (3.0) at the peak resistance and ranged from (6.1) to (7.1) at $R_{80\%}$. However, the axial load had a significant influence on the wall ductility levels. For example, the ductility capacity of *Wall 1* remained at almost 45% lower than that of *Wall 4* at different stages of loading, as shown in Fig. 3.14(b). These results agree with those reported by Paulay and Priestley (1992) regarding the negative

influence of axial (compressive) loads on ductility. As can be also seen in Fig. 3.14(c), the BEs alignment did not influence the μ_{peak} of *Walls 3* and *5*; since BEs-web connection failure only influenced the post-peak response as discussed earlier, whereas, $\mu_{80\%}$ of *Wall 3* exceeded that of *Wall 5* by 30%. Finally, walls with different aspect ratios had different elastic displacement capacities, as discussed earlier and shown in Table 3.2. Wall Ultimate Response Prediction Models

In this section, the wall resistance functions were analytically developed and compared to the corresponding experimental results. The analysis was performed through both fiber section analysis to determine the cross-section flexural capacity; and plastic analysis to predict the wall ultimate resistance, R_{ult} and its corresponding displacement, Δ_{ult}. Accordingly, two approaches, *Approaches I* and *II* are investigated in the current study to develop analytical resistance functions for the tested walls through plastic analyses.

In *Approach I*, the wall was modeled as a structural component that spanned vertically with a cross-section that included both the web and BEs represented as frame element with a flanged cross-section. In *Approach II*, a more detailed analytical model was developed to consider the wall web as a component that is supported on the (top and bottom) wall supports as well as the (right and left) BEs. Thus, this latter approach accounts for the relative displacement between the web and BEs. It is also worth mentioning that, based on the findings of Woodson (1992) and as reported in USDOD (2008) for walls with shear reinforcement in the out-of-

plane direction (i.e. ties in the BEs), the maximum support rotation in the models developed using the two approaches was limited to 6˚.

3.4.7. Fiber Section Analysis

In order to adequately predict R_{ult} using plastic analysis, the cross-section flexural capacity needs to be first quantified accurately by taking into account the material non-linearity. Thus, a non-linear fiber section analysis procedure was carried out in the current study. Both the concrete blocks and grout were lumped as one material with a compressive strength, f'_{av}, of 11.2 MPa, as mentioned earlier. The ultimate unconfined compressive strain for the masonry was assumed 0.0025 as per the CSA-S304(2014) since this strain was not recorded during the compression tests on the concrete prisms. The maximum compressive strain at the BEs region was assigned a higher value of 0.005 to consider the influence of the steel confinement, as reported by Obaidat et al. (2010). The nonlinear behaviors of the unconfined and confined masonry materials were accounted for by using the stress-strain relationship proposed by Chang and Mander (1994) for reinforced concrete components as applied by Ezzeldin et al. (2016) for RM walls. The reinforcement bars were assigned a bi-linear elasto-plastic relation, using f_y from the experimental test. Only the bars in the BEs were allowed to withstand compressive stresses according to CSA S304-14 provisions. For simplicity of the model, the nine loads were considered as a uniformly distributed load to generate the wall resistance function.

In *Approach I*, to account for the BEs alignment (i.e. being flush to the web) that resulted in an asymmetrical system, the flexural capacities at mid-height, ($M_{mid\text{-}height}$) and at support (M_{sup}), were evaluated for both directions separately, as presented in Table 3.3. In *Approach II*, the flexural capacities of the web in both vertical and horizontal directions, ($M_{v\text{-}web}$ and $M_{h\text{-}web}$), respectively, as well as the BEs ($M_{v\text{-}BEs}$) were evaluated. Table 3.3 demonstrates the contribution of the dual layer of reinforcement of the BEs on the section flexural capacity. For example, the flexural capacity of one BE is approximately 30% higher than that of the entire web. In addition, the contribution of the horizontal reinforcement on the web section capacity, of *Walls* 3 and 5 (i.e. ρ_h =0.30%), is obvious when compared to all other walls with lower ρ_h (i.e. 0.16%), as the predicted flexural capacity nearly increased by 100%.

3.4.8. Plastic Analysis

The UFC 3-340-02 (USDOD 2008) provides formulae to evaluate the wall resistances (i.e. at elastic and ultimate stages) and equivalent stiffness values. These formulae coupled with the wall cross-section flexural capacities, estimated using the fiber section analysis, were used to generate an idealized resistance function for each wall through plastic analysis. In *Approach I,* to mimic the wall restraints, fixed-simple supported boundary conditions were adopted. The analysis in this approach resulted in only two mechanisms prior to wall failure, as shown in Fig. 3.15. In *Approach I, Mechanism A* is characterized by a yield line at the bottom support before the formation of another yield line at the wall mid-height (i.e. Mid-

height cross-section), marking *Mechanism B*. Equations (1) and (2) were used to predict the wall resistance at each mechanism, whereas the corresponding equivalent stiffness, K_e and K_p were determined using Eqs. (3) and (4) at the elastic and ultimate stages, respectively.

$$R_e = \frac{8M_{sup}}{H_w} \quad (1) \qquad R_{ult} = \frac{4\left(M_{\sup}+2M_{mid-height}\right)}{H_w} \quad (2)$$

$$K_e = 185\frac{EI_{ef}}{{H_w}^4} \quad (3) \qquad K_p = 384\frac{EI_{ef}}{{H_w}^4} \quad (4)$$

Where, E, is the elastic modulus of concrete, I_{ef}, is the effective moment of inertia of the wall cross-section and H_w is the wall height.

In *Approach II*, the web was assumed to have a fixed- simple supported boundary condition in the vertical direction, while the horizontal direction was simply supported on the BEs that in turn behaved as a beam-column with fixed-simple supported boundary conditions, as shown in Fig. 3.16. To simplify plastic analysis for two-way elements (i.e. the web), UFC 3-340-02 (USDOD, 2008) define each mechanism when a critical cross-section reaches its ultimate flexural capacity. Accordingly, each wall would develop five mechanisms, each triggered by critical cross-section reaching its ultimate flexural capacity, either in the web or in the BEs, as described in Table 3.4 and shown in Fig. 3.16. As can be seen in the figure, *Mechanisms A* to *D* are associated with the web, whereas Eq. (5) and (6) were used to predict the resistance (r) and displacement (δ) of the web mechanisms, where the load and stiffness distribution coefficients (β and γ) in these equations were taken

based on the considered directions (i.e. vertical or horizontal) and the web's aspect ratio and boundary conditions. Further information can be found in the UFC 3-340-02 (USDOD, 2008) document. These coefficients facilitated estimating the load that would produce a yield line in the wall web's bottom support as well as the center of the wall.

$$r_{web} = \frac{M_{web}}{H_w \beta} \quad (5) \qquad K_{web} = \frac{EI_{ef}}{\gamma \cdot H^4} \quad (6)$$

Mechanisms E and *F* materialize through yield line formation at the BEs bottom support and mid-height cross-sections, respectively. Therefore, formulae used in *Approach I* and presented in Eqs. (1 to 4) were utilized for the BEs in *Approach II*. Although all mechanisms can develop independently, in terms of load resistance, as discussed by Neal (1977), these mechanism may overlap when the displacement response is evaluated. Therefore, the analytical resistance functions, shown in Fig. 3.17, combine *Mechanisms A and E*, where yield lines develop at the wall support followed by all other mechanisms that result in yield lines at the center of the wall.

3.4.9. Model Validation

The predicted resistance functions of both approaches were compared to the experimental results as shown in Fig. 3.17. The results of *Approach I* in terms of the resistance (r) and displacement (δ) of each mechanism in addition to each wall's R_{ult} and Δ_{ult} were presented in Table 3.5. The R_{ult} of all the test walls was predicted with an average deviation of merely 7% relative to the experimental results. However, the displacement corresponding to ultimate resistance prediction for all

walls was significantly underestimated, with an average deviation of 74%. This may be attributed to the high resulting stiffness of the wall cross-section when the web and BEs were assumed as a single component.

Approach II predicted the ultimate resistance, $R_{ult,}$ and the corresponding displacements Δ_{ult} more accurately, as shown in Table 3.6. Unlike *Approach I*, where all the walls followed the same yield line development order, in *Approach II*, *Wall* 6 had a different mechanism order compared to all other walls. According to the calculations, *Mechanism B* would develop, in lieu of *Mechanism A*, in *Wall 6* because of the high aspect ratio of this wall that altered the load distribution coefficients. As can be seen in Table 3.6, *Approach II* accurately predicted the ultimate resistance of the test walls with an average deviation of 4.5% relative to its corresponding experimental results.

As for the displacement response, all walls, except *Wall 7*, were predicted using *Approach II*, as shown in Fig. 3.17. The average deviation of the web deformation at ultimate load was 20%. However, the model failed to predict accurately the resistance function of *Wall 7* (i.e. a deviation of 55% in the wall ultimate displacement) which had aspect ratio less than one, this may be attributed to the two-way distribution factors used which may require further investigation. In addition, as presented in Fig. 3.17, *Approach II* was also capable of predicting the wall's mid-height displacement at the BEs with an average deviation of 18.5%.

Based on *Approach II*, the resistance contributions of the wall web and BEs were reported in Table 3.7. The vertical direction of the web, $R_{web\text{-}v}$, carried 37% of

R_{ult}, on average, while the web horizontal direction, $R_{web\text{-}h}$, transferred approximately 9% of R_{ult} to the BEs. Eventually, the BEs resistance (R_{BEs}) reached approximately 63% of R_{ult}. These contribution values were obviously affected by the different wall design parameters. Whereas, when the web reinforcement ratio was doubled in *Walls 3* and *5* compared to *Wall 1*, the contribution of the web increased from 37% in *Wall 1* to 42% in *Wall 3* and 43% in *Wall 5*. In *Wall 2*, the reinforcement ratio increased in the BEs compared to *Wall 1*, accordingly the contribution of the BEs increased from 64% to 69%. Table 3.7 also shows that the influences of the axial load (i.e. *Walls 1* and *4*) and BEs alignment (i.e. *Wall 3* and *5*) on these contributions were negligible. Finally, the aspect ratio effect on the load distribution was evaluated in *Walls 1,6* and *7* as presented in Table 3.6. The increase in the aspect ratio from 0.72 in Wall 7 to 1.2 in Wall 6 increased the load distributed in the horizontal direction from 5% to 10%, respectively.

3.5. CONCLUSIONS

Several recent studies investigated the in-plane response of reinforced masonry shear walls with boundary elements, whereas only a limited number of studies were related to their out-of-plane performance. In this respect, the experimental program (*Phase II*) comprised seven seismically-detailed RM scaled walls with BEs with different design parameters under quasi-static out-of-plane cyclic loading. The experimental results were assessed in terms of the wall resistance functions, damage sequences and ductility capacities. Finally, plastic analyses were performed to

develop and validate an analytical resistance function to simulate the out-of-plane response of RM walls with BEs.

The influence of the different design parameters on the wall resistance function was highlighted, especially at high displacement demands. In this respect, all walls were able to sustain high displacement demands compared to those corresponding to blast standards threshold values, and flexural crushing damage was the dominant mode of failure for all walls. Nonetheless, the torsional behavior of BEs were observed and resulted in either BEs damage or BEs-web connection failure. Such damage may be avoided by properly detailing the BEs and their connection to the wall web to withstand this compatibility-induced torsional moment.

Models based on plastic analyses were developed to generate the wall resistance functions using two different wall representation approaches. Both approaches adequately estimated the ultimate resistance of the wall (i.e. an average deviation of less than 11%). However, *Approach I*, which considered both the wall web and the BEs as one component (i.e. the relative displacement between the web and BEs was ignored), was incapable of predicting the wall displacement response (i.e. an average deviation of 74%) due to overestimated stiffness of the whole cross-section. *Approach II* (modeling both the BEs and web separately) however, accurately predicted resistance function parameters for all the walls.

Although the current study investigated the influence of different design parameters on RM walls with BEs, there are still some aspects that were not

investigated. These aspects include utilizing different BE dimensions, BE spacing and other material properties. Therefore, as would be expected, additional experimental and/or analytical studies would facilitate adoption of RM walls with BEs as an out-of-plane load resistant system within the future editions of blast design standards ASCE 59 and CSA S850.

3.6. ACKNOWLEDGMENTS

The financial support for this project was provided by the Natural Sciences and Engineering Research Council (NSERC) of Canada. Support was also provided by the McMaster University Centre for Effective Design of Structures (CEDS), funded through the Ontario Research and Development Challenge Fund (ORDCF) of the Ministry of Research and Innovation (MRI). Provision of mason time by the Ontario Masonry Contractors Association (OMCA) and the Canada Masonry Design Centre (CMDC) is appreciated.

3.7. NOTATION

The following symbols are used in this paper:

A_R	=	Aspect ratio of the wall;
E	=	Elastic modulus of concrete;
f'_{av}	=	Average compressive strength of prisms;
f'_m	=	Specified masonry strength;
f_y	=	yield strength of reinforcement;
f_{ult}	=	ultimate strength of reinforcement;
h_w	=	Wall height;
I_{ef}	=	Effective moment of inertia of the wall cross-section
l_w	=	Wall length;
K_e	=	Equivalent elastic stiffness;
K_p	=	Equivalent plastic stiffness;
$M_{mid\text{-}height}$	=	Flexural moment capacity at wall mid-height in *Approach I*;
$M_{support}$	=	Flexural moment capacity at wall support in *Approach I*;

$M_{v\text{-}web}$ = Vertical flexural moment capacity of wall web in *Approach II*;
$M_{h\text{-}web}$ = Horizontal flexural moment capacity of wall web in *Approach II*;
$M_{v\text{-}web}$ = Flexural moment capacity of wall BEs in *Approach II*;
r = Resistance of a specific mechanism;
r_{web} = Resistance of a web mechanism;
R_e = Elastic resistance;
R_{peak} = Peak resistance;
R_{ult} = Ultimate resistance;
$R_{80\%}$ = Resistance at degradation to 80% of peak resistance;
α = Stiffness distribution coefficient for two-way elements;
β = Load distribution coefficient for two-way elements;
Δ_{web} = Displacement of the center of the web;
Δ_{BEs} = Displacement of the center of the BEs;
Δ_e = Displacement of the center of the web at elastic resistance;
Δ_{peak} = Displacement of the center of the web at peak resistance;
Δ_{ult} = Displacement of the center of the web at ultimate resistance;
$\Delta_{80\%}$ = Displacement of the center of the web at degradation to 80% of peak resistance;
δ = Displacement at specific mechanism;
μ = Displacement ductility ratio;
μ_{peak} = Displacement ductility ratio at peak resistance;
$\mu_{80\%}$ = Displacement ductility ratio at degradation to 80% of peak resistance;
ρ_h = Horizontal steel reinforcement ratio of the web;
ρ_v = Vertical steel reinforcement ratio of the wall;
$\rho_{v\text{-}BEs}$ = Vertical steel reinforcement ratio of the BEs;
$\rho_{v\text{-}w}$ = Vertical steel reinforcement ratio of the web;
σ_v = Equivalent axial stress ratio applied to each wall including self-weight;
θ_s = Support rotation of the wall;
θ_{peak} = Support rotation of the wall at peak resistance;
$\theta_{80\%}$ = Support rotation of the wall at degradation to 80% of peak resistance;

3.8. REFERENCES

Abboud, B. E., Hamid, A. A., and Harris, H. G. (1990). "Small-scale Modeling of Concrete Block Masonry Structures." *ACI Structural Journal*, (87), 145–155.

Abboud, B., Hamid, A. A., and Harris, H. G., (1996). "Flexural Behavior of Reinforced Concrete Masonry Walls Under Out-of-Plane Monotonic Loads." *ACI Structural Journal*, *93*(3), 327-335.

ACI Committee 318. (2014). *Building Code Requirements for Structural Concrete (ACI 318M-14).* ACI Report, American concrete institute.

Al-Jaberi, Z., Myers, J. J., and ElGawady, M. A. (2018). "Out-of-plane flexural behavior of reinforced masonry walls strengthened with near-surface-mounted fiber-reinforced polymer." *ACI Structural Journal*, 115(4), 997–1010.

ASCE (2011). "Blast Protection of Buildings." *ASCE 59-11*, Reston, Va.

Ashour, A., El-Dakhakhni, W., and Shedid, M. (2016). "Experimental Evaluation of the System-Level Seismic Performance and Robustness of an Asymmetrical Reinforced Concrete Block Building." *Journal of Structural Engineering*, 142(10), 04016072.

Azimikor, N., Brzev, S., Elwood, K. J., Anderson, D. L., and Mcewen, W. (2017). "Out-of-plane instability of reinforced masonry uniaxial specimens under reversed cyclic axial loading." *Canadian J. Civ. Eng.*, 376(March), 367–376.

Banting, B. R., and El-Dakhakhni, W. W. (2012). "Force- and Displacement-Based Seismic Performance Parameters for Reinforced Masonry Structural Walls with Boundary Elements." *Journal of Structural Engineering*, 138(12), 1477–1491.

Banting, B. R., and El-Dakhakhni, W. W. (2014). "Seismic Design Parameters for Special Masonry Structural Walls Detailed with Confined Boundary Elements." *Journal of Structural Engineering*, 140(10), 04014067.

Bonet, J. L., Romero, M. L., and Miguel, P. F. (2011). "Effective flexural stiffness of slender reinforced concrete columns under axial forces and biaxial bending." *Engineering Structures*, Elsevier Ltd, 33(3), 881–893.

Browning, R. S., Dinan, R. J., and Davidson, J. S. (2014). "Blast Resistance of Fully Grouted Reinforced Concrete Masonry Veneer Walls." *Journal of Performance of Constructed Facilities*, 28(2), 228–241.

Chang, G. A., and Mander, J. B. (1994). "Seismic energy based fatigue damage analysis of bridge columns: Part 1—Evaluation of seismic capacity." NCEER Tech. Rep. No. NCEER-94-0006, State Univ. of New York, Buffalo, NY.

Collins, M. P., and Lampert, P., "Redistribution of Moments at Cracking—The Key to Simpler Torsion Design," *Analysis of Structural Systems for Torsion*, SP-35, American Concrete Institute, Farmington Hills, Mich., 1973, pp. 343-383.

CSA (Canadian Standards Association). (2012a). "Design and assessment of buildings subjected to blast loads." *CSA S850-12*, Mississauga, ON, Canada.

CSA (Canadian Standards Association). (2012b). "Post-blast safety evaluation of buildings." *CSA S851-12 (R2017)*, Mississauga, ON, Canada.

CSA (Canadian Standards Association). (2014a). "Design of masonry structures." *CSA S304-14*, Mississauga, ON, Canada.

CSA (Canadian Standards Association). (2014b). "CSA Standards on concrete masonry units." *CSA A165 Series-14*, Mississauga, ON, Canada.

CSA (Canadian Standards Association). (2014c). "Mortar and grout for unit masonry." *CSA A179-14*, Mississauga, ON, Canada.

CSA (Canadian Standards Association). (2014d). "Carbon steel bars for concrete reinforcement." *CSA G30.18-09*, Mississauga, ON, Canada.

Da Porto, F., Mosele, F., and Modena, C. (2010). "Experimental testing of tall reinforced masonry walls under out-of-plane actions." *Construction and Building Materials*, Elsevier, 24(12), 2559–2571.

Dizhur, D., and Derakhshan, H. (2010). "Earthquake-Damaged Unreinforced Masonry Building Tested In-Situ." *Journal of Structural Engineering*, 76–89.

ElSayed, M., El-Dakhakhni, W., and Tait, M. (2015a). "Resilience Evaluation of Seismically Detailed Reinforced Concrete-Block Shear Walls for Blast-Risk Assessment." *Journal of Performance of Constructed Facilities*, 4015087.

ElSayed, M., El-Dakhakhni, W., and Tait, M. (2015b). "Response Evaluation of Reinforced Concrete Block Structural Walls Subjected to Blast Loading." *Journal of Structural Engineering*, 141(11), 04015043.

El-Hashimy, T., Ezzeldin, M., Tait, M. and El-Dakhakhni, W. (2018). "Out-of-Plane Performance of Reinforced Masonry Shear Walls Constructed with Boundary Elements." Journal of Structural Engineering, 10.1061/(ASCE)ST.1943-541X.0002337.

Ezzeldin, M., Wiebe, L., and El-Dakhakhni, W. (2016). "Seismic Collapse Risk Assessment of Reinforced Masonry Walls with Boundary Elements Using the FEMA P695 Methodology." *Journal of Structural Engineering*, 142(11), 04016108.

Ezzeldin, M., El-Dakhakhni, W., and Wiebe, L. (2017). "Experimental assessment of the system-level seismic performance of an asymmetrical reinforced concrete block wall building with boundary elements." *Journal of Structural Engineering*, 143(8)

Ghobarah, A., and El Mandooh Galal, K. (2004). "Out-of-Plane Strengthening of Unreinforced Masonry Walls with Openings." *Journal of Composites for Construction*, 8(4), 298–305.

Hamoush, S.A., McGinley, M.W., Mlakar, P., Scott, D., and Murray, K. (2001). Out-of-plane strengthening of masonry walls with reinforced composites. *Journal of Composites for Construction*, *5*(3), 139-145.

Harris, H. G., and Sabnis, G. (1999). *Structural modeling and experimental techniques*. CRC Press, Boca Raton, FL.

Neal, B. G. (1977). *The Plastic Methods of Structural Analysis*. Chapman & Hall, London.

Noor-E-Khuda, S., Dhanasekar, M., and Thambiratnam, D. P. (2016). "Out-of-plane deformation and failure of masonry walls with various forms of reinforcement." *Composite Structures*, Elsevier, 140, 262–277.

Noor-E-Khuda, S., & Dhanasekar, M. (2017). "Masonry Walls under Combined In-Plane and Out-of-Plane Loadings". *Journal of Structural Engineering*, 144(2), 04017186.

Noor-E-Khuda, S., & Dhanasekar, M. (2018). "Three sides supported unreinforced masonry walls under multi-directional loading". *Construction and Building Materials*, 188, 1207-1220.

Obaidat, A. T., Abo El Ezz, A., and Galal, K. (2017). "Compression behavior of confined concrete masonry boundary elements." *Engineering Structures*, Elsevier Ltd, 132, 562–575.

Park, R., and Paulay, T. (1975). *Reinforced Concrete Structures*, John Wiley & Sons, Inc., Hoboken, NJ, USA.

Paulay, T., and Priestley, M.（1992). *Seismic design of reinforced concrete and masonry buildings*, Wiley, New York, USA.

Robazza, B. R., Brzev, S., Yang, T. Y., Elwood, K. J., Anderson, D. L., and Mcewen, B. (2018). "Out-of-Plane Behavior of Slender Reinforced Masonry Shear Walls under In-Plane Loading : Experimental Investigation." 144(3), 1–16.

Seif ElDin, H. M., and Galal, K. (2017). "In-Plane Seismic Performance of Fully Grouted Reinforced Masonry Shear Walls." *Journal of Structural Engineering*, 143(7), 04017054.

Shedid, M. T., El-Dakhakhni, W. W., and Drysdale, R. G. (2008). "Behavior of fully grouted reinforced concrete masonry shear walls failing in flexure: Analysis." *Engineering Structures*, 31(9), 2032–2044.

Shedid, M. T., El-Dakhakhni, W. W., and Drysdale, R. G. (2010). "Alternative strategies to enhance the seismic performance of reinforced concrete-block shear wall systems." *J. Struct. Eng.*, 10.1061/(ASCE)ST.1943-541X.0000164, 676–689.

Simonds, K. (2014). "Performance of reinforced concrete block structural walls with boundary elements under multiple design basis blast threat levels". M.Eng. thesis, McMaster University, Hamilton, ON, Canada.

Smith, N. L., Tait, M. J., Asce, M., El-dakhakhni, W. W., Asce, F., and Mekky, W. F. (2016). "Response Analysis of Reinforced Concrete Block Infill Panels under Blast." *Journal of Performance of Constructed Facilities*, 30(6), 1–12.

Tanner, J. E., and Klingner, R. E. (2017). *Masonry structural design*. McGraw-Hill Education.

The Masonry Society (TMS). (2016). "Building code requirements and specifications for masonry structures." *TMS 402-16/ACI 530-16/ASCE 5-16*, Detroit.

Tomaževič, M., and Velechovsky, T. (1992). "Some aspects of testing small-scale masonry building models on simple earthquake simulators." *Earthquake Engineering & Structural Dynamics*, 21(11), 945–963.

USDOD (Unified Facilities Criteria). (2008). "Structures to resist the effects of accidental explosions." UFC 3-340-02, U.S. Dept. of Defense, Washington, DC

Winkel, M., and Smith, I. (2010). "Structural Behavior of Wood Light-Frame Wall Segments Subjected to In-Plane and Out-of-Plane Forces." *Journal of Structural Engineering*, 136(7), 826–836.

Woodson, S. C. (1992). *"Lacing versus stirrups - An experimental study of shear reinforcement in Blast-Resistant Structures."* SL-92-2, US Army Corps of Engineers, Vicksburg, Mississippi.

Table 3.1. Test Matrix of RM walls with BEs

Parameter	***Wall* 1***	***Wall* 2**	***Wall* 3**	***Wall* 4**	***Wall* 5**	***Wall* 6**	***Wall* 7**
ρ_v (%)	0.47	0.61	0.61	0.47	0.61	0.47	0.47
$\rho_{v\text{-}BE}$ (%)	0.79	1.10	0.79	0.79	0.79	0.79	0.79
$\rho_{v\text{-}w}$ (%)	0.23	0.23	0.46	0.23	0.46	0.23	0.23
ρ_h (%)	0.16	0.16	0.30	0.16	0.30	0.16	0.16
σ_v (%)	10	10	10	Zero	10	10	10
Loading side	Flush	Flush	Flush	Flush	Non-flush	Flush	Flush
A_R	1.0	1.0	1.0	1.0	1.0	1. 20	0.7
h_w (mm)	1,500	1,500	1,500	1,500	1,500	1,750	1,050
l_w (mm)	1,450	1,450	1,450	1,450	1,450	1,450	1,450

* : Control wall

**: Shaded cells highlight the variable parameter from the control wall

Table 3.2. Summary of experimental wall resistances, displacements and support rotations

Parameter	*Wall* 1*	*Wall* 2	*Wall* 3	*Wall* 4	*Wall* 5	*Wall* 6	*Wall* 7
R_e (kN)	214.00	249.00	223.00	146.00	240.00	193.00	273.00
Δ_e (mm)	9.77	11.43	9.80	6.47	11.48	11.54	7.22
R_{ult} (kN)	258.00	276.90	284.30	230.70	299.60	215.50	398.40
Δ_{ult} (mm)	21.1	16.4	22.9	22.8	24.4	19.1	24.02
R_{peak} (kN)	263.00	290.00	297.00	244.00	301.00	223.00	399.60
Δ_{peak} (mm)	27.66	32.60	29.72	55.56	39.16	38.15	28.80
θ_{peak} (deg)	2.1	2.5	2.3	4.2	3.0	2.5	3.1
$\Delta_{80\%}$ (mm)	66.82	70.00	70.13	109.28	62.07	76.42	37.33
$\theta_{80\%}$ (deg)	5.1	5.3	5.3	8.3	4.7	5.0	4.1

* : Control wall

Table 3.3. Summary of flexural capacity of the predictive fiber-section analysis

Cross-section Flexural Capacity		*Wall* 1	*Wall* 2	*Wall* 3	*Wall* 4	*Wall* 5	*Wall* 6	*Wall* 7
Approach I	$M_{mid\text{-}height}$ (kN.m)	30.28	36.35	31.10	25.00	52.90	30.28	30.28
	$M_{support}$ (kN.m)	37.20	48.67	52.90	30.80	31.10	42.96	42.96
Approach II	$M_{v\text{-}web}$ (kN.m/m)	6.66	6.66	7.97	5.62	7.97	6.66	6.66
	$M_{h\text{-}web}$ (kN.m/m)	2.23	2.23	3.91	2.23	5.03	2.23	2.23
	$M_{v\text{-}BEs}$ (kN.m)/side	10.94	13.82	10.94	9.43	9.61	10.94	10.94

Table 3.4. Developed response mechanisms in *Approach II*

Mechanism	**Critical Cross-section**
A (Web)	• Horizontal cross-section at web support
B (Web)	• Vertical cross-section at Web center
C (Web)	• Horizontal cross-section at web support • Vertical cross-section at Web center
D (Web)	• Horizontal cross-section at web support • Vertical cross-section at Web center • Horizontal cross-section at web center
E (BEs)	• BEs support cross-section
F (BEs)	• BEs support cross-section • BEs mid-height cross-section

Table 3.5. Summary of Plastic analysis *Approach I*

	Wall 1	***Wall 2***	***Wall 3***	***Wall 4***	***Wall 5***	***Wall 6***	***Wall 7***
Mechanism A							
r (kN)	229.1	259.7	282.2	164.3	165.8	196.4	312.5
δ (mm)	3.9	4.0	4.3	2.5	2.5	5.6	1.4
Mechanism B							
r (kN)	47.0	64.1	24.8	51.3	199.1	40.2	64.0
δ (mm)	0.1	0.1	3.4	1.0	6.4	0.0	3.9
R_{ult} (kN)	276.1	323.7	306.9	215.5	365.1	236.6	376.4
R_{ult} ***deviation*** (%)	7%	17%	8%	-7%	22%	10%	-6%
Δ_{ult} (mm)	4.0	4.1	7.8	3.5	9.0	5.6	5.3
Δ_{ult} ***deviation*** (%)	-81%	-75%	-66%	-84%	-63%	-71%	-78%

Table 3.6. Summary of Plastic analysis *Approach II*

	***Wall* 1**	***Wall* 2**	***Wall* 3**	***Wall* 4**	***Wall* 5**	***Wall* 6**	***Wall* 7**
Mechanism	***A***					***B***	***A***
r (kN)	78.3	78.3	93.8	66.2	93.8	62.0	77.8
δ_{web} (mm)	3.1	3.1	3.7	3.2	3.7	3.2	2.0
δ_{BEs} (mm)	0.7	0.7	0.8	0.6	0.8	1.3	0.1
Mechanism	***C***						
r (kN)	0.9	0.9	28.6	8.6	53.6	11.0	20.6
δ_{web} (mm)	0.1	0.1	1.9	0.7	3.6	1.3	2.0
δ_{BEs} (mm)	0.0	0.0	0.4	0.0	0.7	0.0	0.1
Mechanism	***D***						
r (kN)	31.1	31.1	27.2	23.4	18.2	26.3	27.9
δ_{web} (mm)	5.7	5.7	5.0	5.4	3.4	7.7	2.1
Mechanism	***E***						
r (kN)	98.8	129.6	85.3	82.8	62.3	79.3	135.6
δ_{BEs} (mm)	3.8	5.0	3.3	3.3	2.4	4.8	2.2
Mechanism	***F***						
r (kN)	44.1	59.4	44.1	47.9	65.5	37.8	57.5
δ_{BEs} (mm)	4.1	5.5	4.1	4.6	6.1	5.6	2.2
R_{ult} (kN)	253.1	299.3	279.0	228.8	293.4	216.3	343.0
R_{ult} **Deviation**(%)	-2%	8%	-2%	-1%	-2%	0%	-16%
Δ_{ult} (mm)	17.4	20.0	19.2	18.0	20.6	23.9	10.7
Δ_{ult} **Deviation** (%)	-18%	22%	-16%	-21%	-16%	25%	-55%

Table 3.7. Contribution of wall components based on plastic analysis

	***Wall* 1**	***Wall* 2**	***Wall* 3**	***Wall* 4**	***Wall* 5**	***Wall* 6**	***Wall* 7**
$R_{web\text{-}v} / R_{ult}$ (%)	36%	31%	42%	35%	43%	36%	34%
$R_{web\text{-}h} / R_{ult}$ (%)	7%	6%	11%	8%	14%	10%	5%
R_{BEs} / R_{ult} (%)	64%	69%	58%	65%	57%	64%	66%

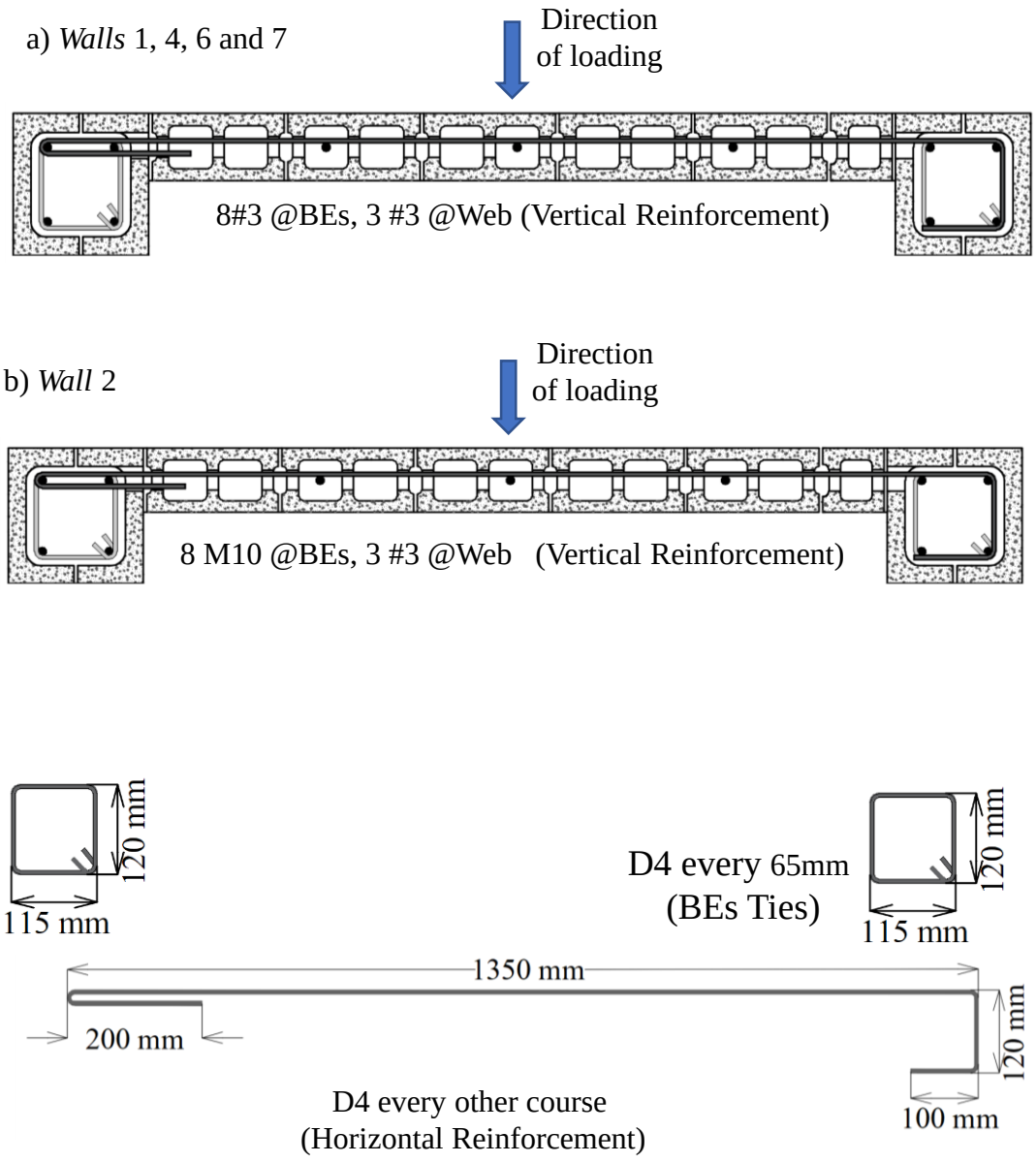

Fig 3.1. Wall Cross-section details

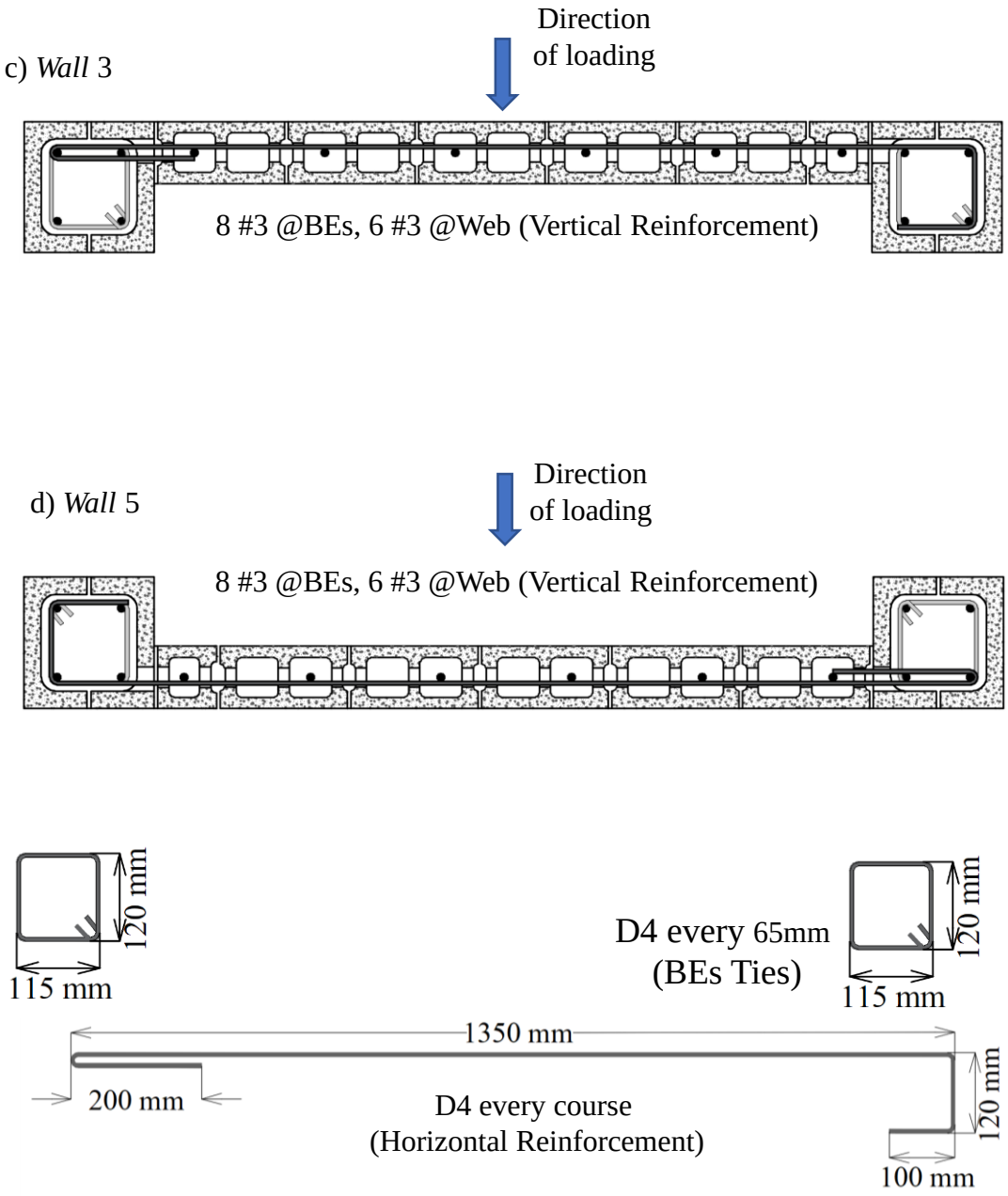

Fig 3.1 (Cont). Wall Cross-section details

(a) (b) (c)

Fig 3.2. Boundary element construction with confined ties

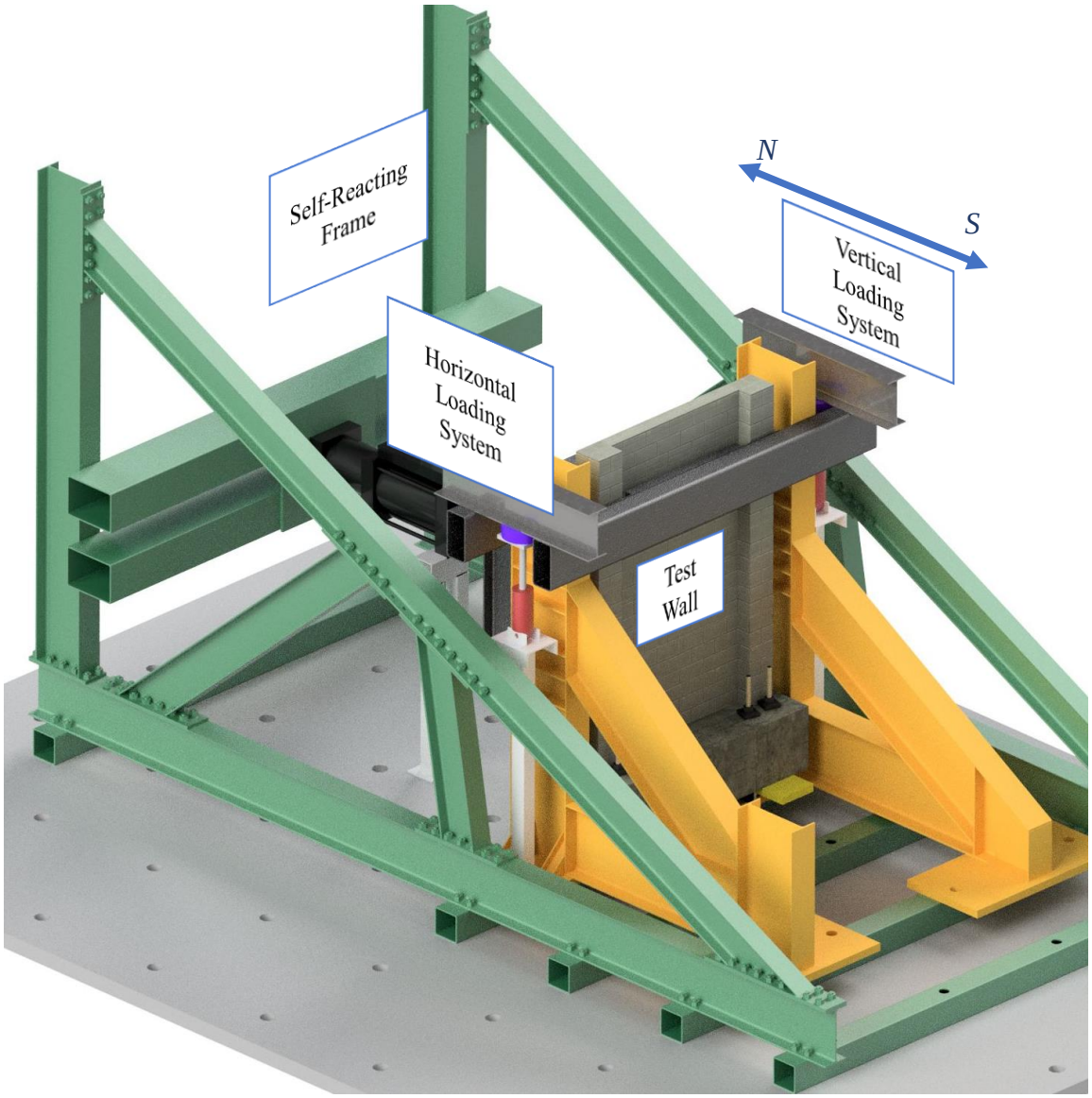

(a)

Fig 3.3. Test setup (a) South view

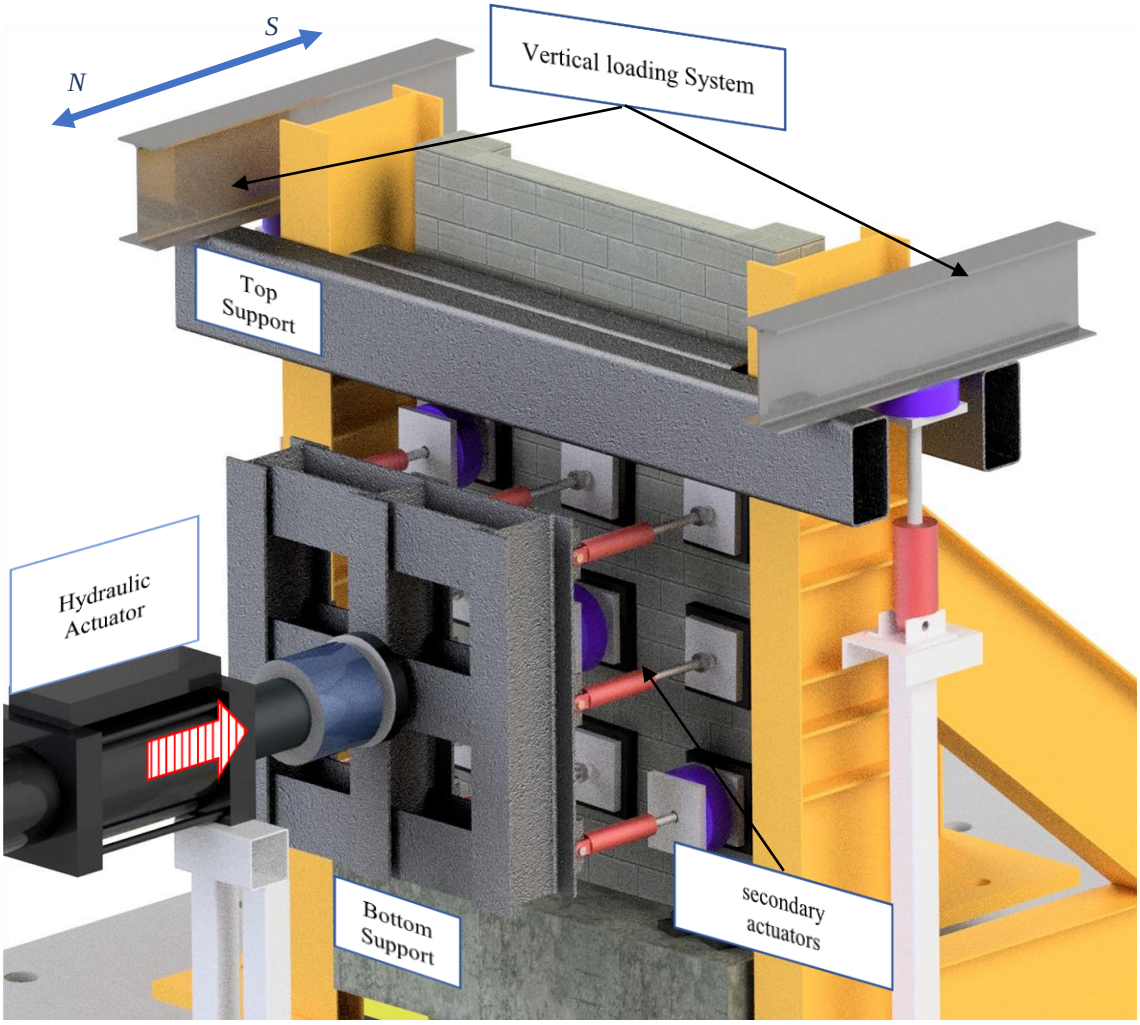

(b)

Fig 3.3 (Cont). Test setup (b) North view

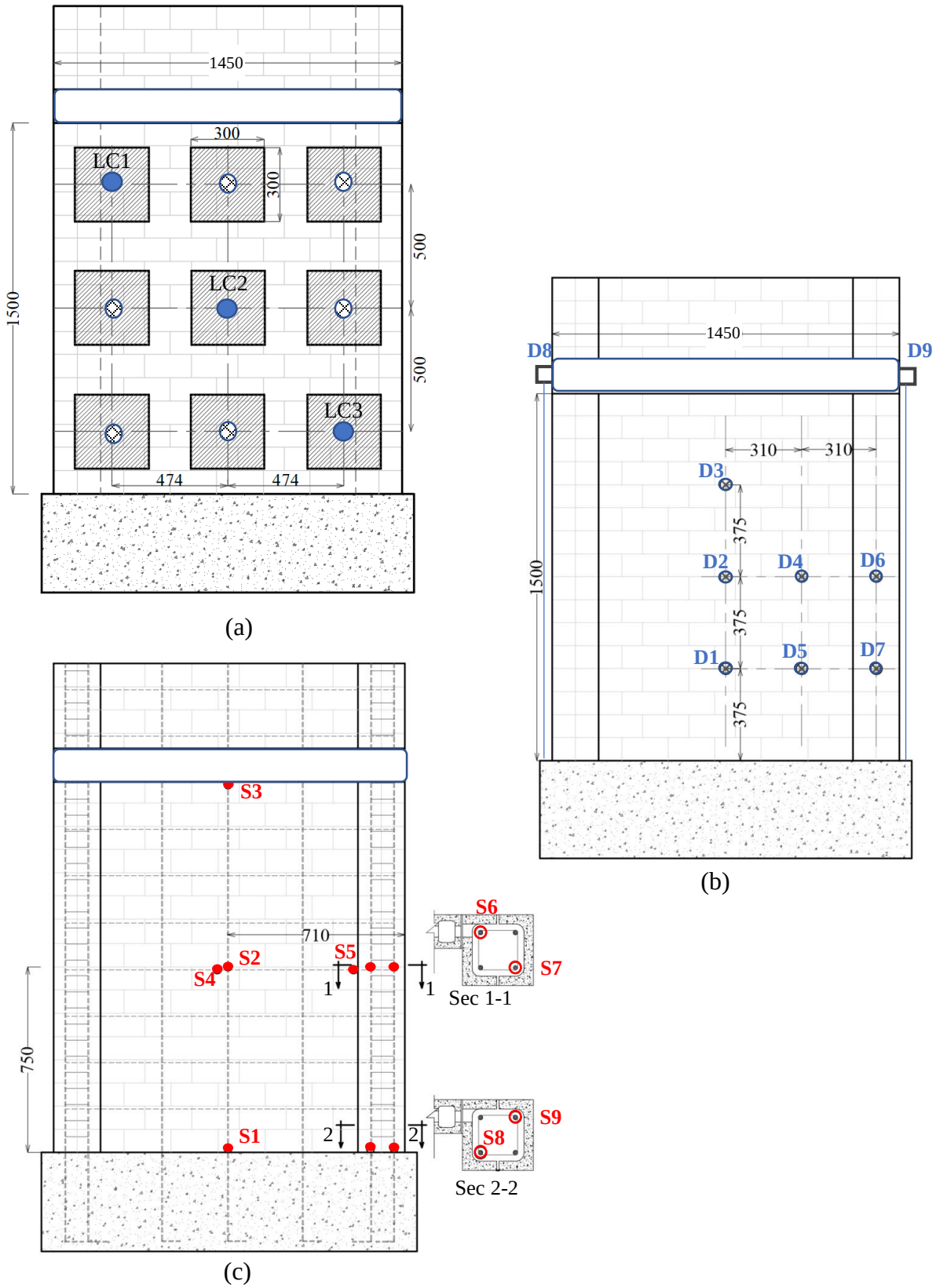

Fig. 3.4. Typical wall instrumentations (All dimensions are in mm):
(a) Rubber pads and load cells positions; (b) Displacement potentiometers; and (c) Strain gauges

	At Elastic Resistance (R_e) Unloaded Side	At Peak Resistance (R_{peak}) Unloaded Side	At Degradation to 80%of peak Resistance ($R_{80\%}$) Unloaded Side	At Degradation to 80%of peak Resistance ($R_{80\%}$) Loading Side
Wall 1	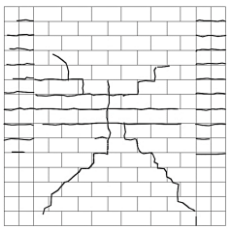	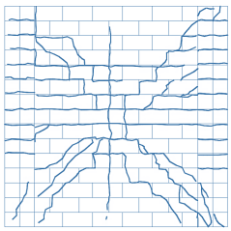	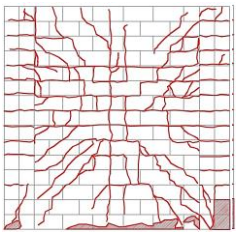	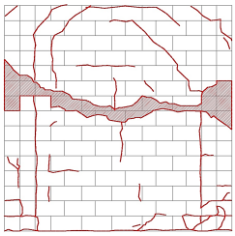
Wall 2	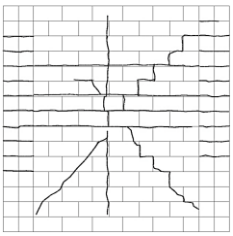	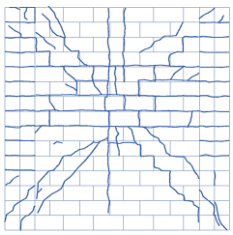	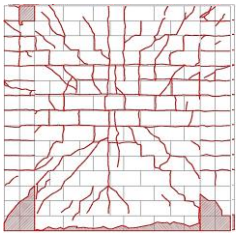	
Wall 3	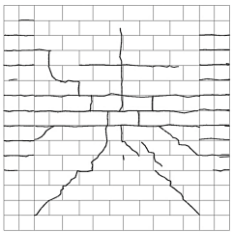	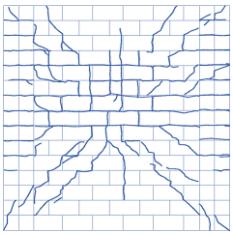	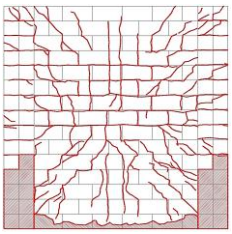	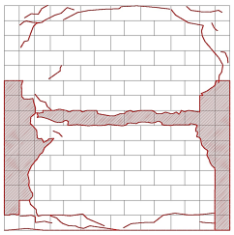
Wall 4	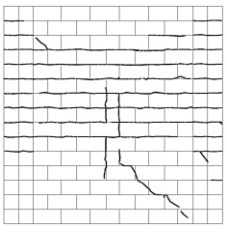	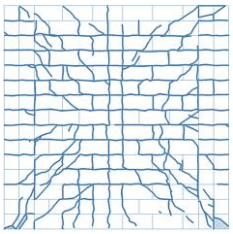	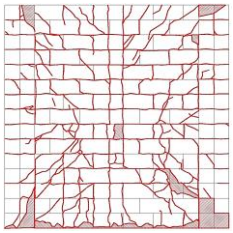	

Fig 3.5. Cracking pattern at different loading stages

	At Elastic Resistance (R_e) Unloaded Side	At Peak Resistance (R_{peak}) Unloaded Side	At Degradation to 80%of peak Resistance ($R_{80\%}$) Unloaded Side	At Degradation to 80%of peak Resistance ($R_{80\%}$) Loading Side
Wall 5	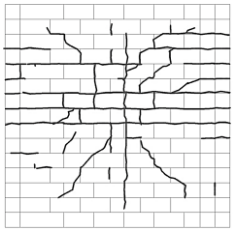	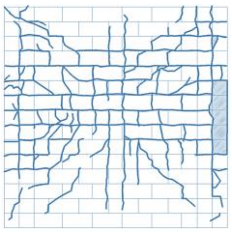	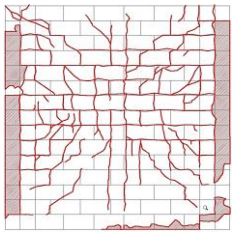	
Wall 6	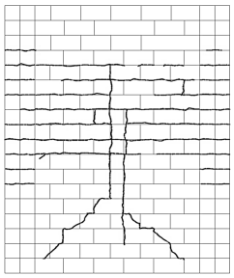	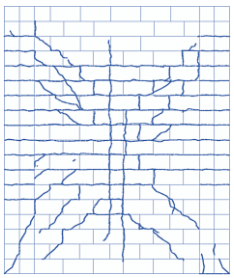	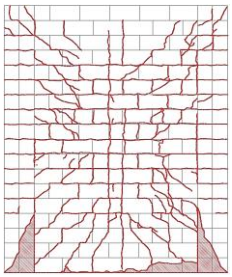	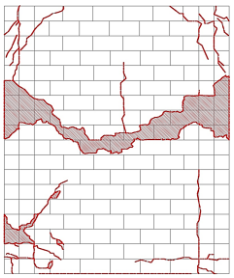
Wall 7	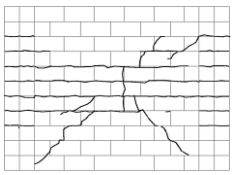	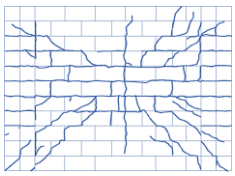	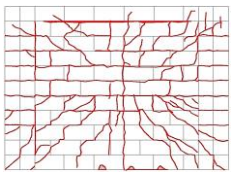	

Fig 3.5 (Cont). Cracking pattern at different loading stages

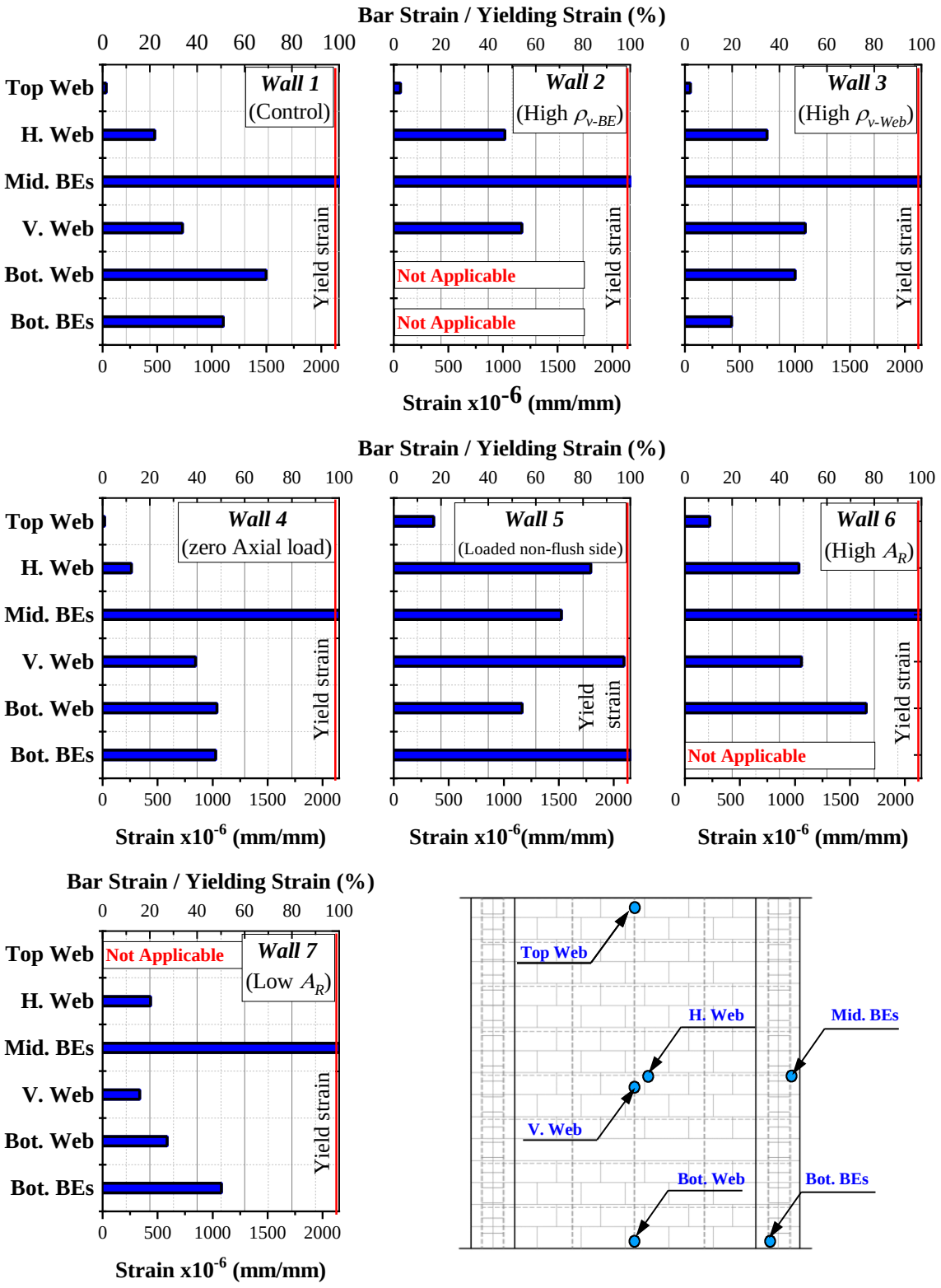

Fig 3.6. Strain measurements for the wall at R_e

Fig 3.7. Local damage at web of *Wall 7*

(a) At Elastic Resistance

(b) At Peak Resistance

(c) At Degradation to
95%of peak Resistance

(d) At Degradation to
90%of peak Resistance

Fig 3.8. Progress of a torsional damage at BEs of *Wall* 3

Fig 3.9. BEs-Web connection failure of *Wall* 5

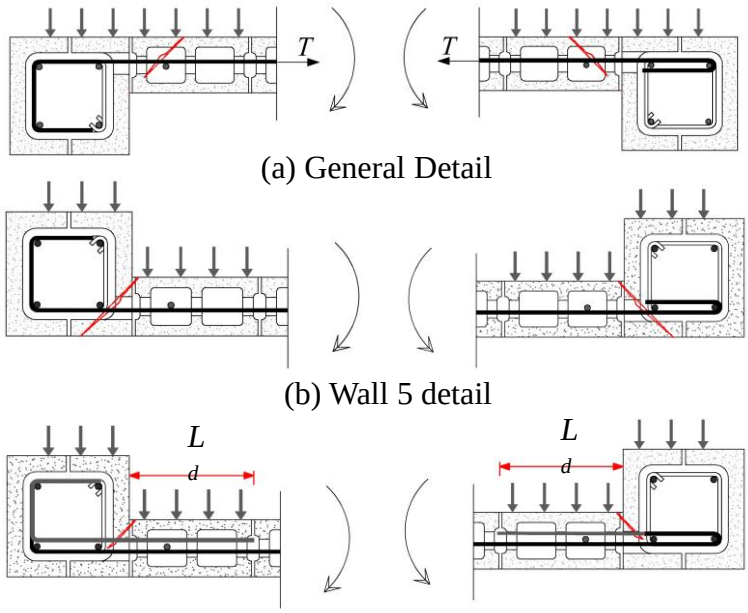

(a) General Detail

(b) Wall 5 detail

(c) Suggested detail

Fig 3.10. BEs-Web connection details and expected developed crack

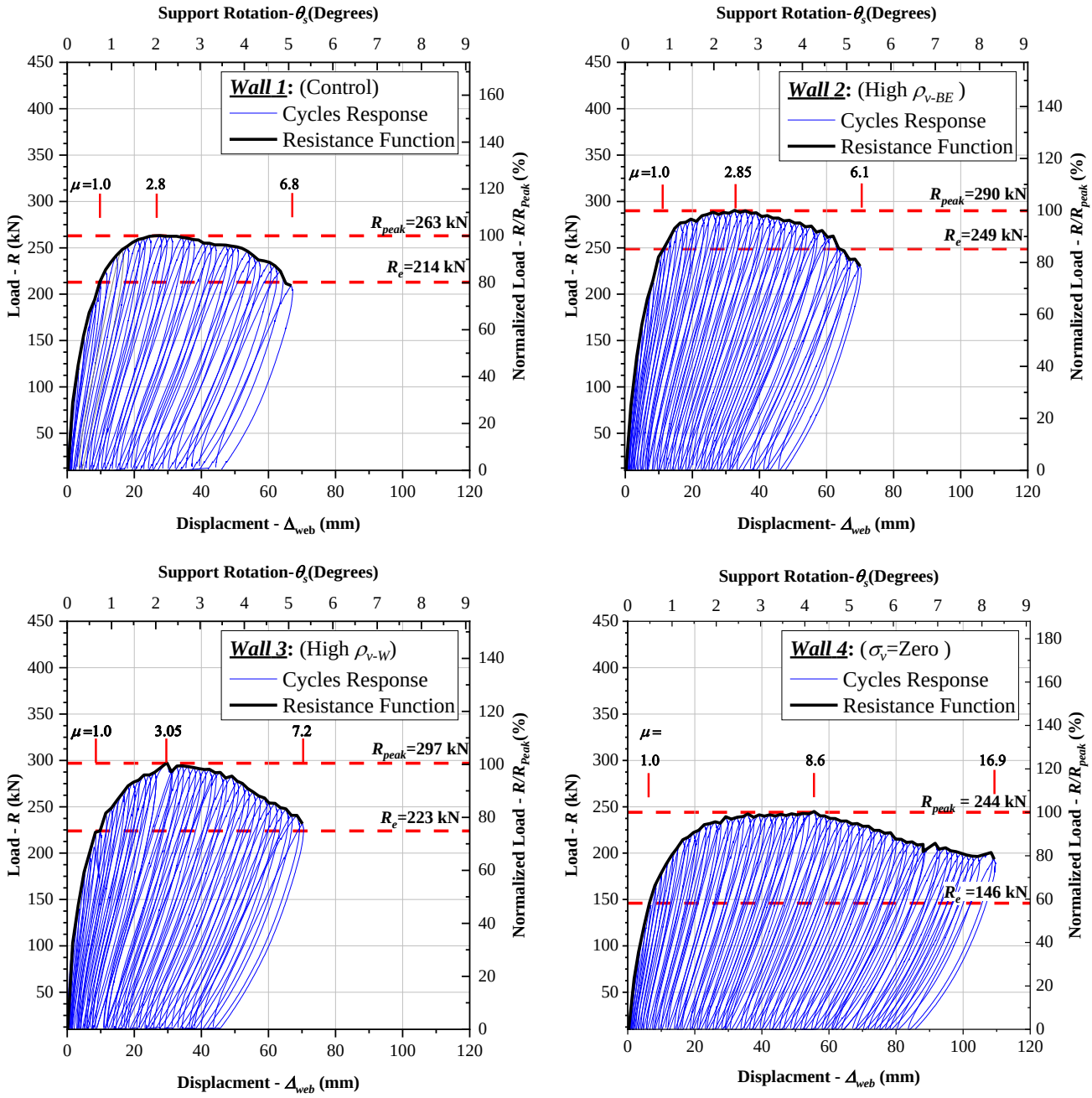

Fig 3.11. . Wall hysteretic load-displacement/rotation relationships

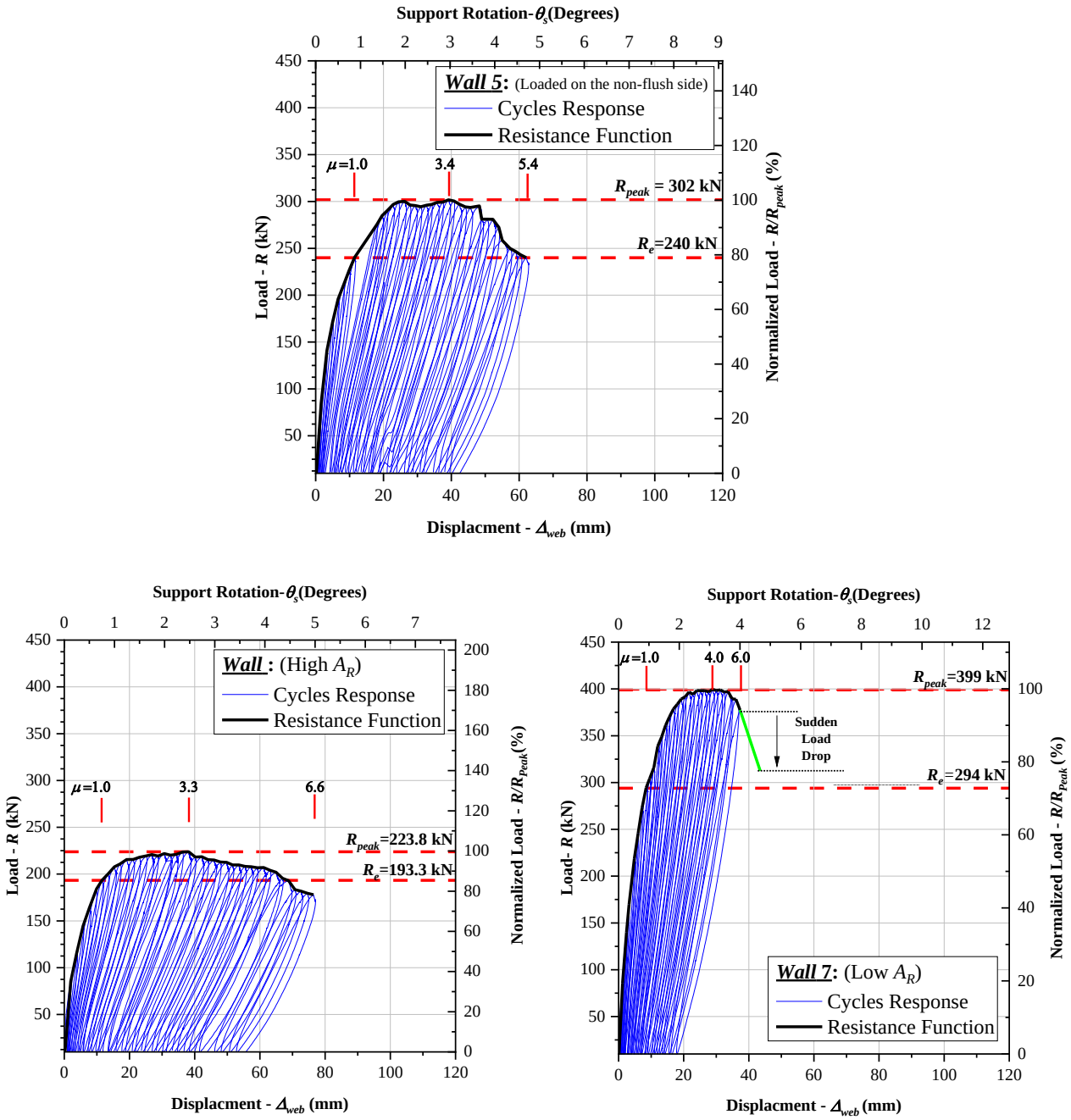

Fig 3.11(Cont). . Wall hysteretic load-displacement/rotation relationships.

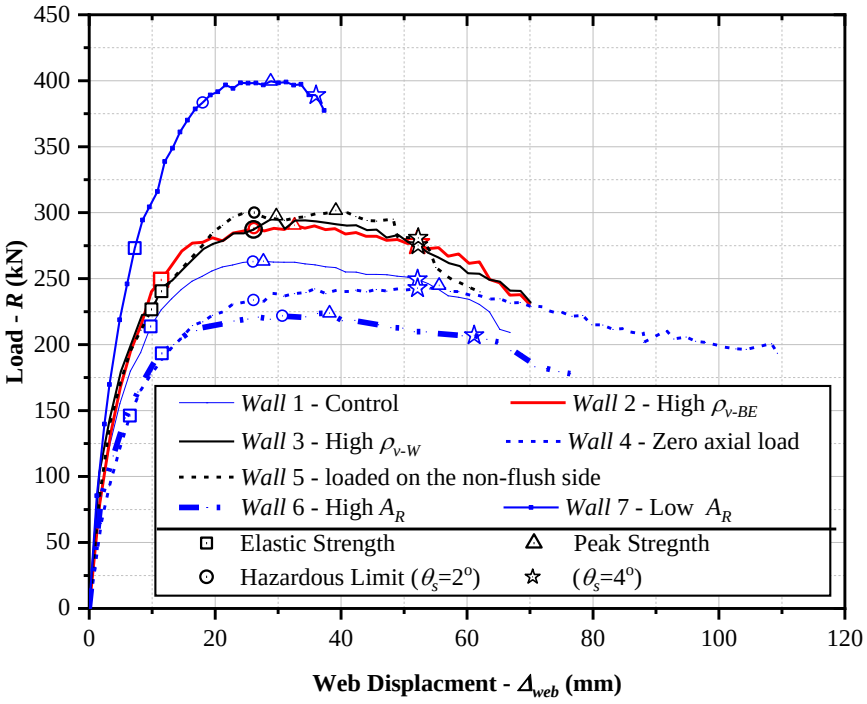

Fig 3.12. Walls resistance functions

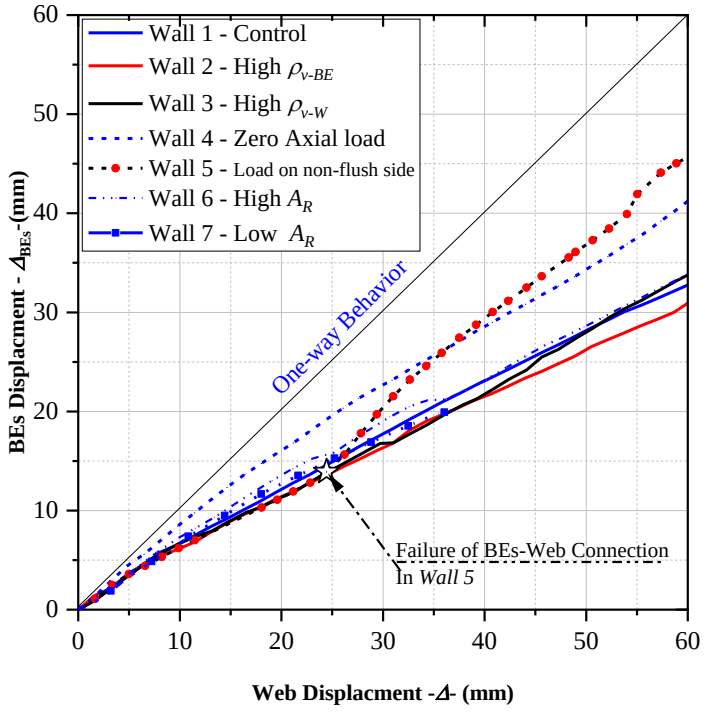

Fig 3.13. Relation between wall BEs and web displacements

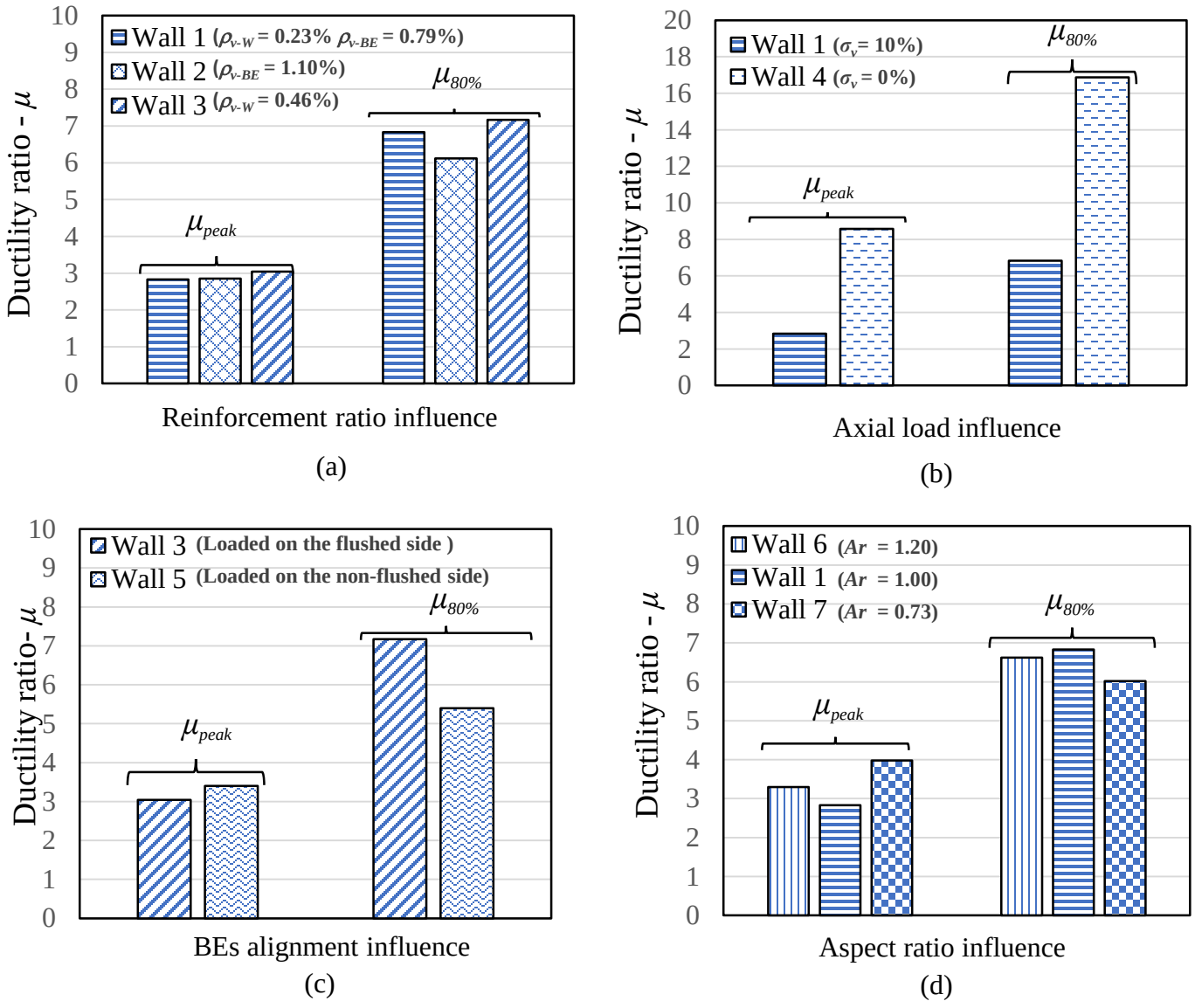

Fig 3.14. Effect of wall design parameters on ductility

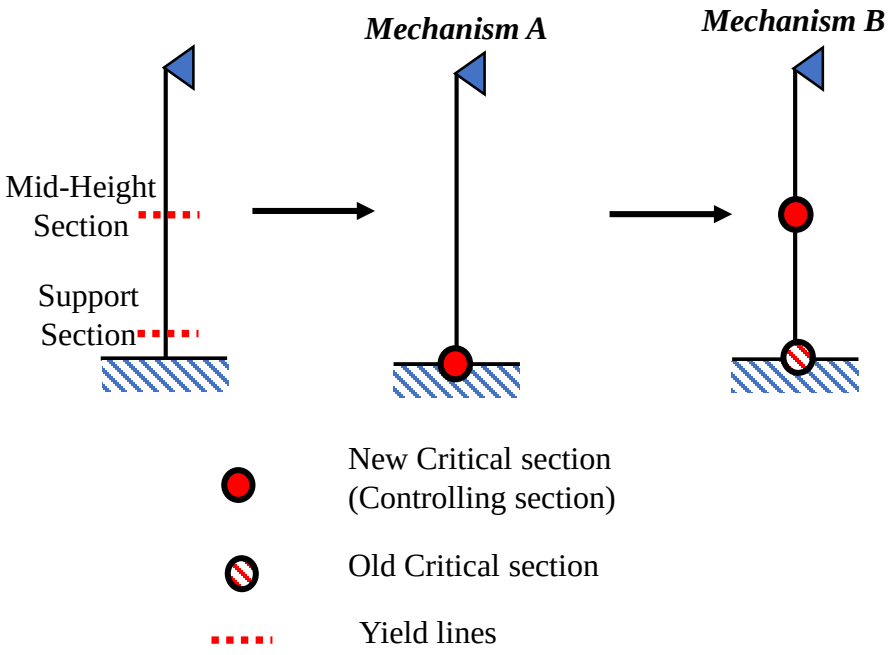

Fig 3.15. Response mechanisms of *Approach I*

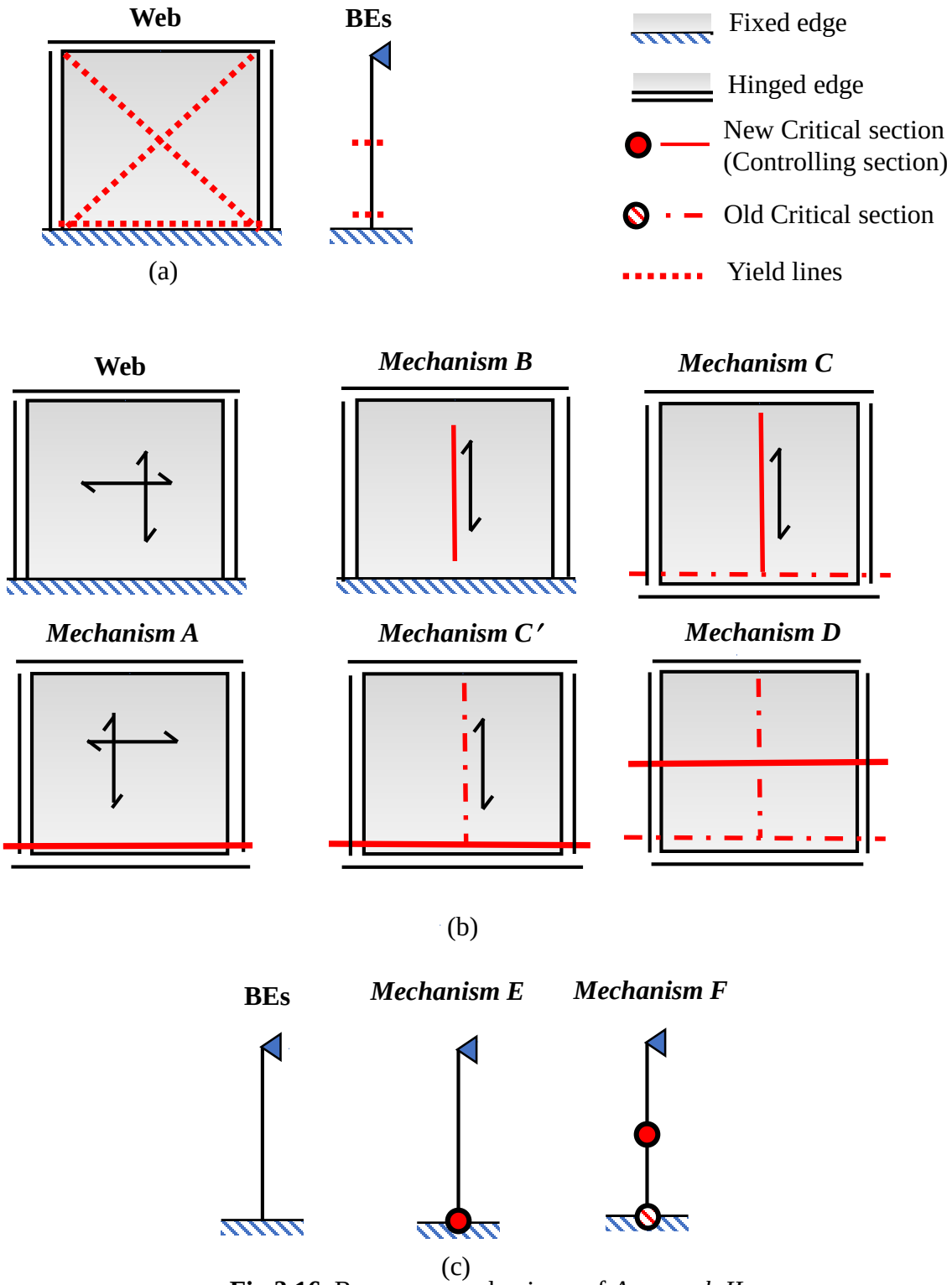

Fig 3.16. Response mechanisms of *Approach II:*
(a) Expected Yield lines; (b) Web Mechanisms and (c) BEs Mechanisms

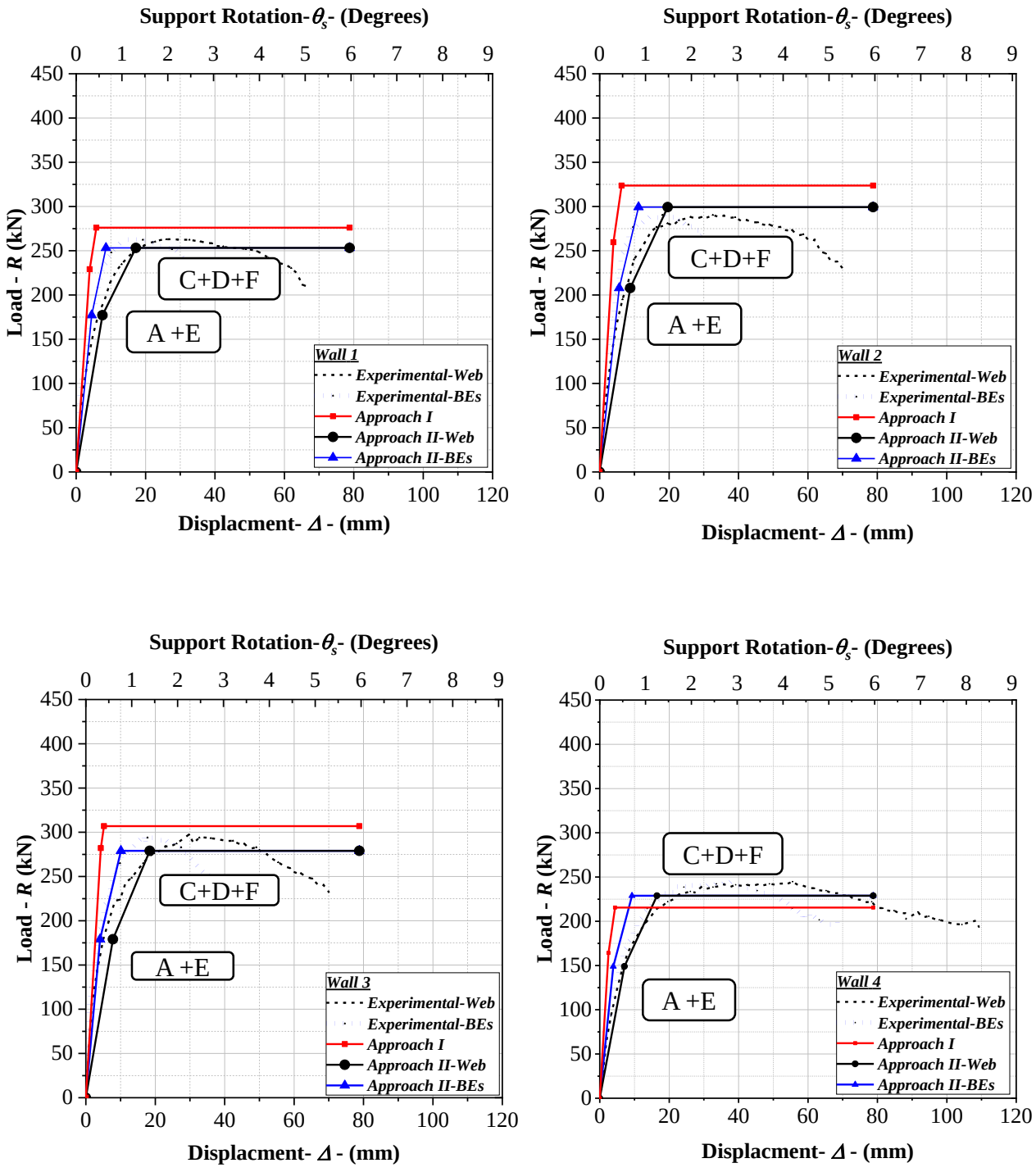

Fig 3.17. Analytical and experimental (resistance functions and predicted mechanisms)

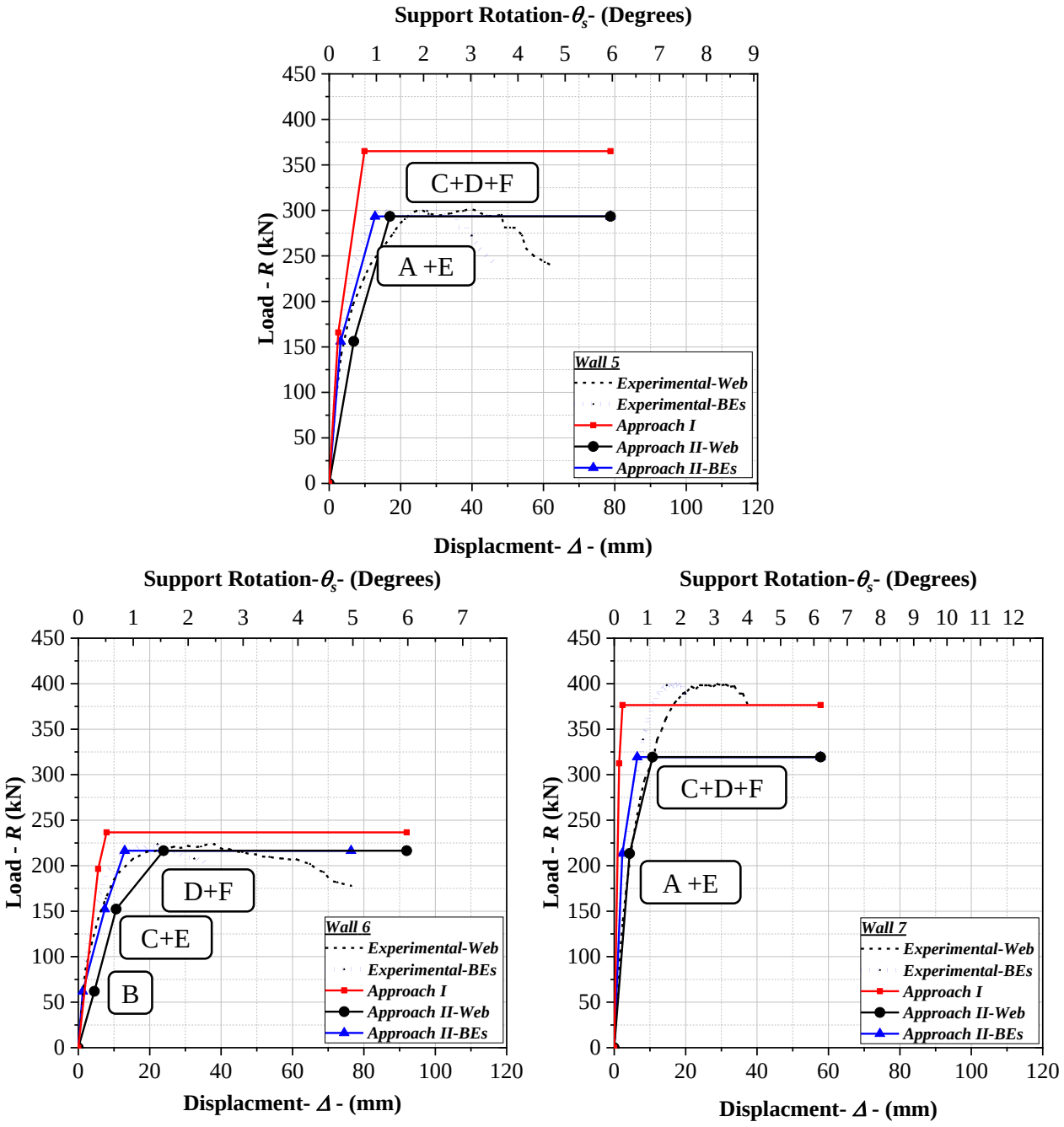

Fig 3.17 (Cont). Analytical and experimental (resistance functions and predicted mechanisms)

CHAPTER 4
REINFORCED MASONRY WALL BLAST RESPONSE LIMITS FOR ASCE 59 AND CSA S850

4.1. ABSTRACT:

The current blast response limits for reinforced masonry walls in North American blast standards (e.g. ASCE 59-11; CSA S850-12) are based on parameters (e.g. support chord rotation) that account for neither the wall ductility capacities nor the influence of different design configurations on the wall damage tolerance levels. For example, reinforced masonry shear walls with boundary elements present a promising blast resisting system due to their enhanced out-of-plane characteristics (e.g. strength and ductility) compared to those of reinforced masonry walls with typical rectangular cross sections. However, the aforementioned standards do not assign separate design requirements or response limits for this new system due to the limited number of relevant experimental and analytical studies available at the time the standards were being developed. To address this knowledge gap, the current study focuses on evaluating the blast response of reinforced masonry shear walls with different configurations and subsequently proposing new related blast response limits for ASCE 59 and CSA S850. In this respect, a finite element model was developed and validated against the results of several previous experimental programs under quasi-static and blast loads. Subsequently, the new response limits were generated using the model and compared to those currently provided by ASCE 59-11 and CSA S850-12 using pressure-impulse diagrams. Finally, the blast

response of reinforced masonry walls without and with boundary elements was evaluated when subjected to different blast scenarios. The results of the current study highlight the blast-resistance enhancements that boundary elements can provide to reinforced masonry shear walls at different damage states and the need to develop category-specific blast response limits within blast design standards.

4.2. INTRODUCTION

Blast-induced demands on structural systems are quite different from those corresponding to seismic loads (NRC 2003; Zhang and Phillips 2016). More specifically, a seismic ground excitation induces forces that are distributed on a structural system based on the mass and stiffness of each component within such a system. Conversely, blast demands affect specific components according to their locations and stand-off distances from the shock wave source (FEMA 2010). Therefore, reinforced masonry (RM) shear walls, designed and detailed to resist in-plane seismic loadings, can be vulnerable to blast loadings on their out-of-plane (i.e. lower stiffness) direction (ElSayed et al. 2015). This is because, unlike in their in-plane direction, these seismically-detailed walls do not necessarily have an adequate ductility capacity to sustain high blast demands in their out-of-plane direction. For this reason, the ASCE 59-11 for blast protection of buildings (ASCE 2011) has indicated in the commentary to Clause 9.2.7.1 regarding *reinforced concrete* walls that "for walls providing gravity load support to beams, columns and slabs, it is recommended that they be constructed with columns at each end of the wall and a beam at each floor level that spans between the columns." In *reinforced*

masonry construction, such walls are termed RM walls with boundary elements (BEs).

Fully grouted RM walls with BEs, shown in Fig. 4.1 (a), were previously reported (e.g. Shedid et al. 2010a; Shedid et al. 2010b; Banting and El-Dakhakhni 2014; Ezzeldin et al. 2017) to have enhanced in-plane seismic performance compared to their conventional counterparts without BEs (i.e. with rectangular cross sections). This is because BEs configuration allows the use of multiple layers of vertical reinforcement confined by steel ties, as shown in Fig. 4.1(b). This configuration increases the masonry maximum compressive strain capacity and subsequently the curvature ductility of the wall cross section. Based on these capacities, the most recent masonry design Canadian standards CSA S304-14 (CSA 2014) have established unique design requirements for RM shear walls with BEs to consider the enhanced seismic performance of such walls.

Very limited studies however have been conducted to investigate the out-of-plane performance of RM walls with BEs (e.g. Simonds 2014; El-Hashimy et al. 2018 and 2019). These studies demonstrated that BEs partially restrained the vertical edges of the wall web, thus enabling the horizontal reinforcement to transfer the applied out-of-plane loads and forming a two-way bending mechanism within the wall web (Simonds, 2014). El-Hashimy et al. (2018) reported also that RM walls with BEs, when subjected to out-of-plane static load demands, experienced different response limits and damage states than those experienced by walls without BEs.

Blast design standards in the United States (ASCE 2011) and Canada (CSA 2012) allow the use of equivalent single-degree-of-freedom (SDOF) models to simulate structural components (e.g. walls) subjected to blast (Mays and Smith 1995; Krauthammer et al. 1999; Krauthammer 1999; Bangash and Bangash 2006). However, there are some limitations associated with such models that may result in inaccurate predictions, as discussed by El-Dakhakhni et al. (2010). For example, for two-way components, such as RM walls with BEs, the ultimate strength can be inaccurately predicted because multiple yield line patterns and corner effects are typically neglected when simplified SDOF models are adopted. In addition, localized failure modes such as torsional damages in the BEs and BEs-web connection failures (El-Hashimy et al. 2019), discussed in the previous chapter, are not explicitly simulated in an equivalent SDOF model (Li and Hao 2011).

Alternatively, finite elements (FE) models can be used to more accurately describe a wall's geometrical details, boundary conditions, and material properties. For example, fiber beam elements were used to simulate the behavior of reinforced concrete members when subjected to localized blast loads (Li et al. 2016). However, their inability to capture shear deformations restricted their applications to further blast studies. Recently, a multi-layer shell element model was proposed by Lu et al. (2011) to simulate the behavior of reinforced concrete shear walls when subjected to seismic demands. The model can capture the coupled in-plane/out-of-plane bending demands taking into account the shear behavior (Lu et al. 2015). El-Hashimy et al. (2018) utilized this layered shell element model to simulate the out-of-of plane response of RM wall with BEs when subjected to out-of-plane quasi-

static demands. The model showed good agreement with the experimental results in terms of wall resistance and displacement response.

The response limits provided by the current blast standards (ASCE 2011, CSA 2012), for the different damage state, can be assessed using pressure-impulse (P-I) diagrams. Such diagrams visualize a component's response to a range of pressure and impulse combinations corresponding to a specific damage state (Baker, 1983; Krauthammer, 2008; Dusenberry, 2010). In this respect, ASCE (2011) and CSA (2012) currently assign unique response limits (e.g. support chord rotation) for each damage state (i.e. Superficial, Moderate, Heavy and Hazardous). However, these limits may not be accurate as they do not account for the different ductility capacities that structural components may posess when different design configurations are adopted. For example, RM walls with BEs typically achieve a higher level of ductility, compared to a RM wall without BEs, and subsequently have chord support rotations that surpass the current limits for the Hazardous damage state (El-Hashimy et al. 2019). To account for the various ductility capacities, NIST (2010) recommended the adoption of wall curvature demands to represent the correpsonding damage states, in which a wall failure, realized through excessive crushing, and/or rupture/buckling of flexural reinforcement, can be successfully evaluated using such limits. For this reason, the current study proposes new blast response limits based on the underlying wall curvature capacity.

The main objective of the current study is to propose new blast response limits using the developed model to consider the wall curvature capacity. In this respect, the SDOF model developed by the Protective Design Center of the U.S. Army

Corps of Engineers PDC-TR 06-08 (2008) was first used and compared to the experimental results of RM walls with BEs under field explosions reported in previous studies. Afterwards, a FE model was constructed using *OpenSees* (McKenna et al. 2013) and validated using seventeen blast loaded RM walls with different configurations and blast load scenarios. Finally, The new limits were evaluated and compared to their current counterparts in the ASCE 59-11 and CSA S850-12 through developing P-I diagrams for RM walls without and with BEs.

4.3. SINGLE-DEGREE-OF-FREEDOM MODEL

SDOF models are commonly used for blast analysis (Mays and Smith 1995, Krauthammer 2008, Bangash and Bangash 2006), given the fact that an equivalent system (i.e. in terms of mass and stiffness) can represent the dynamic response of a structural component and its corresponding failure modes (CSA 2012). Since RM walls with BEs have been shown to experience a two-way bending mechanism due to the restraints provided by the BEs (e.g. Simonds 2014), their simulation as a SDOF model can be challenging (El-Dakhakhni et al. 2010). To investigate this behavior, the experimental results of eight RM walls with BEs, tested under live explosives by Simonds (2014) through different scaled distances, were compared to their analytical response prediction using the *SBEDS* (Single-degree-of-freedom Blast Effects Design Spreadsheet) software PDC-TR 06-08 (2008), originally developed by the Protective Design Center of the U.S. Army Corps of Engineers, and following the provisions of the UFC 3-340-02 (USDOD 2008) in analyzing RM walls with different boundary conditions.

The eight one-third scaled RM walls with BEs were all simply supported. The walls were divided into three sets (each set comprised walls with different designs) with each set subjected to a different scaled distance, *Z*, that ranged from 2.76 to 1.62 m/kg$^{1/3}$. Table 4. 1 summarizes the wall dimensions, vertical, horizontal and BEs reinforcement ratios (ρ_v, ρ_h and $\rho_{v\text{-}BEs}$), masonry compressive strength (f'_m), and reinforcement yield strength (f_y).

To properly simulate a structural component by a SDOF model, a resistance function (i.e. load-displacement relationship) is required. However, the partial restraint provided by the BEs cannot be accurately represented by *SBEDS*. Therefore, the walls were analyzed using a plastic analysis, as discussed in chapter 3, to evaluate their resistance functions, as shown in Fig. 4.2, and the dyanamic increase factors, DIFs, provided by North American standards (ASCE 2011) were used to account for the strain rate effects (i.e. defined as the change in strain developed per time).

The SBEDS results were compared with the experimental tests, as presented in Table 4. 2. Although walls subjected to blast waves with *Z* value of 2.76 m/kg$^{1/3}$ had an average deviation of 9.5 %, when *Z* decreased to 2.2 m/kg$^{1/3}$ and 1.62 m/kg$^{1/3}$ (i.e. the blast load increased), walls had average deviation of 25.7% and 67.0%, respectively. The deviation in *SBEDS* predictions are mainly attributed to the limited details in the simplified SDOF model that does not consider the damage sequence of different wall components (i.e. web and BEs) with different modes of failure. In addition, the existence of partial restraints by the BEs further limited the

accuracy of the SDOF model. The following sections describe the FE model used to overcome these limitations.

4.4. FINITE ELEMENT MODEL DESCRIPTION

Several FE models have been developed in the literature to predict the out-of-plane behavior of different wall types (Eamon et al. 2004; El-Dakhakhni et al. 2010; Syed et al. 2018; Choi et al. 2018). According to Cerioni and Donida (1994) and Hallinan and Guan (2007), layered elements are one of the most effective FE models that can account for both flexural and shear deformations. A layered FE model was recently utilized to simulate the out-of-plane response of unreinforced (Noor-E-Khuda et al. 2016) and reinforced (El-Hashimy et al. 2018) masonry walls. The latter study used *OpenSees* (McKenna et al. 2013) to simulate the out-of-plane load-displacement relationship (i.e. resistance function) of non-load bearing RM walls without and with BEs under quasi-static load. In the current study, the model was further extended to simulate the out-of-plane dynamic response of load-bearing walls when subjected to blast loading demands, in order to evaluate blast response limits, as will be discussed next.

4.4.1. Material Models

In the current study, the fully grouted concrete masonry material was modelled based on the model developed by Lu et al. (2015), adopting the smeared crack approach based on the crack band theory (Bazant and Oh 1983). Since the masonry material within the BEs area are confined by steel ties, the model by Mander et al. (1988) was used to calculate the enhanced compressive strength and strain within

the BEs confined area (Ezzeldin et al. 2016; El-Hashimy et al. 2018). The reinforcement steel was modelled as an equivalent thickness of steel layer with a uniaxial bilinear elastoplastic material model. Full details about the material formulation are presented by Lu et al. (2015) and El-Hashimy et al. (2018).

4.4.2. Model Geometry

Four-node multi-layer shell elements (SHELLMITC4 in *OpenSees*) (Lu et al. 2015) were used for the wall, as shown in Fig. 4.3(a). The cross sections of these shell elements were divided into multiple layers, where materials (i.e. masonry, horizontal and vertical reinforcement) were assigned to different layers according to its corresponding location within the wall, as shown in Fig. 4.3(b). The shell elements were restricted to a square shape to ensure equivalent distribution of strain in both vertical and horizontal directions (Bazant and Oh, 1983). As for the gravity loads, several research studies demonstrated their significant influence on the displacement ductility of load-bearing RM walls (e.g. Shedid et al. 2009; El-Hashimy et al. 2019). Therefore, point loads were introduced to each node at the top of the model in the gravity direction.

Due to the two-way bending mechanism associated with RM walls with BEs (Simonds 2014), BEs would twist to maintain compatibility with the wall web. This behavior develops flexural moments at the BEs-web connection and torsional moments on the BEs. However, if the torsional moments exceed the BEs cracking torsional capacity, cracking develop and the torsional stiffness of the BEs diminishes rapidly and subsequently, internal forces are redistributed within the

wall web. In other words, loads carried by the web in the horizontal direction are redistributed to the vertical direction (El-Hashimy et al. 2019). Similar behavior was reported in studies on spandrel beams (e.g. Collins and Lampert 1973). To simulate such behavior in the developed model, rotational springs were introduced to the nodes at the BEs-web connection, as shown in Fig. 4.3(a). Each spring was modeled as a zero-length plastic spring, following a bilinear response based on the web's horizontal rotational stiffness, K_θ, calculated using mechanics base elastic analysis and the cracking torsional moment capacity, $M_{\tau cr}$, of the BEs predicted using ACI 318M-14, as shown in Fig. 4.3(c).

4.4.3. Quasi-Static Model Validation

The developed model was initially validated using the experimental results of fully grouted RM walls without (Salem et al. 2019) and with (El-Hashimy et al. 2019) BEs under a quasi-static out-of-plane loading. These experimental programs were selected because they included walls with a wide range of reinforcement ratios and distributions, as well as different axial load levels. Table 4. 3 summarizes the RM wall dimensions, vertical, horizontal and BEs reinforcement ratios (ρ_v, ρ_h and $\rho_{v\text{-}BEs}$), masonry compressive strength (f'_m), reinforcement yield strength (f_y) and equivalent axial stress ratio on the wall cross-section (σ_{axial}). In both the model and experiment, the out-of-plane distributed loads were applied through nine-point loads on the wall.

To investigate the sensitivity of the model to the introduced rotational springs at the BEs-web connection, *Wall 2* was modelled without and with

rotational springs. Both model results were then compared to the experimental responses of the web and BEs, as shown in Figs. 4.4(a and b), respectively. As can be seen in Fig. 4.4(a), the influence of the rotational springs on the web displacement response was minor, as both models (i.e. without and with rotational springs) were able to capture the web displacements throughout the test with deviations of 13.0% and 3.2%, respectively. However, the displacement response of the BEs was accurately predicted only when rotational spring were used, as shown in Fig. 4.4(b). For example, without rotational springs model overestimated the BE displacement at degradation to 80% of ultimate resistance with a deviation of 65.0%, whereas the model with rotational springs captured the same displacement with a deviation of 17.0%. These results clearly demonstrate the importance of considering torsion when the out-of-plane behavior of RM walls with BEs is simulated.

Figure 4.5 compares the resistance functions of all walls using the developed model with the corresponding experimental results. The model was capable of predicting the wall ultimate resistances, with maximum deviations of 16.0% and 6.6% for the walls without and with BEs, respectively. In addition, the model accurately captured the displacement responses at the wall mid-heights throughout the test. For example, the displacement corresponding to the wall ultimate resistance was predicted with maximum deviation of 11.0% for RM walls without BEs and of 10.5% and 19.0% for RM walls with BEs at the wall web and BEs, respectively.

4.4.4. Dynamic Model Description

In addition to the above static model features, the dynamic model also accounted for the simulated blast load/wave and the strain rate effect on the material (i.e. masonry and reinforcement) properties. The damping effects were also considered through Rayleigh damping formulation, with damping ratio of 5% as suggested by CSA S850-12 (CSA 2012).

The blast wave is generally defined by a sudden rise in pressure that decays with time and distance. The pressure-time pulse signature is typically divided into two phases: 1) a positive phase, where the incident/reflected pressure immediate rise drops to its ambient value (USDOD 2008); and 2) a negative phase, where the pressure decreases below the ambient pressure. This negative phase is typically not considered in blast design (Krauthammer 2008) due to its low pressure (i.e. absolute magnitude) and long duration relative to those of the positive phase, as it also results in an overall lower impulse. As shown in Fig. 4.6, the positive phase is characterized by a peak pressure (P_o), and an impulse (I_o), where the latter is evaluated through the integration of the pressure over the blast pressure wave duration (t_d).

Blast wave parameter values are accompanied by a high level of uncertainty, as reported by Campidelli et al. (2015). As such, a simple idealization of the positive phase, provided by Biggs (1964) (i.e. triangular load), was implemented in the model using a time-series load object in *OpenSees*, as shown in Fig. 4.6. Finally, since the current study investigates only far-field blast loads (i.e. scaled distance

equal to or greater than 1.2 m/kg$^{1/3}$ (ASCE 2011)), the pressure was considered to be uniformly distributed on the underlying walls (ASCE 2011; CSA 2012; USDOD 2008). Subsequently, the blast wave was simulated uniformly on the wall surface in the out-of-plane direction. The magnitude of such wave changed with time according to predefined pressure-time series.

Impulsive loads (e.g. blast waves) are characterized by a short loading duration, leading high strain rates to develop in the material. Since materials typically experience enhanced properties at such loading rate (Bischoff and Perry 1991; Malvar 1998), ASCE 59 (2011) and CSA S850 (2012) consider this by assigning DIFs, for each material. To account for strain rate effects in the current study, expressions relating the strain rate to the steel yield strength (Malvar 1998) and concrete compressive strength (Wei and Hao, 2009) were used at each shell layer within the developed model.

The dynamic time-step analysis included an iterative procedure to account for the DIFs, as shown in Fig. 4.7. Initially, the analysis was performed assuming static material properties (i.e. DIFs are equal to 1.0). At the yielding strain of the wall web center, the strain rate was calculated and new DIFs were estimated (Malvar 1998; Wei and Hao 2009). Subsequently, the analysis was repeated using the new DIFs until the assumed and resulting strain rates converged.

4.4.5. Dynamic Model Validation

Seventeen walls with three different configurations and RM walls boundary conditions were used to validate the developed model. The first configuration

consisted of five RM walls without BEs (ElSayed et al. 2015) as shown in Fig. 4.8(a), while the second configuration contained eight RM walls with BEs as shown in Fig. 4.8(b) (Simonds 2014). The third configuration comprised of four walls that were supported at their corners to represent infill wall panels as shown in Fig. 4.9(c) (Smith et al. 2016). Tables 4.1 and 4.4 summarize the wall vertical and horizontal reinforcement ratios (ρ_v, ρ_h), masonry compressive strength (f'_m), and reinforcement yield strength (f_y) of all the test walls. All the walls were one-third scale fully-grouted RM walls and were subjected to far-field explosive charges that had different scaled distances ranging from 1.6 to 2.75 m/kg$^{1/3}$. During the validation of the dynamic model response, the blast wave (i.e. pressure-time response history) produced by these charges was used as a time-series load in *OpenSees* according to the corresponding experimental study.

The model predictions were compared to the experimental results in the current study in terms of wall deformations and damage. The out-of-plane wall deformed shape was predicted accurately for the different boundary conditions, as shown in Fig. 4.9. To evaluate the model, Table 4.5 presents the model maximum displacements at the wall center, Δ_{web}, and BEs, Δ_{BEs}, along with deviations relative to the experimental results. The model was able to capture the experimental maximum displacements with maximum deviations of 22 %, 24 % and 16 % for RM walls without and with BEs and the Infill panels, respectively.

For the same walls, Figs. 4.10 (a and b) show the model strain distribution in the vertical and horizontal directions at the wall maximum displacement, respectively. Since high compression strains (i.e. in 0.003) indicate the possibility

of crushed concrete (CSA 2014), Figs. 4.10 (a and b) were compared to the experimental wall damage, as shown in Fig. 4.11. For example, the model showed higher compression strains concentration at the BEs areas relative to those at the wall web. These results demonstrate that extensive crushing occurred at the BEs, which is in good agreement with the experimental results, as shown in Fig. 4.11 (b).

The DIFs for the masonry and reinforcement bars, at yielding of the first reinforcement layer, were compared with their counterparts in the blast standards (ASCE 2011, CSA 2012). The results indicated that the reinforcement bar layers had an average DIFs of 1.30 and a low coefficient of variation (C.O.V) of 0.01. Meanwhile, DIFs at the extreme compression masonry layers had an average of 1.24 with a relatively higher C.O.V of 0.31. Based on the above, it is deemed acceptable to use the DIF values suggested by the standards (i.e. 1.20), should the duration of the analysis need to be reduced.

4.5. ASSESSMENT OF ASCE 59-11 AND CSA S850-12 RM BLAST RESPONSE LIMITS

4.5.1. Damage States and Response limits

As mentioned earlier, both ASCE 59-11 and CSA S850-12 quantify the damage states of a structural component under blast through predefined response limits. The standards indicate that a RM wall, subjected to flexural and axial load demands, will experience only a *Superficial* damage state when the displacement ductility reaches unity, (i.e. the wall is essentially, elastic with its reinforcement starting to yield), while a *Hazardous* damage state is reached when the support chord rotation

exceeds 2°. These fixed response limits clearly do not consider the different out-of-plane capacities for different wall configurations (El-Hashimy et al.,2018).

In the current study, new blast response limits are proposed and compared to their counterparts currently assigned in the ASCE 59-11 and CSA S850-12 to RM walls without BEs, which are currently also implicitly applicable to walls with BEs as no other separate limits are available. The new limits are all based on the curvature capacity of the underlying wall cross section to account for its ductility and subsequently show different levels of damage when different wall configurations are subjected to similar support chord rotation demands. More specifically, based on the developed FE model, three curvature capacities were selected to represent three damage states, namely *Slight*, *Intermediate* and *Severe* damage states. These damage states are reached when a wall critical cross section reaches a curvature that corresponds to 80% of ultimate resistance ($\phi_{80\%ult}$), ultimate resistance (ϕ_{ult}) and 20% ultimate resistance degradation ($\phi_{20\%deg}$), respectively.

4.5.2. Pressure-Impulse (P-I) Diagrams

P-I diagrams can be effectively used to assess the response of structural components at predefined damage states (Baker et al. 1983). A P-I diagram for a specific structural component contains a series of curves, each representing a specific response limit, at different pressure and impulse combinations demands. Such response can be divided into three regimes based on the loading duration: 1) an impulsive regime; 2) a dynamic regime; and 3) a pressure regime. As such, and shown in Fig. 4.12, a P-I diagram has two asymptotes (Impulse- and Pressure-

controlled) and a transition zone in between, where both impulse and pressure affect the response, as discussed by Baker et al(1983).

Figure 4.13 outlines the procedure adopted to construct the P-I diagram for a certain response limit (Δ_{target}). Initially, for a given set of blast wave properties (i.e. P_o and t_d at I_o), the FE model evaluates the wall response, Δ_o. Then, based on the difference between Δ_o and Δ_{target}, P_o is changed while maintaining the same I_o. The analysis is thus repeated until convergence occurs. At this point, P_o and the corresponding I_o mark one point on the P-I diagram. The whole procedure is then repeated for different impulse demands. Further information about the development of these P-I diagrams can be found in the literature (Baker et al. 1983; Krauthammer 2008; El-Dakhakhni et al. 2010; Parlin et al. 2014).

4.5.3. Model Walls Description

To assess the proposed response limits, six model walls were designed according to the TMS-402 (2016), as shown in Fig. 4.14. These six walls included RM walls without and with BEs that had similar in-plane flexural capacities to facilitate direct comparisons, as presented in Table 4.6. The walls were designed to have a ductile flexural failure in the in-plane direction, and therefore, all walls were categorized according to TMS-402 (2016) as *Special* RM shear walls except Wall *WR3* which is described as an *Intermediate* shear wall. In all cases, none of the walls were explicitly designed to resist any specific blast loads in their out-of-plane direction. All walls had the same length and height (i.e. 3.00 m) and were assumed to be constructed using the standard North American concrete block dimensions (i.e. 190

x 190 x 390 mm). All walls were uniformly loaded in the out-of-plane direction, and also subjected to axial compression stresses equivalent to 5% of their corresponding axial compressive strengths.

As shown in Table 4.6, Walls *WR1* and *WB1* had the lowest vertical reinforcement ratios of 0.30% and 0.17%, respectively, with an average flexural in-plane capacity of 1812 kN.m. Walls *WR2* and *WB2* had vertical reinforcement ratios of 0.75% and 0.45%, respectively, which increased their average in-plane flexural capacity to 2980 kN.m. Finally, Walls *WR3* and *WB3* had the highest vertical reinforcement ratios of 1.25% and 0.72%, respectively, with flexural in-plane capacity of 4054 kN.m. As can be seen in Table 4.6, all RM walls with BEs had lower reinforcement ratios than their corresponding walls without BEs by 40% on average, although they had similar in-plane flexural capacities.

The developed FE model was used to evaluate the out-of-plane resistance function of these walls until a degradation to 20% of the ultimate resistance was achieved for each. The DIFs assigned by the ASCE 59-11 were included to account for the strain rate effects. The curvature values of the critical cross-section were evaluated at the different response levels, as presented in Table 4.6, and subsequently used to generate the P-I diagrams of each wall at the corresponding damage states (i.e. *Slight*, *Intermediate* and *Severe*).

4.5.4. Analysis Results

The proposed response limits were compared to the existing limits through the pressure and impulse capacities (i.e. the asymptote values of a P-I diagram for a

specific response limit). Since the out-of-plane ductility capacity at 20% ultimate resistance degradation (μ_{out}) of RM walls with BEs ranged from 14.3 to 3.5, as presented in Table 4.6, the deviation between the *Intermediate* and *Severe* damage states (i.e. reaching the curvature corresponding to the ultimate resistance and the 20% resistance degradation) is significant, as shown in Fig. 4.15. For example, Wall *WB1* (ρ_v = 0.17%) with a ductility capacity of 14.3 suffers a *Severe* damage state that exceeds its *Intermediate* damage state by 48% and 152% for the pressure- and impulse asymptotes, respectively, whereas these values diminish to only 4% and 15%, respectively, in Wall *WB3* (ρ_v = 0.72%) due its low ductility capacity of 3.5. Alternatively, since RM walls without BEs had significantly lower out-of-plane ductility capacities, as presented in Table 4.6, Wall *WR1* (for example) reaches a *Severe* damage state at pressure and impulse asymptotes that are approximately 14% and 56% higher, respectively, than those corresponding to its *Intermediate* damage state, as shown in Fig. 4.16.

As shown in Fig. 4.15, Walls *WB1* and *WB2* suffer a *Hazardous* damage state before even reaching their 20% strength degradation (i.e. *Severe* damage state). Conversely, Wall *WB3* endures the *Hazardous* damage state with pressure and impulse demands that exceed its *Severe* damage state by 13% and 32%, respectively. The above analysis results clearly demonstrate the inconsistency of ASCE 59-11 and CSA S850-12 limits in assessing the wall damage.

From a different prospective, when the response of Wall *WR3* (ρ_v = 1.25%), categorized as an intermediate RM shear wall according to TMS-402 (2016) in the

in-plane direction, is evaluated against the ASCE59-11 limits, both *Superficial* and *Hazardous* P-I diagrams coincided as shown in Fig. 4.16. This is because the wall suffers a brittle failure (i.e. no flexural reinforcement yielding) accompanied by loss of wall resistance prior to the support chord rotation reaching the *Hazardous* response limit of 2 degrees. This further demonstrates the drawbacks of the blast response limits currently assigned by ASCE 59-11 and CSA S850-12 to assess RM walls with different reinforcement ratios.

Finally, a comparison between the six RM walls has been conducted using the proposed damage states to show the performance enhancements through the P-I diagram when BEs configuration is utilized in RM walls. As shown in Fig. 4.17, RM walls with BEs have higher pressure and impulse capacities than those of RM walls without BEs at the different proposed damage states. For example, as shown in Fig. 4.17(a), Wall *WB1* attains higher pressure and impulse asymptotes than Wall *WR1* by 224% and 145%, respectively, at the *Slight* damage state. These enhancements are similarly observed at higher damage states, as shown in Fig. 4.17(c), where as Wall *WB1* pressure and impulse asymptotes are higher than Wall *WR1* by 361% and 332%, respectively. The difference between the performance of both wall configurations is mainly attributed to the dual layer of reinforcement that exists within the BEs. This clearly demonstrates that RM walls with BEs provide a promising blast resisting construction system compared to traditional RM wall systems with rectangular cross-sections.

4.6. CONCLUSIONS

In this study, the out-of-plane behavior of fully grouted RM walls without and with BEs under far-field blast loading demands was numerically evaluated. In this respect, a SDOF analysis for eight walls using SBEDS was carried out and compared to their counterparts, tested under previously reported field explosions. The displacement response predicted by a simplified SDOF resulted in a deviation that increased as the scaled distances decreased. This deviation was mainly attributed to the limited details in the SDOF model that did not consider the BEs-Web connection and the damage sequence of the web and BEs at different locations. As such, a FE model was developed to simulate the blast response of RM walls, considering the strain rate effects within wall materials. The model was then validated to capture the displacement response and crack pattern of seventeen RM walls with different design and support configurations. The model was capable of capturing the experimental wall displacement response and deformed shape through the different selected scaled distances. The analysis results also indicated the capability of the model of capturing the wall's post ultimate response and the corresponding crushing damage.

In addition, to quantify the performance of RM walls with BEs relative to those without BEs, new response limits, based on the wall curvature capacity at different resistance levels, were proposed and subsequently compared to those currently in ASCE 59-11 and CSA S850-12. The results showed that the proposed blast response limits better represent the different damage states, for the different

wall configurations. For example, unlike the current blast response limits in ASCE 59-11 and CSA S850-12, the proposed limits are applicable to identify the damage states for components with low out-of-plane ductility capacities (i.e. RM walls without BEs and/or with high reinforcement ratios). Finally, the pressure and impulse capacities corresponding to the different damage states increased significantly when RM walls without BEs were replaced by RM walls with BEs with similar in-plane flexural capacities.

4.7. ACKNOWLEDGMENTS

The financial support for this project was provided by the Natural Sciences and Engineering Research Council (NSERC) of Canada. Support was also provided by the McMaster University Centre for Effective Design of Structures (CEDS), funded through the Ontario Research and Development Challenge Fund (ORDCF) of the Ministry of Research and Innovation (MRI). Provision of mason time by the Ontario Masonry Contractors Association (OMCA) and the Canada Masonry Design Centre (CMDC) is appreciated.

4.8. NOTATION

The following symbols are used in this paper:

f'_m	=	Specified masonry strength;
f_y	=	Yield strength of reinforcement;
h_w	=	Wall height;
I_o	=	Blast wave reflected impulse;
K_{LM}	=	Load-Mass factor;
K_θ	=	Rotation stiffness;
l_w	=	Wall length;
P_o	=	Blast wave reflected pressure;
t_{BEs}	=	Boundary elements thickness;

t_d	=	Blast wave positive phase duration;
R	=	Wall out-of-plane resistance;
Δ_{wall}	=	Displacement of the center of the wall;
Δ_{web}	=	Displacement of the center of the web;
Δ_{BEs}	=	Displacement of the center of the BEs;
Δ_o	=	Displacement of the center of the wall evaluated using FE model;
Δ_{target}	=	Displacement of the center of the wall according the damage response limits;
ρ_h	=	Horizontal steel reinforcement ratio of the web;
$\phi_{80\% ult}$	=	Curvature at 80% of wall ultimate resistance;
ϕ_{ult}	=	Curvature at wall ultimate resistance;
$\phi_{20\% deg}$	=	Curvature at 20% of wall ultimate resistance degradation;
μ_{out}	=	Web displacement ductility at 20% ultimate resistance degradation;
ρ_v	=	Vertical steel reinforcement ratio of the wall;
$\rho_{v\text{-}BEs}$	=	Vertical steel reinforcement ratio of the BEs;
$\rho_{v\text{-}web}$	=	Vertical steel reinforcement ratio of the web;
σ_{axial}	=	Wall axial equivalent stress ratio;
$M_{\tau cr}$	=	Cracking torsional moment capacity of cross-section;
θ_s	=	Support rotation of the wall; and
Z	=	scaled distance.

4.9. REFERENCES

ASCE (2011). "Blast Protection of Buildings." *ASCE 59-11*, Reston, Va.

Baker, W. E., Cox, P. A., Westine, P. S., Kluesz, J. J., and Strehlow, R. A. (1983). *Explosion Hazards and Evaluation*. Elsevier scientific publishing company, NewYork.

Bangash, M. Y. H., and Bangash, T. (2006). *Explosion-resistant buildings design, analysis, and case studies*, Springer, Berlin, 229–288.

Banting, B. R., and El-Dakhakhni, W. W. (2014). "Seismic Design Parameters for Special Masonry Structural Walls Detailed with Confined Boundary Elements." *Journal of Structural Engineering*, 140(10), 04014067.

Bazant, Z., and Oh, B. (1983). "Crack band theory of concrete." *Materials and Structures*, 16, 155–177

Biggs, J. M. (1964). *Introduction to structural dynamics*. McGraw-Hill Inc.

Bischoff, P. H., and Perry, S. H. (1991). "Compressive behaviour of concrete at high strain rates." *Materials and Structures*, 24(6), 425–450.

Campidelli, M., El-Dakhakhni, W. W., Tait, M. J., and Mekky, W. (2015). "Blast Design-Basis Threat Uncertainty and Its Effects on Probabilistic Risk Assessment." *ASCE-ASME Journal of Risk and Uncertainty in Engineering Systems, Part A: Civil Engineering*, 1(4), 04015012.

Cerioni, R., and Donida, G. (1994). "A finite element model for the nonlinear analysis of reinforced and prestressed masonry walls." *Computers & Structures*, 53(6), 1291–1306.

Choi, J.-H., Choi, S.-J., Kim, J.-H. J., and Hong, K.-N. (2018). "Evaluation of blast resistance and failure behavior of prestressed concrete under blast loading." *Construction and Building Materials*, Elsevier, 173, 550–572.

Collins, M. P., and Lampert, P., "Redistribution of Moments at Cracking—The Key to Simpler Torsion Design," *Analysis of Structural Systems for Torsion*, SP-35, American Concrete Institute, Farmington Hills, Mich., 1973, pp. 343-383.

Canadian Standards Association (CSA). (2012). "Design and assessment of buildings subjected to blast loads." *CSA S850-12*, Mississauga, ON, Canada.

Canadian Standards Association (CSA). (2014). "Design of masonry structures." *CSA S304-14*, Mississauga, ON, Canada.

Dusenberry, D. O. (2010). *Handbook for blast-resistant design of buildings*. *Assessment*.

Eamon, C. D., Baylot J. T., O'Daniel, J. L. (2004). "Modeling Concrete Masonry Walls Subjected to Explosive load" *Journal of Engineering Mechanics*, 130(9), 1098-1106.

ElSayed, M., El-Dakhakhni, W., and Tait, M. (2015). "Response Evaluation of Reinforced Concrete Block Structural Walls Subjected to Blast Loading." *Journal of Structural Engineering*, 141(11), 04015043.

Ezzeldin, M., Wiebe, L., and El-Dakhakhni, W. (2016). "Seismic collapse risk assessment of reinforced masonry walls with boundary elements using the FEMA P695 methodology." *Journal of Structural Engineering*, 142(11: 04016108. https://doi.org/10.1061/(ASCE)ST.1943-541X.0001579.

Ezzeldin, M., El-Dakhakhni, W., and Weibe, L. (2017). "Experimental assessment of the system-level seismic performance of an asymmetrical reinforced concrete block wall building with boundary elements." *Journal of Structural Engineering*, 143(8): 04017063. https://doi.org/10.1061/(ASCE)ST798 .1943-541X.0001790.

El-Dakhakhni, W. W., Mekky, W. F., and Rezaei, S. H. C. (2010). "Validity of SDOF Models for Analyzing Two-Way Reinforced Concrete Panels under Blast Loading." *Journal of Performance of Constructed Facilities*, 24(4), 311–325.

El-Hashimy, T., Ezzeldin, M., Tait, M. and El-Dakhakhni, W. (2018). "Out-of-Plane Performance of Reinforced Masonry Shear Walls Constructed with Boundary Elements." Journal of Structural Engineering, 10.1061/(ASCE)ST.1943-541X.0002337.

El-Hashimy, T., Ezzeldin, M., El-Dakhakhni, W., and Tait M. (2019). "Out-of-Plane performance of Seismically-Detailed Reinforced Masonry Shear Walls with Boundary Elements." Journal of Structural Engineering. submitted 2018.

FEMA. (2010). *Blast-Resistant Benefits of Seismic Design. Phase 2 Study: Performance of Structural Steel Strengthening Systems (FEMA P-439B).*

Hallinan, P., and Guan, H. (2007). "Layered Finite Element Analysis of One-Way and Two-Way Concrete Walls With Openings." *Advances in Structural Engineering*, 10(1), 55–72.

Krauthammer, T. (1999). "Blast-resistant structural concrete and steel connections." *Int. J. Impact Eng.*, 22(1999), 887–910.

Krauthammer, T., Conrath, E. J., Marchand, K. A., and Mlakar, P. F. (1999). *Structural design for physical security—State of the practice*, ASCE, Reston, Va.

Krauthammer, T. (2008). *Modern Protective Structures*. *CRC press*, Boca Raton.

Li, J., and Hao, H. (2011). "Development of a Simplified Numerical Method for Structural Response Analysis to Blast Load." *Procedia Engineering*, Elsevier, 14, 2558–2566.

Li, Z., Zhong, B., and Shi, Y. (2016). "An effective model for analysis of reinforced concrete members and structures under blast loading." *Advances in Structural Engineering*, 19(12), 1815–1831.

Lu, X., Lu, X., Zhang, W., and Ye, L. (2011). "Collapse simulation of a super high-rise building subjected to extremely strong earthquakes." *Science China Technological Sciences*, SP Science China Press, 54(10), 2549–2560.

Lu, X., Xie, L., Guan, H., Huang, Y., and Lu, X. (2015). "A shear wall element for nonlinear seismic analysis of super-tall buildings using OpenSees." *Finite Elements in Analysis and Design*, Elsevier, 98, 14–25.

Malvar, L. J. (1998). "Review of static and dynamic properties of steel reinforcing bars." *ACI Materials Journal*, 95(5), 609–616.

Mander, J. B., Priestley, M. J. N., and Park, R. (1988). "Theoretical Stress-Strain Model for Confined Concrete." *Journal of Structural Engineering*, 114(8), 1804–1826.

Mays, G. C., and Smith, P. D. (1995). *Blast effects on buildings*, Telford, London.

McKenna, F., Fenves, G. L., and Scott, M. H. (2013). "Open system for earthquake engineering simulation." Univ. of California, Berkeley, CA.

National Institute of Standards and Technology (NIST). (2010). "Evaluation of the FEMA P-695 Methodology for Quantification of Building Seismic Performance Factors." *Nist Gcr 10-917-8*, 268.

Noor-E-Khuda, S., Dhanasekar, M., and Thambiratnam, D. P. (2016). "An explicit finite element modelling method for masonry walls under out-of-plane loading." *Engineering Structures*, Elsevier, 113, 103–120.

National Research Council (NRC). (2003). *ISC Security Design Criteria for New Federal Office Buildings and Major Modernization Projects: A Review and Commentary*. National Academies Press, Washington, D.C.

U.S. Army Corps of Engineers Protective Design Center (PDC-TR 06-08). (2008). "Single degree of freedom structural response limits for antiterrorism design." ⟨https://pdc.usace.army.mil/library/tr/ 06-08⟩ (Jan. 18, 2013).

U.S. Department of Defense (USDOD). (2008). "Structures to resist the effects of accidental explosions." Whole building design guide, UFC 3-340-02, Washington, DC.

Parlin, N. J., Davids, W. G., Nagy, E., and Cummins, T. (2014). "Dynamic response of lightweight wood-based flexible wall panels to blast and impulse loading." *Construction and Building Materials*, Elsevier Ltd, 50, 237–245.

Salem, S., Ezzeldin, M., El-Dakhakhni, W., and Tait, M. (2018). "Out-of-Plane Behavior of Load-Bearing Reinforced Masonry Shear walls." *Journal of Structural Engineering*, Submitted 2018.

Shedid, M. T., El-Dakhakhni, W. W., and Drysdale, R. G. (2009). "Behavior of fully grouted reinforced concrete masonry shear walls failing in flexure: Analysis." *Engineering Structures*, 31(9), 2032–2044.

Shedid, M., El-Dakhakhni, W., and Drysdale, R. (2010a). "Characteristics of rectangular, flanged, and end-confined reinforced concrete masonry shear walls for seismic design." *Journal of Structural Engineering*, 136(12), 1471–1482.

Shedid, M. T., El-Dakhakhni, W. W., and Drysdale, R. G. (2010b). "Alternative Strategies to Enhance the Seismic Performance of Reinforced Concrete-Block Shear Wall Systems." *Journal of Structural Engineering*, 136(6), 676–689.

Simonds, K. (2014). "Performance of reinforced concrete block structural walls with boundary elements under multiple design basis blast threat levels". M.Eng. thesis, McMaster University, Hamilton, ON, Canada.

Smith, N. L., Tait, M. J., M., El-Dakhakhni, W. W., and Mekky, W. F. (2016). "Response Analysis of Reinforced Concrete Block Infill Panels under Blast." *Journal of Performance of Constructed Facilities*, 30(6), 1–12.

Syed, Z. I., Raman, S. N., Ngo, T., Mendis, P., and Pham, T. (2018). "The Failure Behaviour of Reinforced Concrete Panels Under Far-field and Near-field Blast Effects." *Structures*, Elsevier, 14, 220–229.

The Masonry Society. (2016). *TMS 402/602 Building Code Requirements and Specification for Masonry Structures, 2016 - The Masonry Society*.

Wei, X., and Hao, H. (2009). "Numerical derivation of homogenized dynamic masonry material properties with strain rate effects." *International Journal of Impact Engineering*, Elsevier Ltd, 36(3), 522–536.

Zhang, R., and Phillips, B. M. (2016). "Performance and Protection of Base-Isolated Structures under Blast Loading." *Journal of Engineering Mechanics*, 142(1), 04015063.

Table 4.1. Characteristics of the RM Walls with BEs based on data from Simonds (2014)

Walls ID	*Length* (mm)	*Height* (mm)	ρ_v (%)	ρ_h (%)	$\rho_{v\text{-}BEs}$ (%)	f'_m (MPa)	f_y (MPa)
B-L	945	990	0.46	0.12	0.63	19.4	477
B-M			0.62	0.26	0.63	19.4	477
B-H			1.10	0.26	1.13	19.4	481

Table 4.2. Summary of SDOF model prediction and experimental maximum displacement.

Z (m/kg$^{1/3}$)	Walls ID	Experimental Results Δ_{web} (mm)	SDOF Model Predictions Δ_{web} (mm)	Deviation (%)
2.76	**B-L**	27.6	25.6	7.0%
	B-M	27.2	23.3	14.3%
	B-H	20.2	18.8	7.1%
2.20	**B-L**	47.3	31.0	34.4%
	B-M	55.2	66.0	19.6%
	B-H	34.6	42.6	23.3%
1.62	**B-L**	171.2	258	51.0%
	B-M	130.0	238	83.1%

Table 4.3. Characteristics of the RM walls used for the static model validation based on data from Salem et al. (2018) and El-Hashimy et al. (2018)

Wall Type	Walls ID	*Length* (m)	*Height* (m)	ρ_v (%)	ρ_h (%)	$\rho_{v\text{-}BEs}$ (%)	f'_m (MPa)	f_y (MPa)	σ_{axial} (%)
Rectangular RM Walls [a]	***M-05***	1.45	1.50	0.61	0.14	N.A.	13.5	436	5
	M-15			0.61	0.14	N.A.	13.5	436	15
RM Walls with BEs [b]	***Wall 1***			0.47	0.16	0.79	11.2	477	10
	Wall 2			0.61	0.16	1.10	11.2	477	10
	Wall 3			0.61	0.30	0.79	11.2	477	10

[a] Based on data from Salem et al. (2018).
[b] Based on data from El-Hashimy et al. (2018).
N.A.: not applicable

Table 4.4. Characteristics of RM walls used for the dynamic model validation based on data from ElSayed et al. (2015) and Smith et al. (2016)

Wall Set	Walls ID	ρ_v (%)	ρ_h (%)	$\rho_{v\text{-}BEs}$ (%)	f'_m (MPa)	f_y (MPa)	Boundary conditions
Rectangular RM Walls[a]	**R-M**	0.62	0.26	N/A	18.4	515	Fixed
	R-H	1.10	0.26	N/A	18.4	481	
Infill RM Panels [b]	**I-M**	0.62	0.26	N/A	18.2	478	Supported at corners only
	I-H	1.10	0.26	N/A	18.2	484	

[a] based on data from ElSayed et al. (2015).
[b] based on data from Smith et al. (2016).

Table 4.5. Summary of experimental and numerical results.

Wall Type	Walls ID	Charge Eq. TNT (kg)	Z (m/kg$^{1/3}$)	Experimental Results		*OpenSees* Predictions			
				Δ_{web}	Δ_{BEs}	Δ_{web}		Δ_{BEs}	
				(mm)	(mm)	(mm)	Deviation	(mm)	Deviation
Rectangular RM Walls	R-M	6	2.76	14.8	N.A.	13.8	-6.90%	N.A.	N.A.
		12	2.20	32.3	N.A.	39.3	+21.6%	N.A.	N.A.
		30	1.62	76.5	N.A.	88.2	+15.3%	N.A.	N.A.
	R-H	12	2.20	23.6	N.A.	21.6	-8.40%	N.A.	N.A.
		30	1.62	69.4	N.A.	77.8	+12.1%	N.A.	N.A.
RM Walls with BEs	B-L	6	2.76	27.6	N.R.	30.2	+9.80%	13.6	N.R.
		12	2.20	47.3	N.R.	53.0	+12.2%	40.0	N.R.
		30	1.62	171.2	86.12	129.9	-24.1%	94.7	+10.0%
	B-M	6	2.76	27.2	21.24	27.7	+2.00%	14.4	-32.1%
		12	2.20	55.2	43.2	48.2	-12.7%	39.9	-7.63%
		30	1.62	130	87.4	119.1	-8.38%	92.7	+6.00%
	B-H	6	2.76	20.2	N.R.	19.9	-1.67%	9.32	N.R.
		12	2.20	34.6	24.64	41.6	+20.1%	20.8	-15.4%
Infill RM Panel	I-M	6	2.76	13.7	N.A.	12.2	-10.9%	N.A.	N.A.
		12	2.20	30.4	N.A.	25.6	-15.7%	N.A.	N.A.
	I-H	6	2.76	12.8	N.A.	12.0	-6.25%	N.A.	N.A.
		12	2.20	26.1	N.A.	25.1	-3.80%	N.A.	N.A.

N.A.: not applicable
N.R.: not reported

Table 4.6. Analyzed wall characteristics

		Conventional RM walls			RM walls with BEs		
		WR1	***WR2***	***WR3***	***WB1***	***WB2***	***WB3***
ρ_v	**(%)**	0.3	0.75	1.25	0.17	0.45	0.72
μ_{out}		2.5	1.3	N/A	14.3	8.4	3.5
$\phi_{80\%ult}$	**$\times 10^{-5}$ (m^{-1})**	2.26	3.13	2.65	0.72	1.08	1.21
ϕ_{ult}	**$\times 10^{-5}$ (m^{-1})**	5.23	5.33	4.94	5.36	6.51	4.30
$\phi_{20\%deg}$	**$\times 10^{-5}$ (m^{-1})**	13.07	7.83	6.25	20.37	15.41	5.22

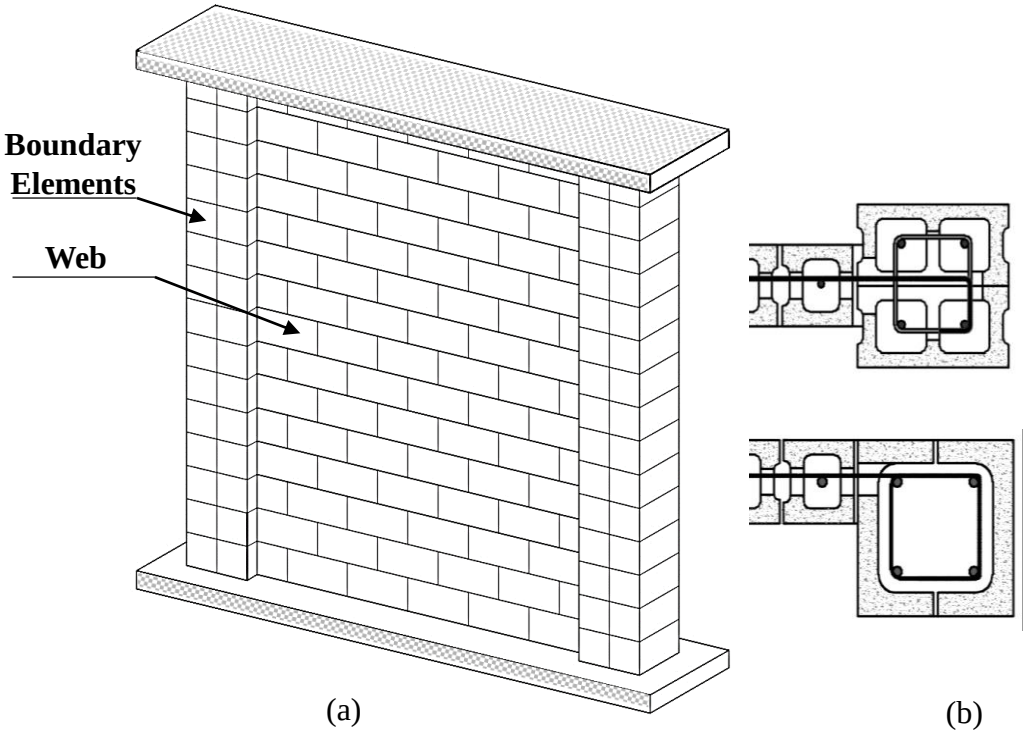

Fig 4.1. Reinforced masonry walls with Boundary elements
(a) Isometric – (b) Boundary elements configuration

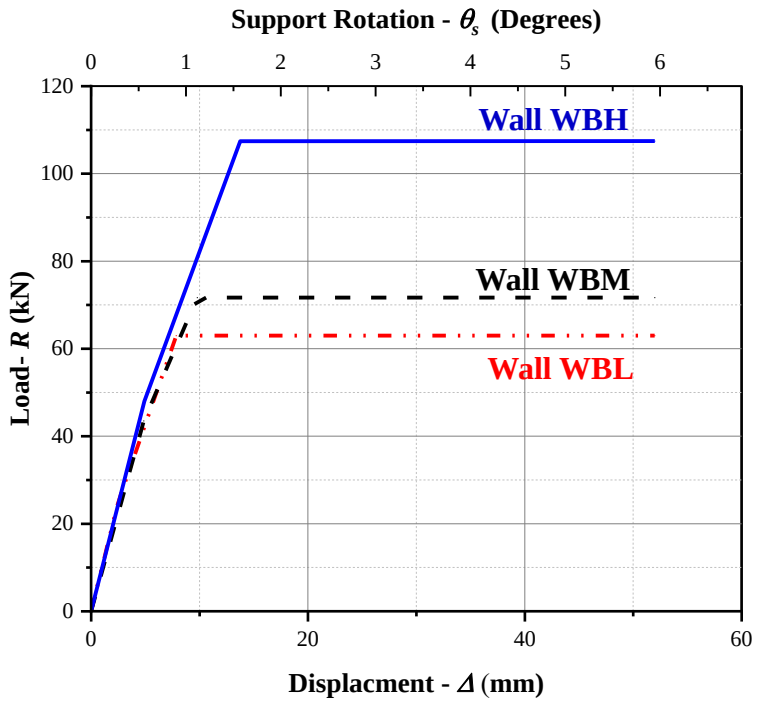

Fig 4.2. Analytical resistance function of RM walls with BEs.

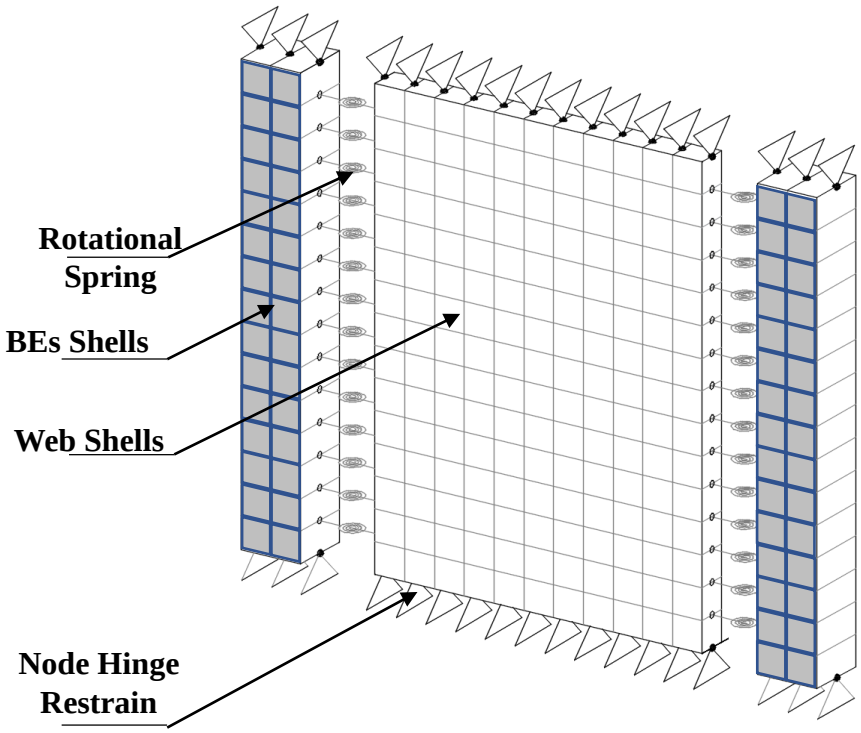

Fig 4.3(a). Three-dimensional model for RM walls with BEs

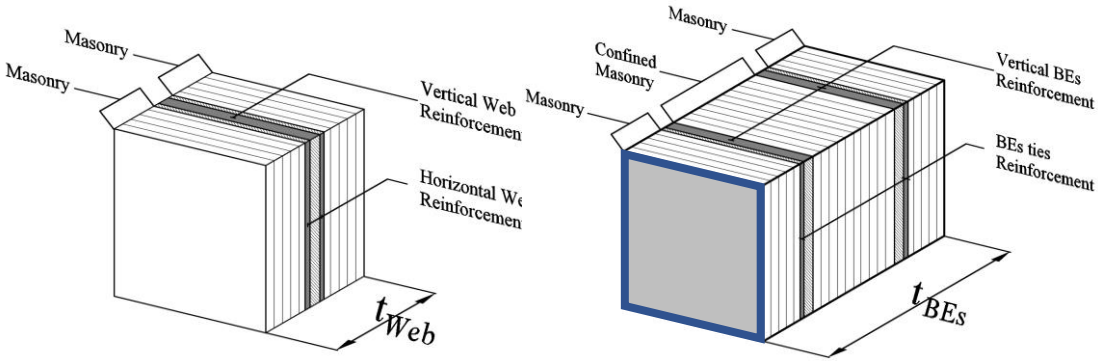

Fig 4.3(b). Multi-layer shell elements modeled for Web and BEs dimensions

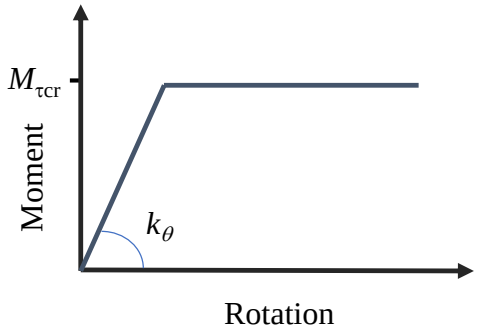

Fig 4.3(c). Rotational spring behavior

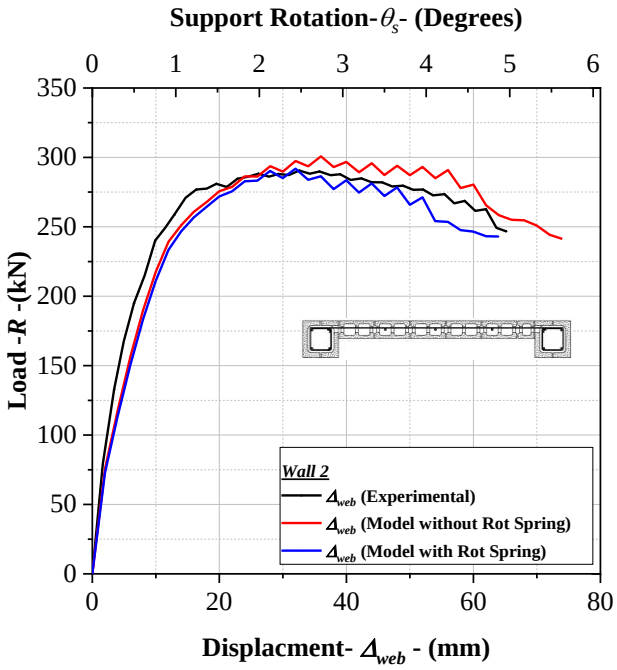

(a)

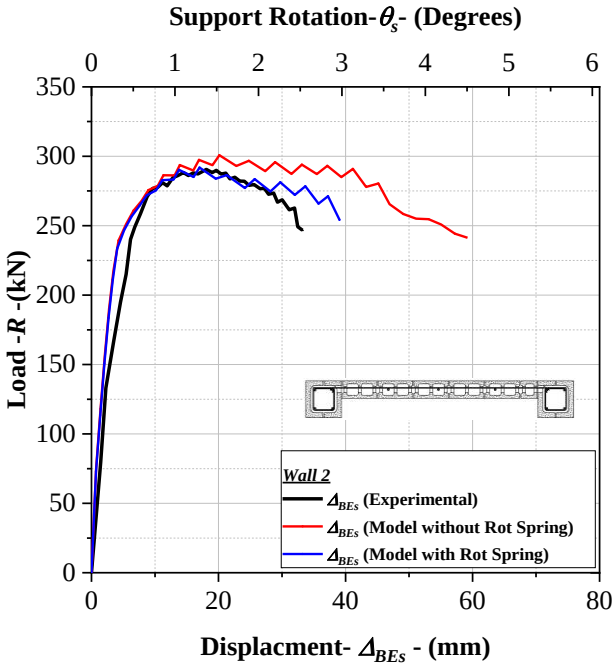

(b)

Fig 4.4. Influence of the rotational spring on
(a) Web displacement response – (b) BEs displacement response

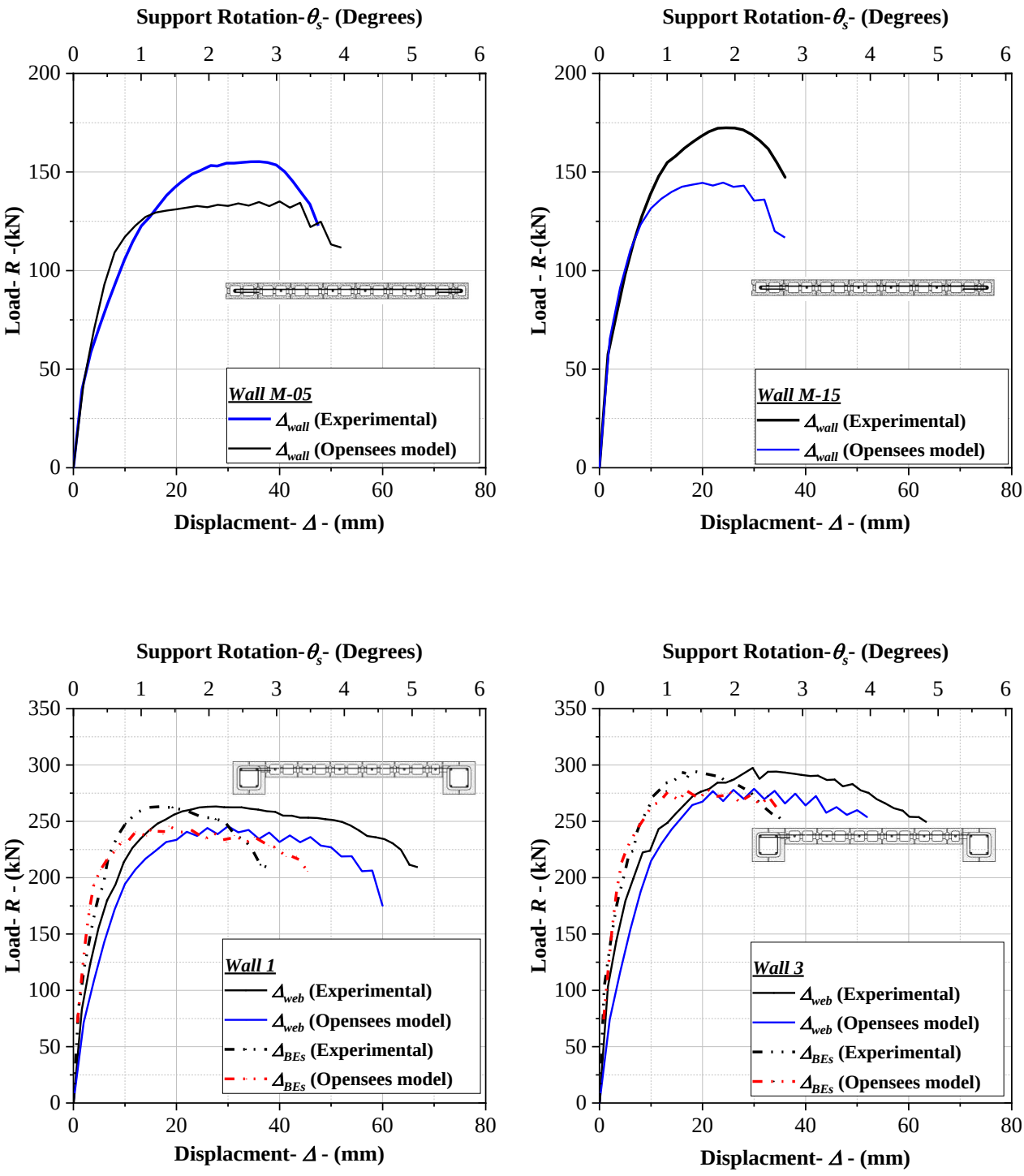

Fig 4.5. Wall static pushover analysis compared to the experimental results

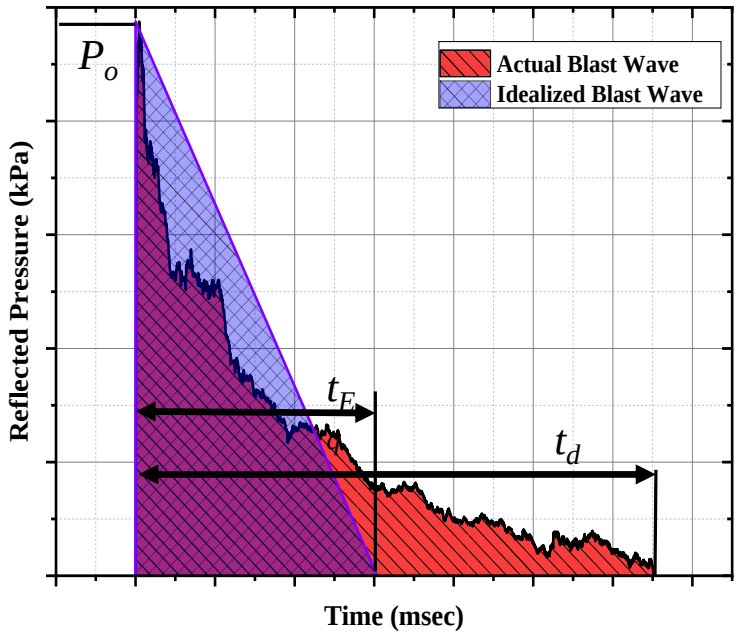

Fig 4.6. Real blast wave positive-phase versus that of an idealized one

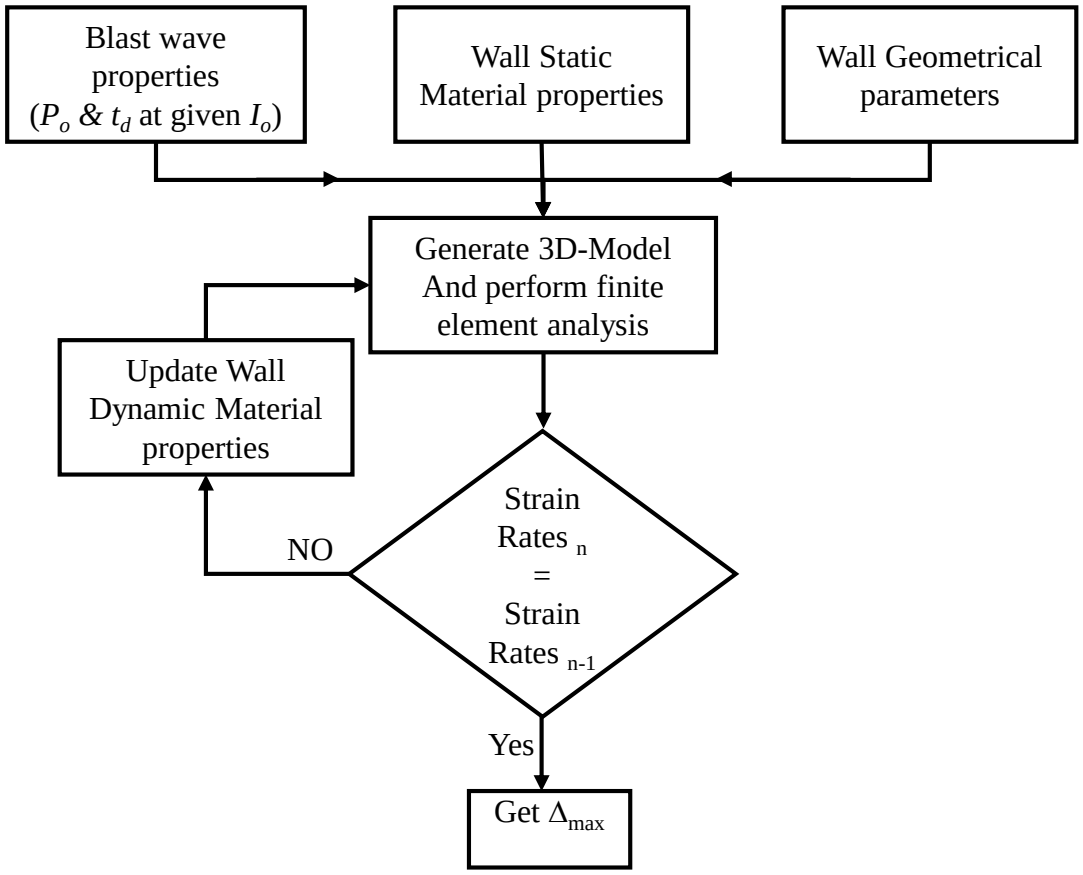

Fig 4.7. Flow chart of the model procedure for strain rate effects inclusion.

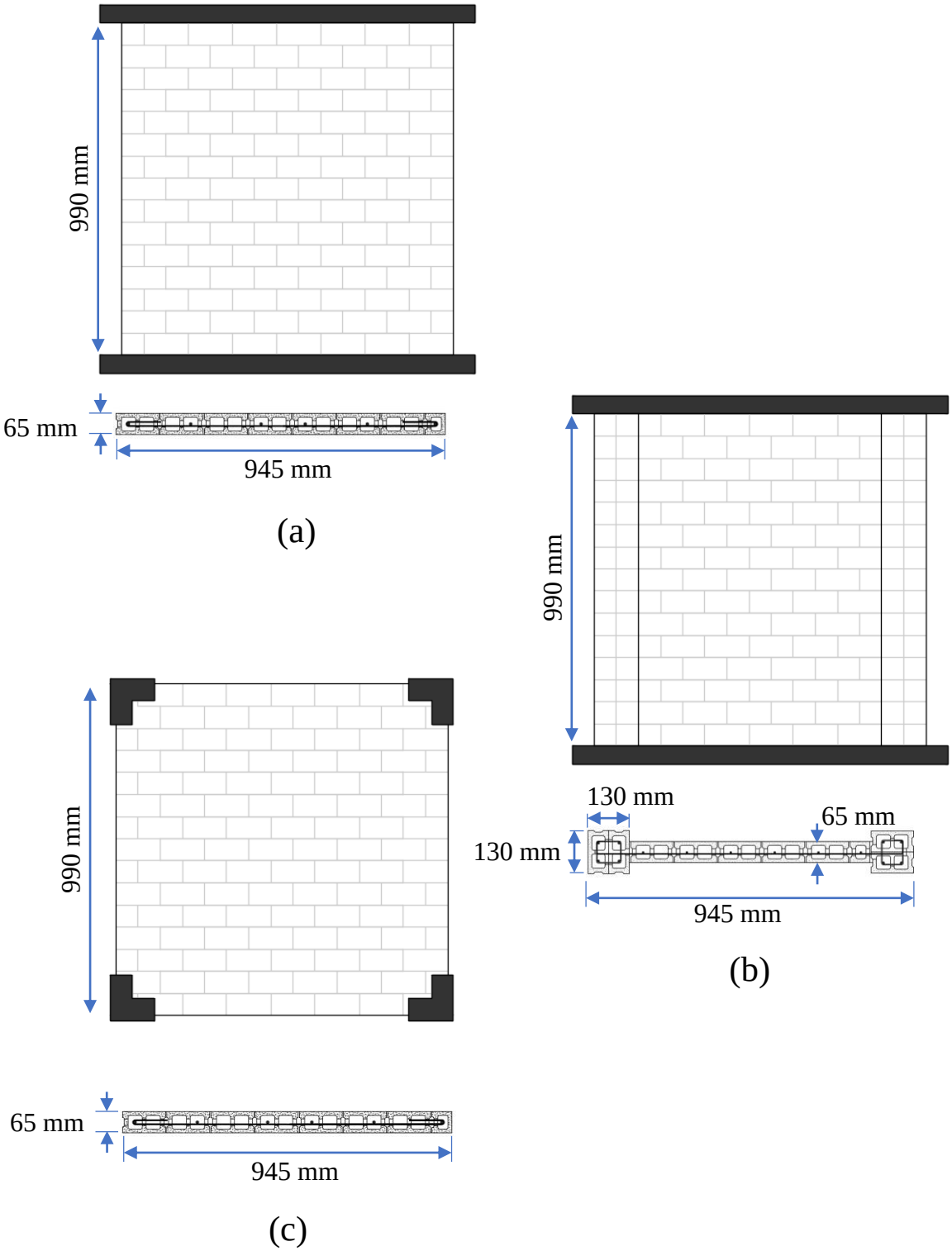

Fig 4.8. RM walls configurations validated by the model:
(a) Rectangular RM wall; (b) RM wall with BEs; and (c) Infill RM Panel

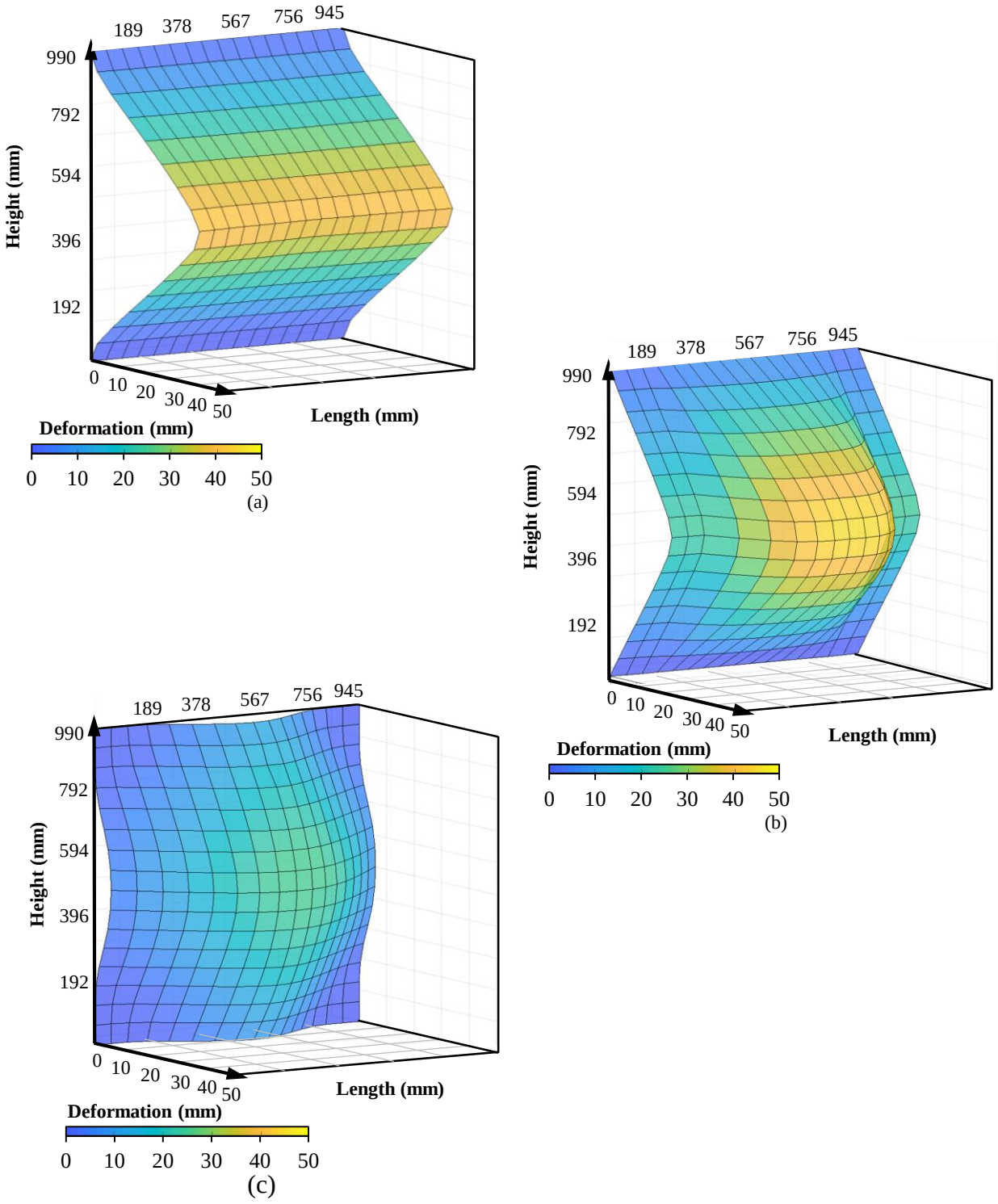

Fig 4.9. Predicted Deformed Shape of different RM walls:
(a) R-M ; (b) B-M; (c) P-M

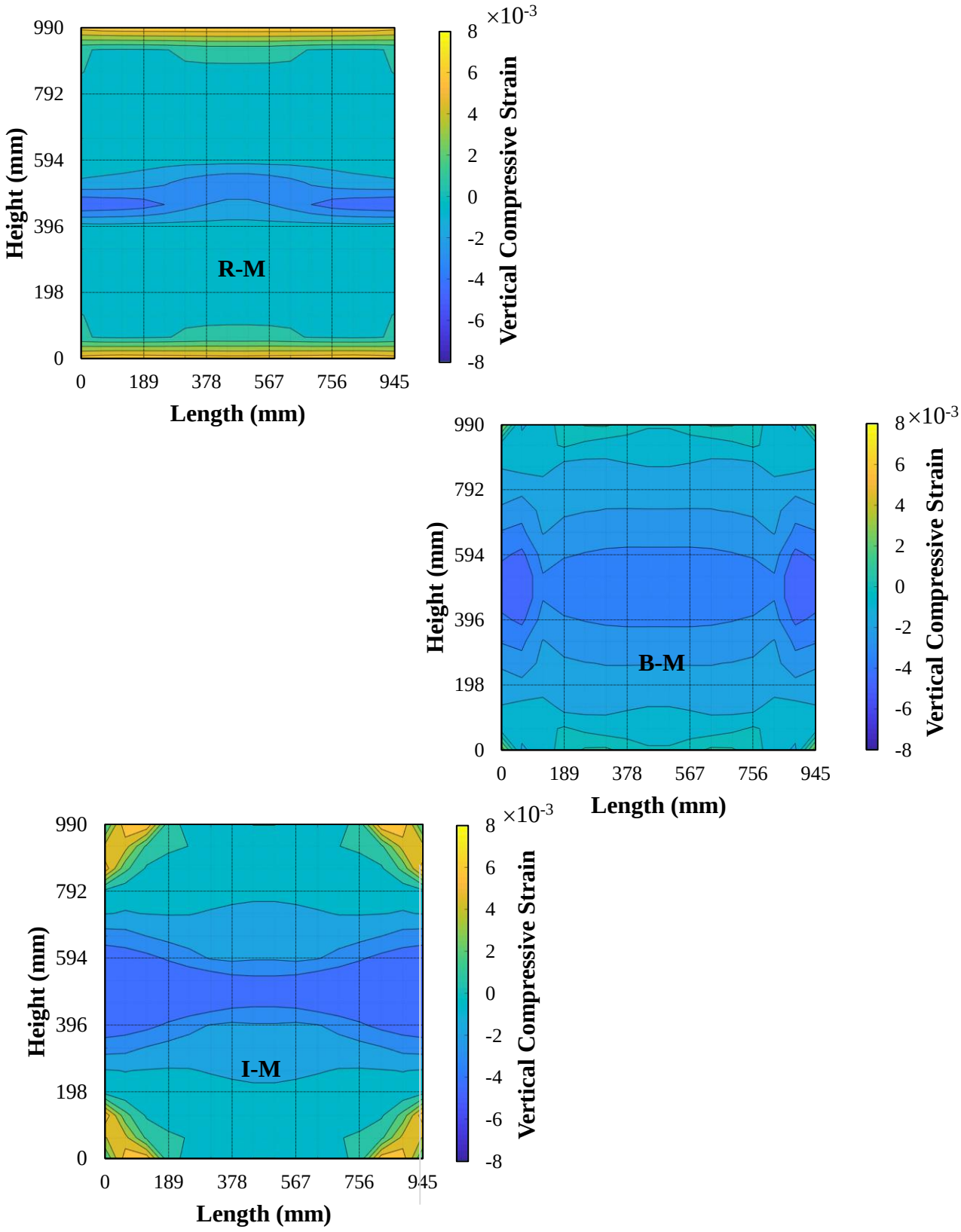

Fig 4.10. Strain distribution at compression face at maximum deformation (a) Vertical strain distribution.

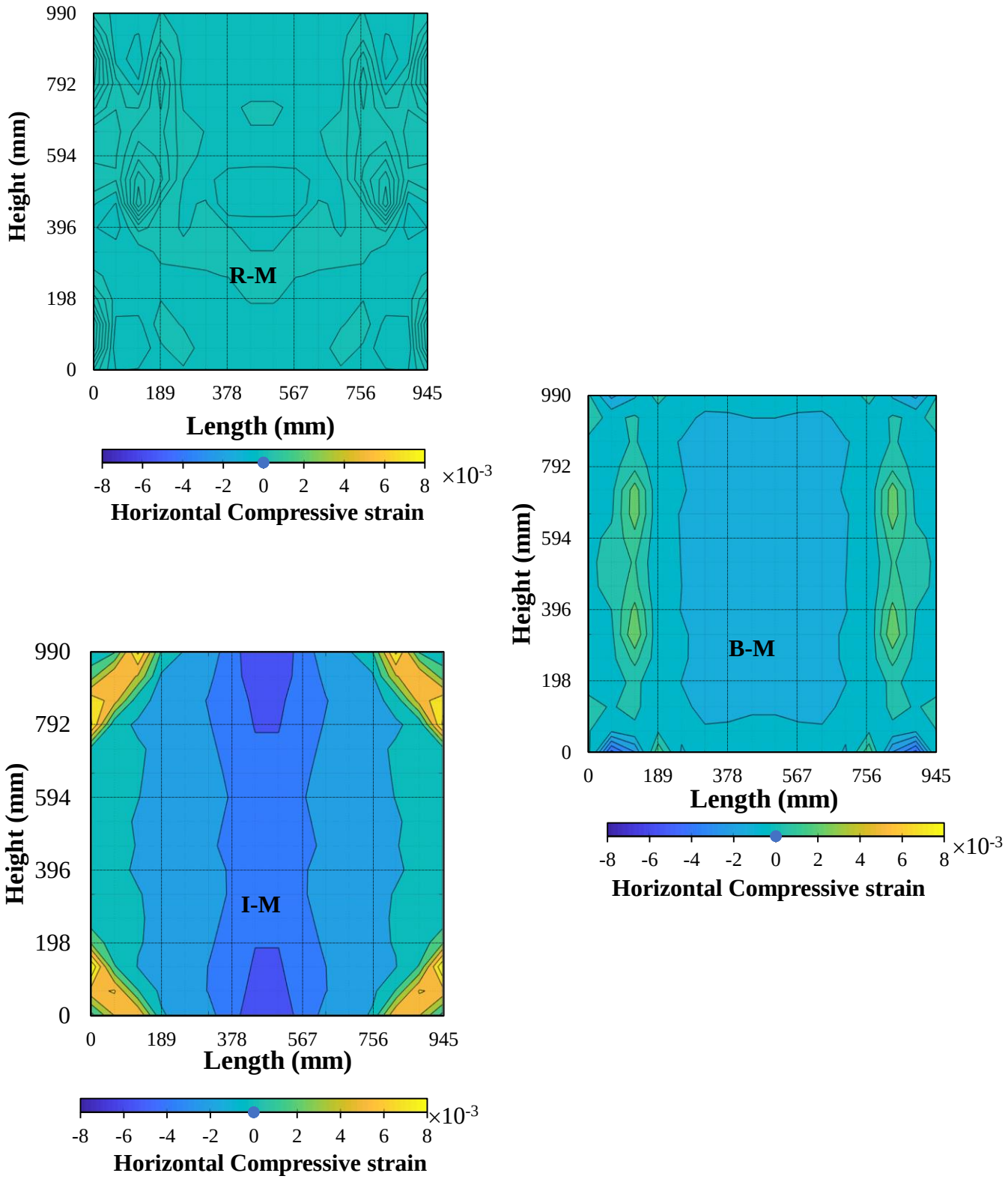

Fig 4.10 (Cont). Strain distribution at compression face at maximum deformation (b) Horizontal strain distribution.

(a)

(b)

(c)

Fig 4.11. Walls actual crushing damage at (Z = 2.2 m/kg$^{1/3}$)
(a) R-M ; (b) B-M; (c) I-M.

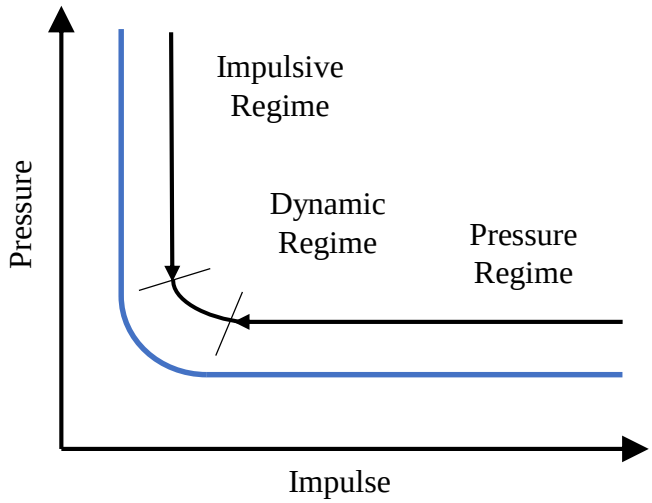

Fig 4.12. General form of a pressure-impulse diagram

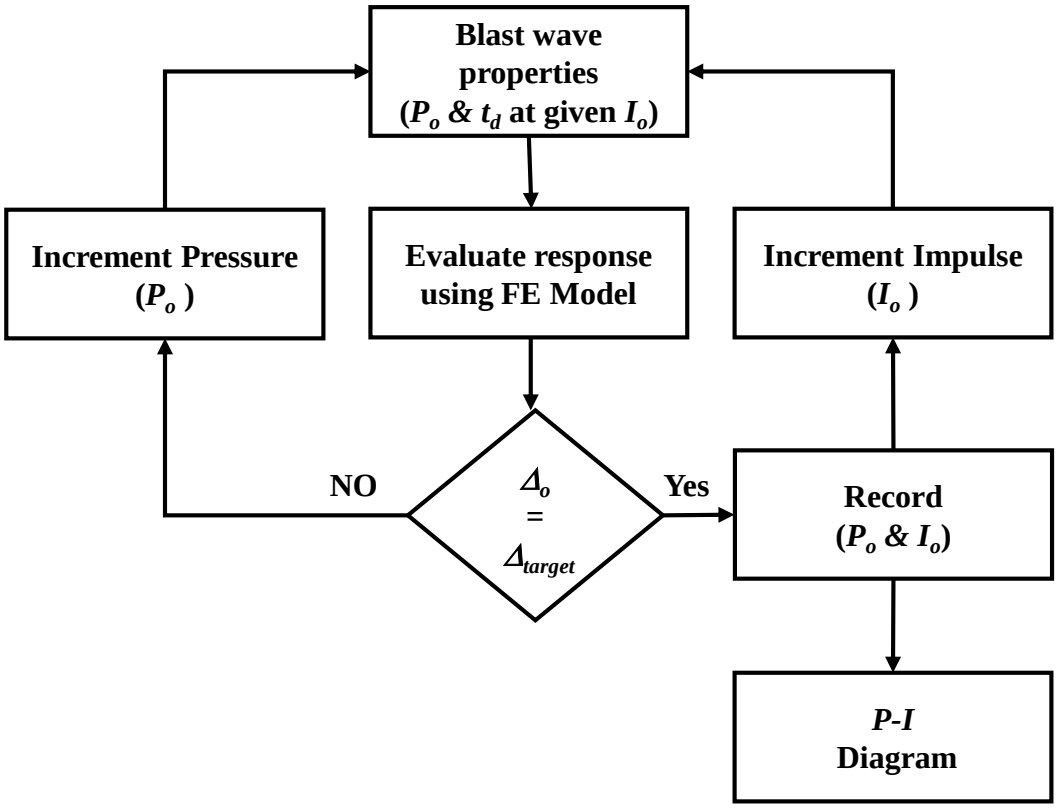

Fig 4.13. Flowchart to generate the P-I diagram

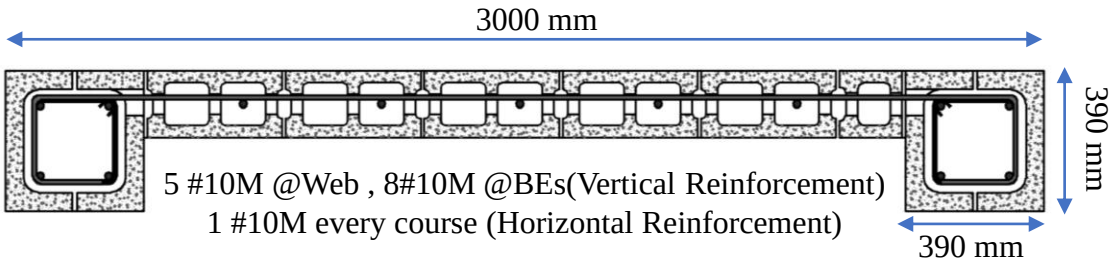

Wall *WB1*

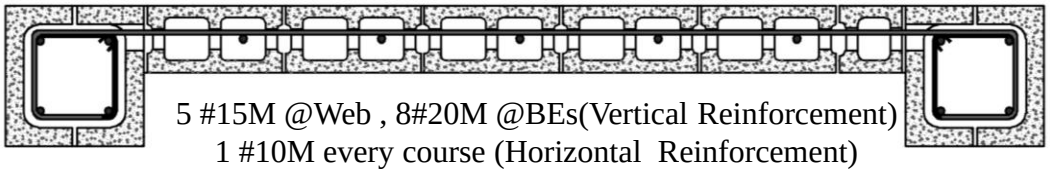

Wall *WB2*

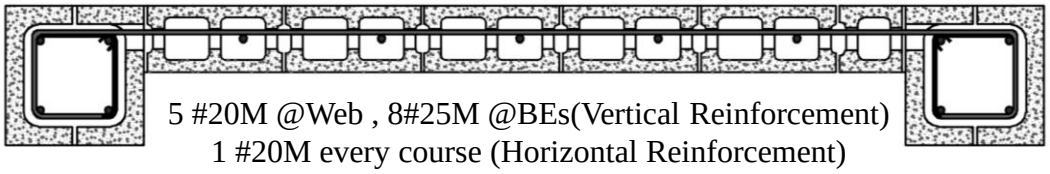

Wall *WB3*

Fig 4.14. Cross sections of RM walls used to assess the response limits of blast loads (a) with BEs used to assess response limits of blast loads

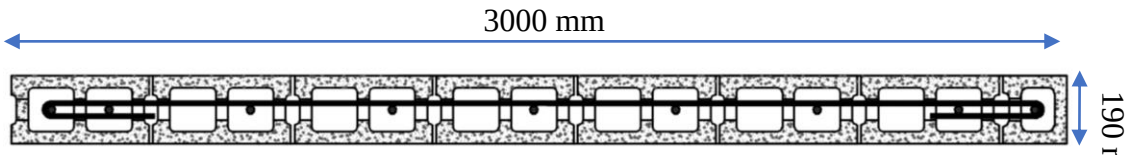

9 #20M (Vertical Reinforcement)
1 #10M every course (Horizontal Reinforcement)

Wall *WR1*

9 #25M (Vertical Reinforcement)
1 #10M every course (Horizontal Reinforcement)

Wall *WR2*

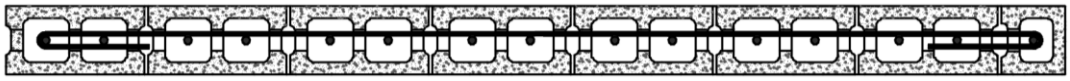

15 #25M (Vertical Reinforcement)
1 #20M every course (Horizontal Reinforcement)

Wall *WR3*

Fig 4.14(Cont). Cross sections of RM walls used to assess the response limits of blast loads (b) with BEs used to assess response limits of blast loads

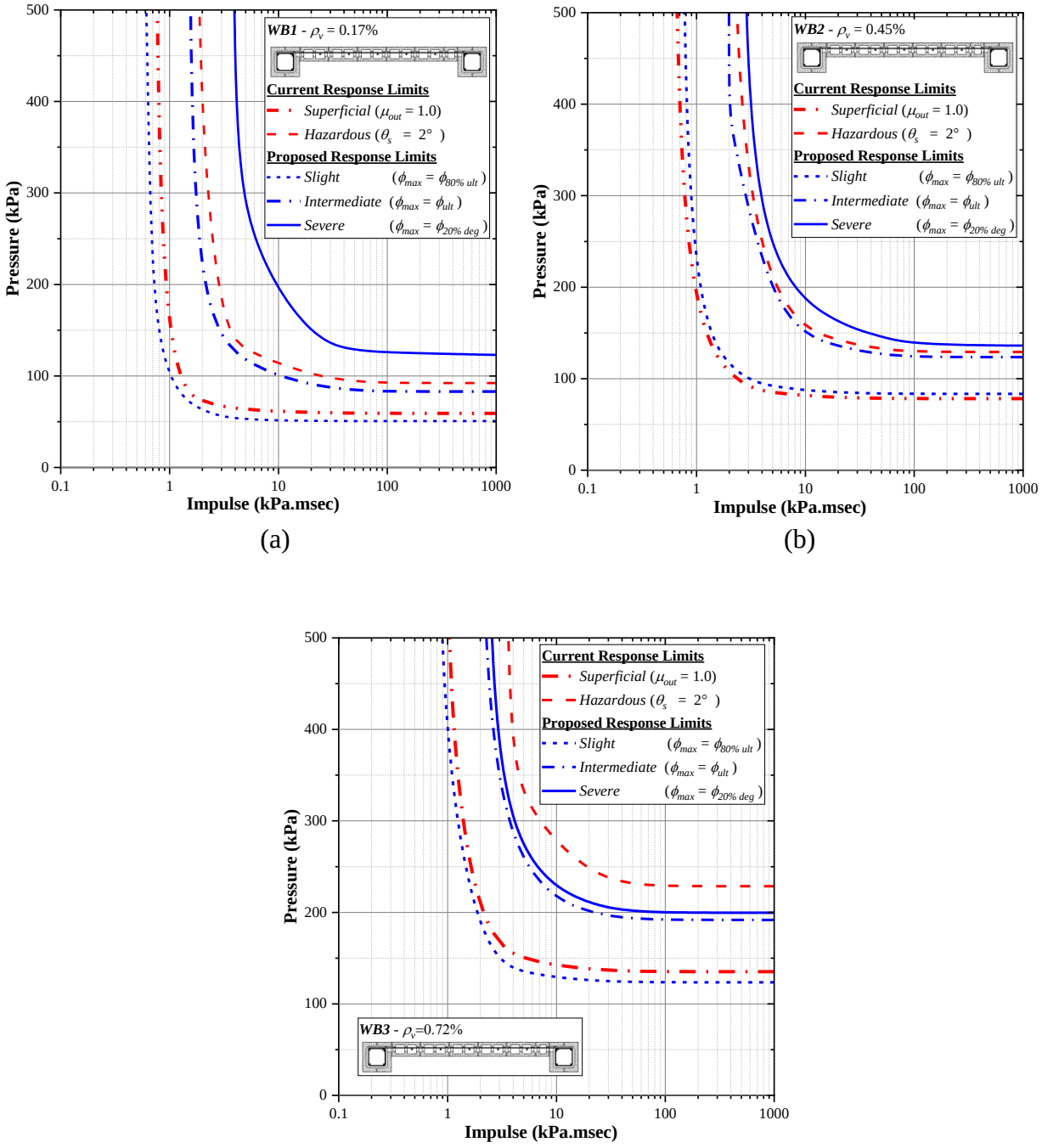

Fig 4.15. Response limits of (ASCE 59-11 and CSA S850-12) and proposed response limits for RM walls with BEs: (a) Wall *WB1;* (b) Wall *WB2;* and (c) Wall *WB3*

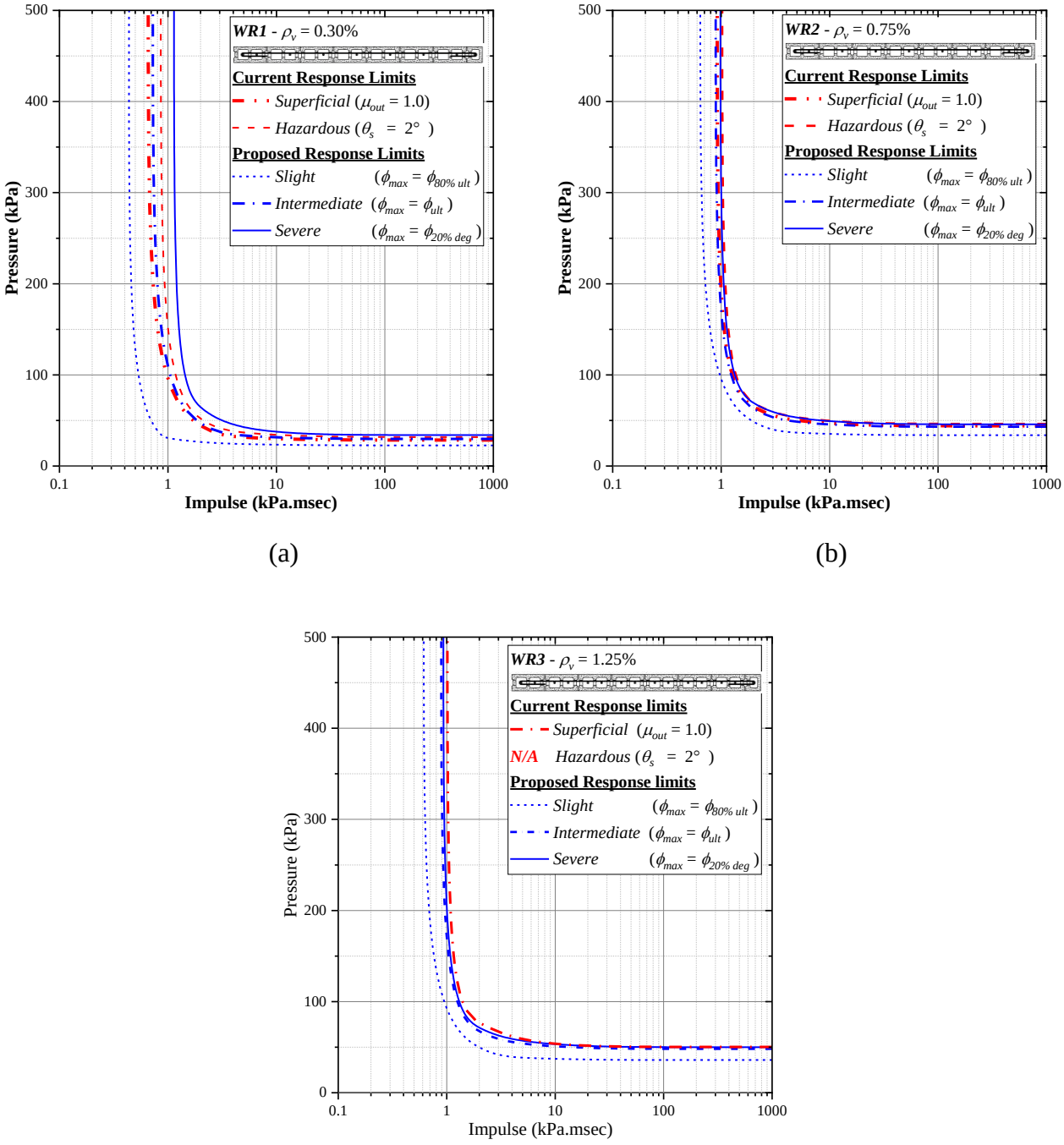

Fig 4.16. Response limits of (ASCE 59-11 & CSA S850-12) and proposed response limits for RM walls without BEs: (a) Wall *WR1;* (b) Wall *WR2;* and (c) Wall *WR3*

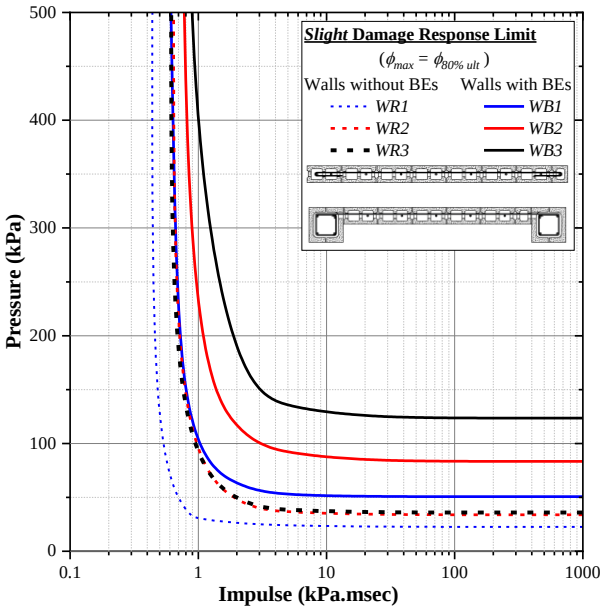

(a)

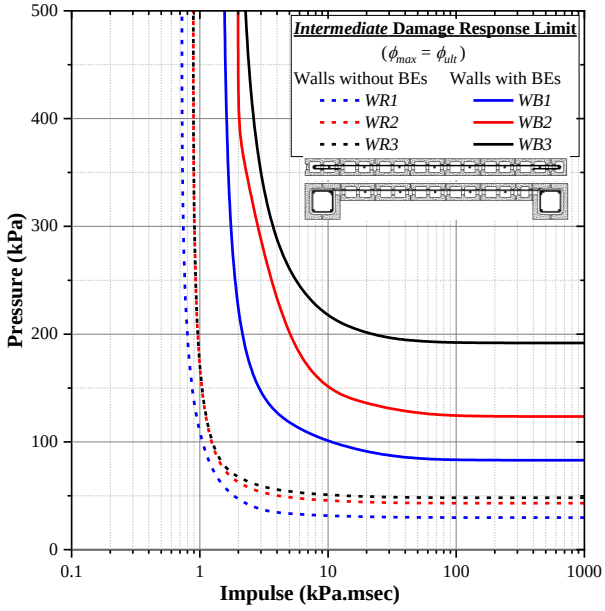

(b)

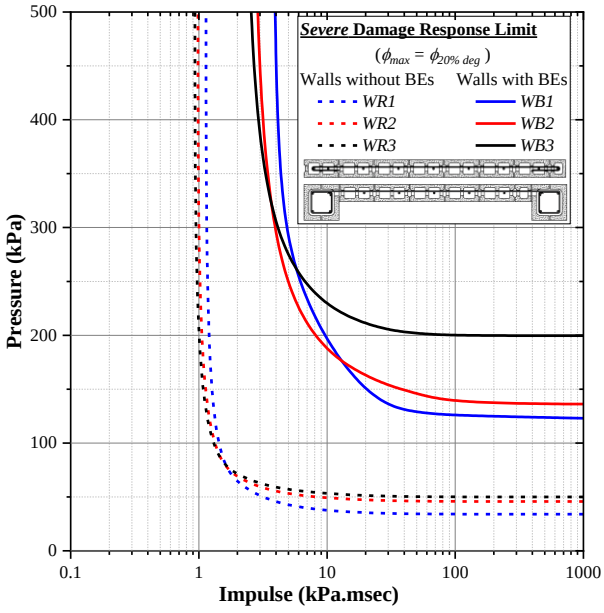

(c)

Fig 4.17. P-I Diagrams for RM walls with and without BEs at different response limits (a) *Slight* Damage*;* (b) *Intermediate* Damage*;* and (c) *Severe* Damage

CHAPTER 5

SUMMARY, CONCLUSIONS, AND RECOMMENDATIONS

5.1 SUMMARY

Recently, several studies have focused on the enhanced in-plane performance that RM walls with BEs provide to seismic force resisting systems. However, no similar studies have been conducted on the influence of BEs on the out-of-plane performance of such walls (e.g. when subjected to blast loads). Therefore, the main goal of this dissertation is to assess this out-of-plane performance of such walls experimentally and numerically in order to facilitate their adoption in the future editions of the ASCE 59-11 and CSA S850-12 standards. In this respect, this dissertation presents the experimental results of ten different RM walls with BEs on a two study phases, where the damage sequence and the influence of different design parameters were observed. Results show that BEs restrained the wall edges, resulting in the development of a two-way bending mechanism in the wall web, and a torsional behavior in the BEs, which led to different failure mechanisms than that occurred by conventional RM walls. Accordingly, an analytical model based on plastic analysis was developed to evaluate the resistance function of such walls taking into account the influence of BEs. In addition, a numerical finite element (FE) model using layered shell elements was developed to evaluate the out-of-plane resistance functions of different wall configurations and simulate the dynamic effects of blast load. Finally, the response limits of the different damage states specified in current ASCE59-11 for conventional RM walls as well as new proposed limits that consider the curvature capacity of the wall were assessed

through pressure-impulse diagrams that highlighted the discrepancy between the response limits in quantifying the damage of the alternative RM walls configurations.

5.2 CONCLUSIONS

The experimental, numerical and analytical results reported in this dissertation highlight the enhancements that boundary elements contribute to RM wall out-of-plane performance and proposes new response limits that provide a better quantification for the different damage states than the currently utilized response limits in the ASCE59-11. The following conclusions are based on the research results reported in the preceding chapters:

- The experimental load-displacement results coupled with the observed crack patterns confirmed the presence of two-way bending mechanism within the wall web, which forced the horizontal reinforcement to contribute to the out-of-plane resistance, unlike the case in conventional RM shear walls (i.e. RM walls without BEs).
- The interaction between the web and BEs also led to compatibility torsion issues that affected the BEs and subsequently damaged the BEs in the wall post-peak response stage. Although current North American standards do not provide separate provisions for RM walls with BEs when subjected to out-of-plane loading, it is recommended that BEs be designed to withstand torsional moments to minimize such damage.

- Test results confirmed that current seismic details for horizontal reinforcement in both CSA S304 (2014) and TMS 402 (2016) do not provide adequate measure to control the cracks propagation that develop either at the corner of the walls or at the BEs-web interface under out-of-plane load. as observed in the experimental investigation and consequently limited the development of the wall's ductility. Accordingly, it is suggested to add horizontal shear dowels at the BEs-web interface that would extend to the applicable development length in order to minimize such crack propagation.
- The influence of the reinforcement ratio on altering the out-of-plane ultimate resistance of walls with BEs was evident from the experimental results. This influence was mainly attributed to the geometrical configuration of the BEs that allowed for the use dual layer of vertical reinforcement at the wall end regions.
- All walls were able to sustain high displacement demands compared to those predicted by current blast standards (ASCE 2011; CSA 2012) corresponding to different response limitations. However, similar to in-plane response, axial load level as small as 10% of the wall axial capacity had a significant negative influence on the wall out-of-plane displacement response and ductility capacity. Therefore, it is critically important to consider the axial load effects when analyzing the wall response, especially when progressive collapse is a concern.
- Plastic analysis accurately predicted resistance for all the walls and predicted the displacement response of all walls with dominant flexural behavior. Plastic analysis also quantified the contribution of the web and BEs in resisting the load. Although the analyses indicate that most of the load was carried by the

BEs, the reinforcement ratio distribution and wall aspect ratio, as expected, had an influence on the load carried by the web.

- A simplified single degree of freedom (SDOF) model for RM walls with BEs failed to predict the out-of-plane response. This is attributed to the partial restraint provided by the BEs, which affected the boundary conditions of the wall, as well as the different damage mechanisms that are not accounted for with the simplified SDOF model (i.e. torsional damage in BEs and BEs-web interface failure).
- The developed numerical finite element model was successfully validated using different static and dynamic experimental program results that included walls with different configurations (i.e. without and with BEs), boundary conditions, aspect ratios, axial loads and reinforcement ratios. More specifically, the model was able to determine the crushing damage location and intensity based on the compressive strain distribution on the wall.
- The model numerically evaluated the influence of BEs on the wall performance compared to conventional walls. The results showed that RM shear walls with BEs had higher initial stiffness values and energy absorption levels compared to their conventional counterparts, when both types of walls were designed to have either identical in-plane or out-of-plane load resistance.
- Pressure-Impulse diagrams generated by the numerical model, using the response limits provided by ASCE 59-11 and CSA S850-12, for different wall parameters were used to evaluate such limits. The diagrams demonstrated that support rotation as a response limit failed to assess the damage level of RM

walls as it does not account for the different out-of-plane ductility capacities that alternative wall configurations may possess.

- The new response limits proposed based on the curvature capacities of the walls provided a better quantification for the walls damage states by accounting for the different ductility capacities that different walls may exhibit.
- Finally, the pressure and impulse capacities corresponding to different damage states increased significantly when conventional RM shear walls were replaced by walls with BEs with similar in-plane flexural capacities.

5.3. RECOMMENDATIONS FOR FUTURE RESEARCH

In light of the research findings reported in this dissertation; this section presents possible research extensions to expand the out-of-plane blast resistance knowledge base of RM walls with BEs.

- Although the current dissertation investigated ten scaled RM walls with BEs that have different design parameters, some aspects remain not studied. As usual additional experimental tests would facilitate more reliable judgment on the test parameters. These additional tests should cover other wall design parameters such as different BE dimensions and different levels of axial load.
- It is recommended to study the influence of adding the BEs configuration (i.e. pilasters) at regular intervals of the wall length rather than only the edges to maximize their contribution to long walls out-of-plane resistance.

- Considering the fact that only a limited knowledge is available in the literature regarding RM elements torsional resistance, more relevant investigation pertaining to the BEs-web connection is still required.
- Additional investigations for a wider spectrum of wall aspect ratios are still required to further determine influence of BEs on the walls' displacement response and damage state. In addition, field/arena blast tests for load-bearing RM shear walls with BEs are also necessary to provide more data that can assist the research and code communities in determining more reliable response limits that can quantify the damage states.
- Although the chosen numerical model (layered-shell elements) reproduces the experimental results very well, there are other numerical models (e.g. the discrete element method for masonry) that may require more investigation.

5.4 REFERENCES

ASCE. (2011). "Blast Protection of Buildings." *ASCE 59-11*, Reston, Va.

CSA. (2012). "Design and assessment of buildings subjected to blast loads." *CSA S850-12*, CSA (Canadian Standards Association). (2014). Design of masonry structures. CSA S304-14, Mississauga, ON, Canada.